DAGAN, ZEEV

ENTRANCE EFFECTS IN STOKES FLOW THROUGH A PORE

City University of New York PH.D. 1981

ENTRANCE EFFECTS IN STOKES FLOW THROUGH A PORE

by

ZEEV DAGAN

A dissertation submitted to the Graduate Faculty in Engineering in partial fulfillment of the requirements for the degree of Doctor of Philosophy,
The City University of New York.

1980

This manuscript has been read and accepted for the Graduate Faculty in Engineering in satisfaction of the dissertation requirement for the degree of Doctor of Philosophy.

12/11/80
date

Sheldon Weinbaum
Chairman of Examining Committee

12/11/80
date

Paul R Kramer
Executive Officer

Prof. Sheldon Weinbaum, Chairman

Prof. Chan-Mou Tchen

Prof. Robert Pfeffer

Prof. Peter Ganatos

Supervisory Committee

The City University of New York

Abstract

ENTRANCE EFFECTS IN STOKES FLOW
THROUGH A PORE

by

Zeev Dagan

Adviser: Professor Sheldon Weinbaum
Co-Adviser: Professor Robert Pfeffer

This thesis presents a study of entrance effects in the creeping motion through a pore of finite length and the motion of a sphere towards a circular aperture in a plane wall. The solution technique used incorporates a newly developed procedure for handling axisymmetric flows in the presence of confining boundaries that do not conform to natural co-ordinate systems with an extension of the collocation technique previously developed for treating both bounded and unbounded three-dimensional multiparticle Stokes flow problems.

The first part of this study (chapter II) presents a closed form analytic solution for the classic problem of creeping flow through a pore of finite length, including entrance and exit effects. The flow field is divided into two simply bounded regions: a cylindrical

volume bounded by the walls of the pore and the entrance and exit planes, and an infinite half space outside the pore. Analytic solutions are first obtained in each region in terms of unknown functions representing arbitrary axial and radial velocity components at the pore entrance (or exit). These functions are then determined by matching the normal and tangential stress at the pore opening using integral transform methods. Results are presented for various aspect ratio pores and a simple expression is derived for the pressure drop across an orifice of finite length.

In chapter III, the analytic matching procedure developed in chapter II is used in conjunction with the boundary collocation technique to treat the slow axisymmetric motion of a sphere in viscous fluid towards an orifice. The accuracy of the solution technique is tested by detailed comparison with the exact solution for the drag on a sphere moving perpendicular to a plane wall (Brenner, 1961). The collocation solutions converge to the exact solution to five significant figures for all spacings tested between 0.1 and 10.0 sphere radii. The solution procedure is also extended to obtain the solution for the problem of uniform flow past a sphere moving axisymmetrically towards a rigidly held disk. These results are required for the formulation of the approximate theory for the three-dimensional motion of a sphere approaching a pore presented in chapter IV.

Although in principle an exact analysis, similar to

that used for the axisymmetric motion, can be applied for the arbitrary motion of a sphere into a finite pore, the numerical computation time required in applying the collocation technique would be excessive. Therefore, an approximate theory is developed for determining the trajectory of a neutrally buoyant sphere carried by the fluid towards a pore, which is valid when the spacing between the sphere and the orifice wall is of the order of the sphere diameter. The equation for the quasi-steady motion of the sphere is derived by considering separately the motions parallel and perpendicular to the wall. Due to the linearity of the governing equations for Stokes flow, the total force acting on the sphere is determined from the vector sum of the individual contributions for the motion of a sphere in quiescent fluid, the flow past a stationary sphere and the forces acting on a rotating sphere. An overall hydrodynamic interaction function is obtained by neglecting higher order contributions and transverse curvature effects. Results indicate that the sphere trajectory departs significantly from the fluid streanlines and that the particle motion is greatly retarded as it approaches the orifice wall. The theoretical results were compared with a series of careful experimental measurements and have been found to be in good agreement. The theoretical predictions and experimental observations reveal that in the limit of zero Stokes number the "critical trajectory" concept for the exclusion of particles that is widely used in nuclepore filter theory is invalid.

The present analysis indicates that when the hydrodynamic interaction of the particles with the wall of the pore is not neglected all particles will eventually enter the pore regardless of their initial position but that the time for each trajectory differs. Therefore, it is necessary to modify the critical trajectory concept using "time dependent exclusion" description of particles approaching a pore. The theory is also used to predict the initial change in average particle concentration that one observes when particles approach a tube from a feed reservoir when the particle dimensions are not small compared to the tube diameter, the Fahreaus effect. In addition, the concentration profiles are determined indicating aggregation of particles near the orifice wall and dilution near the pore axis.

ACKNOWLEDGEMENTS

My largest debt is to Professor Sheldon Weinbaum and Professor Robert Pfeffer for their unfailing counsel and assistance in directing this research.

I am also thankful to Mr. William Hall for his instrumental help in performing the experimental measurements, and to the staff of The City University of New York Computer Center for the use of their facilities.

This research was sponsored by the National Science Foundation under Grant no. ENG78-22101. Their support is gratefully acknowledged.

Above all, I thank Nina.

TABLE OF CONTENT

LIST OF TABLES

LIST OF FIGURES

CHAPTER I

INTRODUCTION

While significant progress has been made in recent years in the internal flows in infinitely long tubes and external flows past more general boundary shapes, there are no existing solutions for the creeping motion through finite length pores or the motion of a particle towards an orifice or a finite length pore. In general, the entire question of finite length entrance and exit effects for creeping flows has not been previously studied although these effects are believed to have an important influence at low Reynolds numbers, where the influence of boundaries decays algebraically.

Particle entrance effects have been of considerable interest in connection with internal flows at low Reynolds numbers in the presence of body forces and hydrodynamic interaction between the particle and the confining boundaries. Such flows occur in many different areas of engineering and the biological and physical sciences. Typical applications include filtration of aerosols, transport processes in biological and synthetic membranes and the study of phloem flow. The biological sciences, in particular, have been an extremely fertile field for new applications of low Reynolds number flows. A brief list of related applications include the motion of solute molecules and proteins through pores and channels in membranes, blood flow in capillary blood vessels and the Fahraeus effect.

In general, problems involving particle interaction

with the confining boundaries cannot be treated by exact theoretical analysis because of the lack of a natural co-ordinate system that can be used to satisfy the no-slip boundary conditions on the confining boundaries and on the surface of the particle simultaneously. Some special cases which permit exact theoretical treatment, by using spherical bipolar co-ordinates, include the motion of a sphere perpendicular to a plane wall (Brenner, 1961) or parallel to it (Goldman, Cox and Brenner, 1967). Exact solutions for the motion of a sphere in bounded fluid involving infinite cylindrical boundaries have been obtained by Haberman and Sayre (1958) for the axisymmetric motion of a sphere in an infinite tube and by Wang and Skalak (1969) for the flow in a cylindrical tube containing a line of spheres. Bounded flows involving finite confining boundaries, a finite length pore, and discontinuous infinite planar boundaries, an orifice, cannot be treated by similar techniques.

More general methods for treating flows involving particle-boundaries interaction include the method of reflection, the finite element method and the boundary collocation technique.

The method of reflection is an iterative approximation technique which alternately satisfies the no-slip boundary conditions on the surface of the particle and on the confining boundaries. The convergence characteristics of this iterative series solution diminishes rapidly

as the distance between the particles and the boundaries decreases resulting in a poor description of the flow when there is strong boundary interaction.

Skalak, Chen and Chien (1972) have used the finite element method in treating an idealized model for capillary blood flow. The red cells are modeled as bi-concave disk-shaped solid particles equally spaced and axisymmetrically located in a circular tube. This method is a very promising technique for irregular but identical particles; however, it cannot be easily extended to steady or unsteady problems where the particle boundary conditions are not periodic.

A more promising technique that can be utilized for treating flows with irregular confining boundaries is the collocation technique. This technique is based on the work of Payne and Pell (1960) who have shown that the infinite set of simply separable singular solutions for each co-ordinate system provides a complete set of generating functions which can be used to describe an arbitrary disturbance along any constant co-ordinate surface of the same orthogonal co-ordinate system. The technique has been applied for both unbounded flows (Gluckman, Pfeffer and Weinbaum, 1971; Ganatos, Weinbaum and Pfeffer, 1978) and bounded flows (Leichtberg, Pfeffer and Weinbaum, 1976; Ganatos, Pfeffer and Weinbaum, 1980). The technique requires that the no-slip boundary conditions on the confining boundaries be satisfied analytically, while on the surface of the particle the no-slip boundary conditions are satisfied at discrete points.

The success of the collocation technique dependes

greatly on the ability to perform the integral transform of the disturbances produced by the particle and detected on the confining boundaries analytically. Otherwise, the computation time required for the inversion integrals can be prohibitively long. Furthermore, confining boundaries that are either discontinuous or of finite dimensions require new solution techniques which had not previously been developed. The problems of creeping flow through a finite length pore and the motion of a particle approaching an orifice are salient examples of this more complicated bounded flow geometry. The logical starting point is, therefore, to first develop a method for treating flows confined by finite or discontinuous boundaries. Once the exact no-slip boundary conditions are imposed along the boundaries of the system, the problem is reduced to a previously developed collocation procedure that can be applied on the surface of each particle in the flow field.

In chapter II the problem of creeping motion through an orifice of finite length is first presented in detail to illustrate the general solution method employed when the boundaries require that the flow field be partitioned into more than one flow region. The important problem of the axisymmetric motion of a sphere towards an orifice is presented in chapter III. Here, in addition to the solution procedure discussed in chapter II for imposing the no-slip boundary conditions on the orifice wall, the collocation technique is utilized to satisfy the no-slip boundary

conditions on the surface of the sphere. This formulation can be easily modified to obtain results for the drag acting on a sphere moving axisymmetrically towards a stationary disk in uniform flow. These results are presented in chapter III as well. Finally, due to the excessive computation time required in applying similar analysis for the three-dimensional motion of a sphere towards an orifice, an approximate solution procedure for determining the trajectory of a neutrally buoyant sphere approaching a pore is developed based partly on the results in chapter III. The theoretical predictions, presented in chapter IV, are compared with experimental measurements which are used to describe the particle trajectory in the vicinity of the pore entrance.

CHAPTER II

AN EXACT SOLUTION FOR THE CREEPING MOTION THROUGH AN ORIFICE OF FINITE LENGTH

II-1. Introduction

The creeping flow through a pore of finite length, including entrance and exit effects, has important applications for transport and filtration processes in biological and synthetic membranes. Some salient examples involving such motion include filtration of particle contaminants and aerosols, the molecular sieving effects that are known to occur at the entrance of the so called "small pores" in biological membranes, the diffusion of macromolecules through vesicle attachment stalks in an endothelial cell layer (Weinbaum and Caro, 1976) and the Fahraeus-Lindqvist effect in blood capillaries (Fahraeus, 1929; Fahraeus and Lindqvist, 1931).

Existing analytic solutions of related problems have been limited to either the slow viscous flow in an infinite half space for an arbitrary prescribed velocity at the pore exit (Parmet and Saibel, 1965) or the classic solution of Sampson (1891) for the flow through a circular hole in a zero thickness plane wall. A number of studies have also examined the locally valid two-dimensional flow near a sharp corner (Dean and Montagnon, 1949; Lugt and Schwiderski, 1965; Weinbaum, 1968). The more difficult problem of analytically determining the interaction between the flow inside and outside the pore has heretofore been unsolved. Weinbaum (1968) demonstrated the importance of the upstream influence on the pressure field and velocity profile for flow approaching the trailing edge of a blunt base body.

If upstream influence is neglected and a Blasius boundary layer profile is assumed just upstream of the corner, the pressure field corresponding to this solution cannot be matched with the uniform pressure field of the Blasius solution and an erroneous velocity field is predicted with separation occuring at the trailing edge. Similarly, the assumption that the flow inside the pore is fully developed and has a Poiseuille profile (Manton, 1978) excludes the upstream influence of the pressure field across the edge of the orifice. Due to the difficulty of analytically treating a three-dimensional corner flow interaction, several investigators (Kanaoka, Emi and Nskada, 1974; Smith and Phillips, 1978; Parker and Buzzard, 1978) have recently undertaken finite difference Navier-Stokes solutions for representative pore geometries. However, the finite difference method is limited due to the admissibility of a weak singularity in the pressure field at the edge of the pore. The locally singular shear stress prevents accurate numerical description of the pressure field because of the mesh size limitation.

The problem of creeping flow through a finite length pore has eluded exact theoretical treatment because of the lack of a natural co-ordinare system which can be used to satisfy the no-slip boundary conditions simultaneously inside on the orifice wall and outside on the wall which lies in the plane of the entrance or exit. The purpose of the present chapter is to develop an efficient matching

technique which could be used to treat an important class of previously unsolved axisymmetric creeping motion problems where the general flow field can be divided into a set of simply bounded fields which cover the original flow field geometrically. Thus, the partitioning of a complex field may establish well defined regions in which the solution for the velocity distribution is unique. One first satisfies the kinematic boundary conditions on the velocity in each region independently by prescribing in a general form the unknown velocity profile at the interface between any two adjacent regions. For a finite interface one chooses a convenient series representation with unknown constant coefficients. Hence, in each region one has a well posed boundary value problem which will admit a unique solution in terms of the unknown velocity at the interface with an adjacent region. This procedure assures continuity of the velocity field without accounting for the influence of the pressure field across the interfacial surfaces. In order to satisfy continuity of the pressure field the normal and tangential stress at each interface has to be matched. This dynamic matching condition can be used to solve for the unknown coefficients in the general series representation of the local velocity profile. The method can be applied as well to problems which also include finite particles by making use of the collocation technique, described in chapter I, to satisfy the no-slip boundary conditions on finite closed surfaces. This extension of the technique

to a sphere approaching an orifice or a disk is described in chapter III.

Section II-2 contains the mathematical formulation of the problem at hand for a pore of arbitrary dimensions and a prescribed pressure drop across the pore. In section II-3 the solution obtained by the new technique is presented and the far field solution compared to Sampson's solution (1891) for the zero thickness orifice. In addition, a simple expression is derived for the pressure drop across the pore. Finally, in section II-4 the extension of the present method to bounded external flows with particles present is discussed.

II-2. Formulation for the creeping flow through a pore.

The flow of interest is axisymmetric, so that the Stokes stream function can be used. It is convenient to formulate the problem in terms of dimensionless (unprimed) co-ordinates which are defined in terms of dimensional (primed) co-ordinates (Fig. II-1) by:

$$R = \frac{R'}{a} \qquad Z = \frac{Z'}{a} \qquad \text{(II-2.1a,b)}$$

where a is the radius of the pore and (R',Z') are the cylindrical co-ordinates. The dependent variables are expressed in dimensionless form, using the fluid density ρ, the kinematic viscosity ν and the pore radius a as follows

$$\psi = \frac{\psi'}{a\nu} \qquad P = \frac{P' a^2}{\rho \nu^2} \qquad \text{(II-2.2a,b)}$$

where ψ' is the stream function and P' is the pressure.

By omitting the inertial terms from the steady state Navier-Stokes equations and introducing the axisymmetric stream function, the following equation is obtained

$$D^2 (D^2 \psi) = 0 \qquad \text{(II-2.3a)}$$

where D^2 is the generalized axisymmetric Stokesian operator, given by

$$D^2 = \frac{\partial^2}{\partial R^2} - \frac{1}{R}\frac{\partial}{\partial R} + \frac{\partial^2}{\partial Z^2} \qquad \text{(II-2.3b)}$$

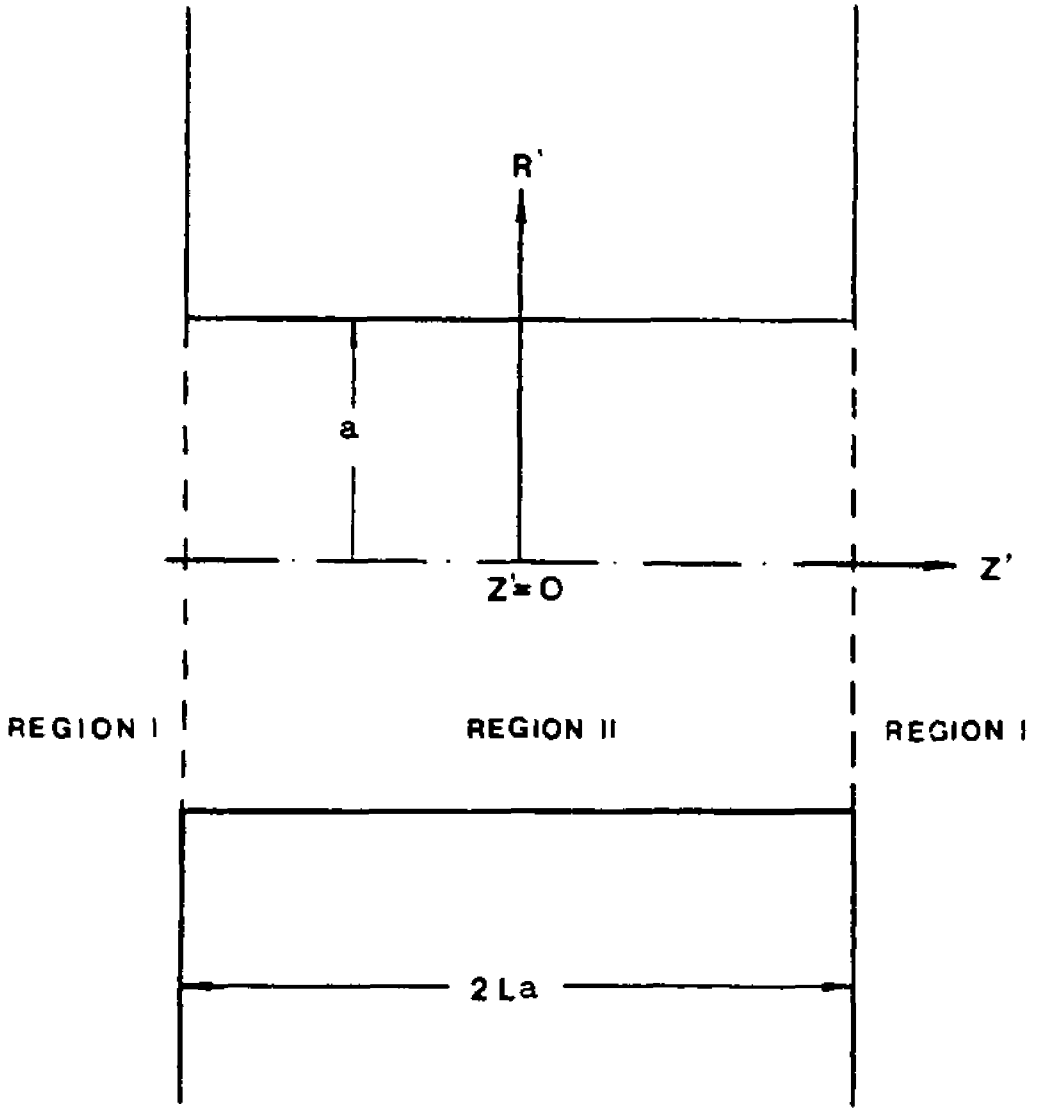

Figure II-1. Geometry of an orifice of finite length and diameter.

and the velocity components in the axial and radial directions are

$$u_z = \frac{1}{R}\frac{\partial \psi}{\partial R} \qquad u_R = -\frac{1}{R}\frac{\partial \psi}{\partial z} \qquad \text{(II-2.4a,b)}$$

In accord with the comments in the previous section, we divide the flow field into two simply bounded regions: a cylindrical volume bounded by the walls of the pore the exit plane and the symmetry plane at Z=0, and the infinite half space outside the pore. Solutions to equation (II-2.3) which are suitable for representing an arbitrary disturbance generated by the wall at Z=L and which yield a finite velocity everywhere in the outer region are given by Parmet and Saibel (1965) in the form

$$\psi^{I}(R,z) = \int_0^\infty R\, J_1(\omega R)\left[A(\omega) + z\, B(\omega)\right] e^{-\omega z}\, d\omega, \quad (z \geq L) \quad \text{(II-2.5)}$$

where $A(\omega)$ and $B(\omega)$ are unknown functions of ω, J_1 is the ordinary Bessel function of the first kind and L is the aspect ratio or the dimensionless pore length. Inside the pore a symmetric solution about Z=0, which generates finite velocities at R=0, is constructed by superimposing the disturbances from the cylindrical boundary R=1 (Haberman and Sayre, 1958), the vertical plane Z=0 and the unknown flow that must match the solution in the infinite half space $Z \geq L$.

$$\psi^{II}(R,Z) = C_0 R^4 + D_0 R^2 + \sum_{n=1}^{\infty} \left[C_n R I_1(\alpha_n R) + D_n R^2 I_0(\alpha_n R) \right] \cos \alpha_n Z + \sum_{n=1}^{\infty} \left[F_n Z \sinh(\lambda_{n,1} Z) + G_n \cosh(\lambda_{n,1} Z) \right] R J_1(\lambda_{n,1} R) \qquad (0 < Z < L) \qquad \text{(II-2.6)}$$

where $C_0, D_0, C_n, \ldots, F_n$ are unknown constant coefficients, I_0 and I_1 are the modified Bessel functions of the first kind, $\lambda_{n,\nu}$ are the zeros of J_ν and $\alpha_n = n\pi/L$.

The kinematic solution for each region can now be obtained independently provided the velocity at the exit of the pore is specified. This velocity, at the pore opening, is prescribed in a general form by a Fourier-Bessel series as follows

$$\vec{u}(R,L) = \frac{f(R)}{R}\hat{z} - \frac{g(R)}{R}\hat{r} = \sum_{n=1}^{\infty} \left[a_n J_0(\lambda_{n,0} R)\hat{z} - b_n J_1(\lambda_{n,1} R)\hat{r} \right] \qquad \text{(II-2.7)}$$

where $f(R)/R$ and $-g(R)/R$ are the axial and radial velocity components at $Z=L$ and $R \leq 1$, and a_n and b_n are unknown constant coefficients.

Using the definition (II-2.7) for the exit velocity, the no-slip boundary conditions on the wall $Z=L$ are:

$$u_z^I(R,L) = \frac{1}{R}\frac{\partial \psi^I}{\partial R}(R,L) = F(R) = \begin{cases} \dfrac{f(R)}{R} & 0 < R < 1 \\ 0 & 1 < R \end{cases} \qquad \text{(II-2.8a)}$$

$$u_R^I(R,L) = -\frac{1}{R}\frac{\partial \psi^I}{\partial z}(R,L) = G(R) = \begin{cases} -\frac{q(R)}{R} & 0<R<1 \\ 0 & 1<R \end{cases} \qquad \text{(II-2.8b)}$$

while equation (II-2.7) and the following no-slip boundary conditions

$$u_z^{II}(1,z) = \frac{1}{R}\frac{\partial \psi^{II}}{\partial R}(1,z) = 0 \qquad (0 \le z \le L) \qquad \text{(II-2.9a)}$$

$$u_R^{II}(1,z) = -\frac{1}{R}\frac{\partial \psi^{I}}{\partial z}(1,z) = 0 \qquad (0 \le z \le L) \qquad \text{(II-2.9b)}$$

have to be satisfied in the inner region.

Finally, the shear stress matching condition at Z=L and $0 \le R < 1$ requires

$$\tau_{ij}^{I} = \tau_{ij}^{II} \qquad \text{(II-2.10)}$$

where τ_{ij} is the stress tensor.

Application of the boundary conditions (II-2.8a,b) along the wall Z=L results in

$$\int_0^\infty \omega J_0(\omega R)\, F^*(\omega,L)\, d\omega = F(R) \qquad \text{(II-2.11a)}$$

$$-\int_0^\infty \omega J_1(\omega R)\, G^*(\omega,L)\, d\omega = G(R) \qquad \text{(II-2.11b)}$$

where

$$F^*(\omega,z) = [A(\omega) + zB(\omega)]\, e^{-\omega z} \qquad \text{(II-2.12a)}$$

$$G^*(\omega,z) = \frac{1}{\omega}[(1-\omega z)B(\omega) - \omega A(\omega)]\, e^{-\omega z} \qquad \text{(II-2.12b)}$$

The right hand side of equation (II-2.11) represents the disturbances produced by the plane Z=L and propagate downstream. These disturbances are functions only of the radial co-ordinate R. Inspection of (II-2.11) shows that the unknown functions F^* and G^* evaluated at the plane of the opening, are simply Hankel transforms of these disturbances. The equations may be inverted to give

$$F^*(\omega,L) = \int_0^1 f(\xi)\, J_0(\omega\xi)\, d\xi \qquad \text{(II-2.13a)}$$

$$G^*(\omega,L) = \int_0^1 g(\xi)\, J_1(\omega\xi)\, d\xi \qquad \text{(II-2.13b)}$$

Equations (II-2.13) give the F* and G* functions evaluated at Z=L in terms of the yet unknown velocity components at the pore exit. To obtain these functions at any value of Z one must determine the unknown functions $A(\omega)$ and $B(\omega)$ in (II-2.12). The expressions for F* and G* obtained from (II-2.13) are substituted into (II-2.12) whose right hand sides are evaluated at the plane Z=L. This gives rise to two linear algebraic equations which can be solved simultaneously to yield the unknown functions $A(\omega)$ and $B(\omega)$. Once these functions are obtained, they are substituted back into (II-2.12) to give the F* and G* functions at any value of Z. The resulting expressions are:

$$F^*(\omega,z) = \left\{ [1+\omega(z-L)] \int_0^1 f(\xi) J_0(\omega\xi)\, d\xi + \omega(z-L) \int_0^1 g(\xi) J_1(\omega\xi)\, d\xi \right\} e^{-\omega(z-L)} \qquad \text{(II-2.14a)}$$

$$G^*(\omega,\bar{z}) = \left\{ -\omega^2(\bar{z}-L)\int_0^1 f(\xi)\,J_0(\omega\xi)\,d\xi + \omega\left[1-\omega(\bar{z}-L)\int_0^1 g(\xi)\,J_1(\omega\xi)\,d\xi\right\} e^{-\omega(\bar{z}-L)} \qquad \text{(II-2.14b)}$$

Using the definition of the stream function, one can write the local fluid velocity at any point in the outer region as a function of the Hankel transforms of F* and G*, which in turn are functions of the unknown velocity components f and g at the pore exit

$$u_{\bar{z}}^{I}(R,\bar{z}) = \int_0^\infty \omega\, F^*(\omega,\bar{z})\, J_0(\omega R)\, d\omega \qquad \text{(II-2.15a)}$$

$$u_R^{I}(R,\bar{z}) = -\int_0^\infty \omega\, G^*(\omega,\bar{z})\, J_1(\omega R)\, d\omega \qquad \text{(II-2.15b)}$$

where from equation (II-2.5) the expression for the stream function in the outer region is given by

$$\psi^{I}(R,\bar{z}) = \int_0^\infty R\, F^*(\omega,\bar{z})\, J_1(\omega R)\, d\omega \qquad \text{(II-2.16)}$$

The solution (II-2.16) satisfies the no-slip boundary conditions along the wall at the plane of the opening for any arbitrary velocity profile at the pore exit.

The boundary conditions to be satisfied in the inner region at R=1 and Z=L are most conveniently applied by using the series representation of the exit velocity rather than the f and g functions. At R=1 the no-slip boundary conditions (II-2.9) require that

$$4C_0 + 2D_0 + \sum_{n=1}^{\infty} \left\{ C_n \alpha_n I_0(\alpha_n) + D_n \left[2 I_0(\alpha_n) + \alpha_n I_1(\alpha_n) \right] \right\} \cos \alpha_n z$$

$$= - \sum_{n=1}^{\infty} \left[F_n z \sinh(\lambda_{n,1} z) + G_n \cosh(\lambda_{n,1} z) \right] \lambda_{n,1} J_0(\lambda_{n,1}) \qquad \text{(II-2.17a)}$$

$$\sum_{n=1}^{\infty} \left[C_n I_1(\alpha_n) + D_n I_0(\alpha_n) \right] \sin \alpha_n z = 0. \qquad \text{(II-2.17b)}$$

The left hand sides of (II-2.17) are simply the Fourier representation of the right hand sides on the interval [0,L]. They may be inverted to give

$$4C_0 + 2D_0 =$$

$$-\frac{1}{L} \sum_{n=1}^{\infty} \left\{ F_n \left[L \cosh(\lambda_{n,1} L) - \frac{\sinh(\lambda_{n,1} L)}{\lambda_{n,1}} \right] \right.$$

$$\left. + G_n \sinh(\lambda_{n,1} L) \right\} J_0(\lambda_{n,1}) \qquad \text{(II-2.18a)}$$

$$C_n \alpha_n I_0(\alpha_n) + D_n \left[2 I_0(\alpha_n) + \alpha_n I_1(\alpha_n) \right] =$$

$$(-1)^{n+1} \frac{2}{L} \sum_{m=1}^{\infty} \left\{ F_m \left[\lambda_{m,1} \cosh(\lambda_{m,1} L) - \frac{\lambda_{m,1}^2 - \alpha_n^2}{\lambda_{m,1}^2 + \alpha_n^2} \sinh(\lambda_{m,1} L) \right] \right.$$

$$\left. + G_m \lambda_{m,1} \sinh(\lambda_{m,1} L) \right\} \frac{\lambda_{m,1} J_0(\lambda_{m,1})}{\lambda_{m,1}^2 + \alpha_n^2} \qquad \text{(II-2.18b)}$$

$$C_n I_1(\alpha_n) + D_n I_0(\alpha_n) = 0 \qquad \text{(II-2.18c)}$$

At the pore exit the solution must satisfy the arbitrary velocity profile (II-2.7). Using the expression for the stream function in the inner region (II-2.6), we

require that

$$2D_0 + \sum_{n=1}^{\infty} \left[F_n L \sinh(\lambda_{n,1} L) + G_n \cosh(\lambda_{n,1} L)\right] \lambda_{n,1} J_0(\lambda_{n,1} R) =$$

$$-4C_0 R^2 - \sum_{n=1}^{\infty} (-1)^n \left\{C_n \alpha_n I_0(\alpha_n R) + D_n \left[2 I_0(\alpha_n R) + \alpha_n R I_1(\alpha_n R)\right]\right\}$$

$$+ \sum_{n=1}^{\infty} a_n J_0(\lambda_{n,0} R) \qquad (0 \leq R \leq 1) \qquad \text{(II-2.19a)}$$

$$\sum_{n=1}^{\infty} \left\{F_n \left[L \lambda_{n,1} \cosh(\lambda_{n,1} L) + \sinh(\lambda_{n,1} L)\right] + G_n \lambda_{n,1} \sinh(\lambda_{n,1} L)\right\} J_1(\lambda_{n,1} R) =$$

$$\sum_{n=1}^{\infty} b_n J_1(\lambda_{n,1} R) \qquad (0 \leq R \leq 1) \qquad \text{(II-2.19b)}$$

Here the disturbance from the outer region at the pore exit is represented by the Fourier-Bessel series expressing the exit velocity components. The left hand side is observed to be a Dini series representation of the right hand side in equation (II-2.19a), while in (II-2.19b) it is a Fourier-Bessel representation of the right hand side. Inversion of these equations together with equation (II-2.18c) yields the following relations:

$$C_0 + D_0 = \sum_{n=1}^{\infty} a_n \frac{J_1(\lambda_{n,0})}{\lambda_{n,0}} \qquad \text{(II-2.20a)}$$

$$\left[F_p L \sinh(\lambda_{p,1} L) + G_p \cosh(\lambda_{p,1} L)\right] \lambda_{p,1} J_0(\lambda_{p,1}) + \frac{16}{\lambda_{p,1}^2} C_0$$

$$+ 4\lambda_{p,1}^2 \sum_{n=1}^{\infty} \frac{(-1)^n \alpha_n}{(\lambda_{p,1}^2 + \alpha_n^2)^2} I_1(\alpha_n) D_n = 2 \sum_{n=1}^{\infty} a_n \frac{\lambda_{n,0} J_1(\lambda_{n,0})}{\lambda_{n,0}^2 - \lambda_{p,1}^2}$$

$$\text{(II-2.20b)}$$

$$F_n \left[L \lambda_{n,1} \cosh(\lambda_{n,1} L) + \sinh(\lambda_{n,1} L) \right] + G_n \lambda_{n,1} \sinh(\lambda_{n,1} L) = b_n \qquad \text{(II-2.20c)}$$

The kinematic solution in each region is now known in terms of the unknown velocity at the pore opening. The functions $A(\omega)$ and $B(\omega)$, introduced in the stream function representation of the outer region, have been obtained in terms of the f and g functions (equations II-2.14), while the solution for the constant coefficients in the expression for the stream function in the inner region are known implicitly in terms of the constant coefficients in the series representation of the pore exit velocity (equations II-2.18 and II-2.20). However, these two solutions have been obtained without accounting for the upstream influence in the pressure field across the pore opening . It is this latter dynamic condition which we now use to determine a unique solution for $f(R)$ and $g(R)$.

The stress tensor, to be matched at Z=L, can be written in the general dimensionless form

$$\tau_{ij} = -\delta_{ij} P + 2 e_{ij} \qquad \text{(II-2.21)}$$

where δ_{ij} is the Kronecker delta, P is the pressure and $2e_{ij}$ is the rate of the strain tensor. By matching the pressure at the pore opening, the normal and tangential components of e_{ij} are left to be matched. These components are given by

$$e_{RR} = \frac{\partial u_R}{\partial R} \qquad e_{zz} = \frac{\partial u_z}{\partial z} \qquad \text{(II-2.22a,b)}$$

$$e_{RZ} = \frac{1}{2}\left(\frac{\partial u_Z}{\partial R} + \frac{\partial u_R}{\partial Z}\right) \qquad \text{(II-2.22c)}$$

Examination of (II-2.22) indicates that e_{RR}, e_{ZZ} and $\frac{\partial u_\theta}{\partial R}$ are continuous across the interface by virtue of the matched radial and axial velocity components. The remaining term, $\frac{\partial u_R}{\partial Z}$, can be replaced by requiring continuous pressure gradient which is directly related to the rate of strain tensor in the creeping motion equations. Hence, at Z=L, we require that

$$P^{I} = P^{II} \qquad (0<R<1) \qquad \text{(II-2.23a)}$$

$$\frac{\partial P^{I}}{\partial Z} = \frac{\partial P^{II}}{\partial Z} \qquad (0<R<1) \qquad \text{(II-2.23b)}$$

The general relations between the pressure and the stream function in steady creeping flow may be readily established from the Navier-Stokes equations. In dimensionless form these relations are:

$$\frac{\partial P}{\partial R} = -\frac{1}{R}\frac{\partial}{\partial Z}(D^2\Psi) \qquad \text{(II-2.24a)}$$

$$\frac{\partial P}{\partial Z} = \frac{1}{R}\frac{\partial}{\partial R}(D^2\Psi) \qquad \text{(II-2.24b)}$$

The pressure field in each region is determined by integration of equations (II-2.24) with the appropiate stream function representation. For the outer region the resulting equation is

$$P^{I}(R,Z) = P_\infty + 2\int_0^\infty \omega J_0(\omega R) B(\omega) e^{-\omega Z} d\omega \qquad \text{(II-2.25)}$$

and for the inner region

$$P^{II}(R,Z) = P_0 + 16 C_0 Z + 2\sum_{n=1}^{\infty} D_n \alpha_n I_0(\alpha_n R) \sin \alpha_n Z$$
$$+ 2\sum_{n=1}^{\infty} F_n \lambda_{n,1} \sinh(\lambda_{n,1} L) J_0(\lambda_{n,1} R) \qquad \text{(II-2.26)}$$

where P_0 is the uniform pressure at the plane of symmetry $Z=0$, and P_∞ is the downstream pressure as $Z \to \infty$.

Introducing the expressions for the pressure (II-2.25) and (II-2.26) into the matching conditions (II-2.23), and substituting $B(\omega)$ from equations (II-2.12) and (II-2.14) yields the following coupled integral equations

$$\int_0^\infty \omega^2 J_0(\omega R) \left[F^*(\omega,L) + G^*(\omega,L)\right] d\omega$$
$$= \frac{\overline{\Delta P}}{2} + 8 L C_0 + \sum_{n=1}^{\infty} F_n \lambda_{n,1} \sinh(\lambda_{n,1} L) J_0(\lambda_{n,1} R)$$
$$(0 \le R < 1) \qquad \text{(II-2.27a)}$$

$$-\int_0^\infty \omega^3 J_0(\omega R) \left[F^*(\omega,L) + G^*(\omega,L)\right] d\omega = 8 C_0 + \sum_{n=1}^{\infty} D_n (-1)^n \alpha_n^2 I_0(\alpha_n R)$$
$$+ \sum_{n=1}^{\infty} F_n \lambda_{n,1}^2 \cosh(\lambda_{n,1} L) J_0(\lambda_{n,1} R) \qquad (0 \le R < 1) \qquad \text{(II-2.27b)}$$

where

$$\overline{\Delta P} = P_0 - P_\infty \qquad \text{(II-2.28)}$$

is half the pressure drop across the pore.

The above integral equation, to the best of the

author's knowledge, cannot be solved explicitly for the F* and G* functions unless the behaviour of the integrals in (II-2.27) is specified for R > 1 (Tranter, 1951). Clearly, such information cannot be provided because it requires knowledge of the solution for the pressure and its gradient along the exterior wall of the pore. Therefore, it is advantageous to replace these functions by their series representations given by (II-2.7) and (II-2.13), and determine the unknown coefficients a_n and b_n in the expansions. Furthermore, in order to eliminate the weak singularity in the pressure field exhibited by the divergence of the integral expressions at R=1, the pressure is integrated over the area of a circle of radius R. The resulting conditions represent the force acting on the interface between the two regions and its gradient, which are analytic everywhere in the interval $0 \leq R \leq 1$. Following the outlined procedure one obtains the equations

$$\sum_{n=1}^{\infty} a_n J_0(\lambda_{n,0} R) = a^*(R) \qquad \text{(II-2.29a)}$$

$$\sum_{n=1}^{\infty} b_n J_1(\lambda_{n,1} R) = b^*(R) \qquad \text{(II-2.29b)}$$

where

$$a^*(R) = \sum_{n=1}^{\infty} a_n + 2C_0 R^2 + \sum_{n=1}^{\infty} D_n (-1)^n [I_0(\alpha_n R) - 1]$$
$$- \sum_{n=1}^{\infty} F_n \cosh(\lambda_{n,1} L) [J_0(\lambda_{n,1} R) - 1] \qquad \text{(II-2.30a)}$$
$$- \sum_{n=1}^{\infty} b_n \int_0^{\infty} d\omega\, \omega [J_0(\omega R) - 1] \int_0^1 d\xi\, \xi J_1(\lambda_{n,1} \xi) J_1(\omega \xi)$$

$$b^*(R) = \left(4LC_0 + \frac{\bar{\Delta P}}{4}\right)R + \sum_{n=1}^{\infty} F_n \sinh(\lambda_{n,1}L)\, J_1(\lambda_{n,1}R)$$
$$- \sum_{n=1}^{\infty} a_n \int_0^{\infty} d\omega\, \omega\, J_1(\omega R) \int_0^1 d\xi\, \xi\, J_0(\lambda_{n,0}\xi)\, J_0(\omega\xi)$$

(II-2.30b)

Equations (II-2.29) are simply the Fourier-Bessel series representation of the functions a*(R) and b*(R). A solution for a_n and b_n is readily available in the form:

$$a_n = \frac{2}{J_1^2(\lambda_{n,0})} \int_0^1 t\, a^*(t)\, J_0(\lambda_{n,0}t)\, dt \qquad \text{(II-2.31a)}$$

$$b_n = \frac{2}{J_0^2(\lambda_{n,1})} \int_0^1 t\, b^*(t)\, J_1(\lambda_{n,1}t)\, dt \qquad \text{(II-2.31b)}$$

The integrals in (II-2.31) are performed analytically (see Appendix) resulting, after some rearrangement in

$$b_n \frac{J_0(\lambda_{n,1})}{\lambda_{n,1}} + 2\sum_{k=1}^{\infty} a_k \lambda_{k,0} J_1(\lambda_{k,0}) A_{kn}$$
$$- F_n \sinh(\lambda_{n,1}L) \frac{J_0(\lambda_{n,1})}{\lambda_{n,1}} + \frac{8LC_0}{\lambda_{n,1}^2} = -\frac{\bar{\Delta P}}{2\lambda_{n,1}^2} \qquad \text{(II-2.32a)}$$

$$a_n \frac{J_1(\lambda_{n,0})}{\lambda_{n,0}} - \frac{2}{\lambda_{n,0}^2}\sum_{k=1}^{\infty} a_k + 2\sum_{k=1}^{\infty} b_k \lambda_{k,1} J_0(\lambda_{k,1}) B_{kn}$$
$$+ 2\sum_{k=1}^{\infty} F_k \cosh(\lambda_{k,1}L)\left[\frac{J_0(\lambda_{k,1})}{\lambda_{n,0}^2 - \lambda_{k,1}^2} - \frac{1}{\lambda_{n,0}^2}\right]$$
$$- 2\sum_{k=1}^{\infty} D_k (-1)^k \left[\frac{I_0(\alpha_k)}{\alpha_k^2 + \lambda_{n,0}^2} - \frac{1}{\lambda_{n,0}^2}\right] - \frac{4C_0}{\lambda_{n,0}^2}\left(1 - \frac{4}{\lambda_{n,0}^2}\right) = 0$$

(II-2.32b)

where

$$A_{kn} = \frac{S(\lambda_{k,0}) - S(\lambda_{n,1})}{\lambda_{k,0}^2 - \lambda_{n,1}^2} \qquad \text{(II-2.33a)}$$

$$B_{kn} = \frac{1}{\lambda_{n,0}^2}\left[\frac{\pi}{2} H_1(\lambda_{k,1}) - 1\right] + A_{nk} \qquad \text{(II-2.33b)}$$

and the function $S(x)$ is given by

$$\frac{2}{\pi} + S(x) = \int_0^1 H_1\left(2x\sqrt{1-t^2}\right)dt$$

$$= \frac{16x^2}{9\pi}\, {}_2F_3\left(2,1;\, 3/2, 5/2, 5/2;\, -x^2\right)$$

Here H_1 is the Struve function of order one and ${}_2F_3$ is the generalized hypergeometric series.

Equations (II-2.18), (II-2.20) and (II-2.32) constitute the fundamental infinite set of linear algebraic equations for all six sets of unknown constant coefficients (C_n, D_n, F_n, G_n, a_n and b_n) and the constants C_o and D_o. This set can be reduced, by a standard elimination procedure, to include only four sets of unknown coefficiens (D_n, F_n, G_n and a_n) and the constant C_o. In addition, it is advantageous, for the purpose of numerical computation, to define the unknown coefficients as follows

$$\bar{C}_n = C_n I_1(\alpha_n) \qquad \text{(II-2.35a)}$$

$$\bar{D}_n = D_n I_0(\alpha_n) \qquad \text{(II-2.35b)}$$

$$\bar{F}_n = F_n L \sinh(\lambda_{n,1} L) \qquad \text{(II-2.35c)}$$

$$\bar{G}_n = G_n \cosh(\lambda_{n,1} L) \qquad \text{(II-2.35d)}$$

Consequently, the resulting system of equations is

$$8LC_o + \sum_{i=1}^{\infty} a_i a_{ij}^{I} + \bar{F}_j F_j^{I} + \bar{G}_j G_j^{I} = -\frac{\overline{\Delta p}}{2} \qquad \text{(II-2.36a)}$$

$$16 C_o + \sum_{i=1}^{\infty} \left(a_i a_{ij}^{\bar{II}} + \bar{D}_i D_{ij}^{II} \right) + \bar{F}_j F_j^{\bar{II}} + \bar{G}_j G_j^{II} = 0 \qquad \text{(II-2.36b)}$$

$$\bar{D}_j D_j^{\bar{III}} + \sum_{i=1}^{\infty} \left(\bar{F}_i F_{ij}^{\bar{III}} + \bar{G}_i G_{ij}^{\bar{III}} \right) = 0 \qquad \text{(II-2.36c)}$$

$$C_{oj} C_o + \sum_{i=1}^{\infty} \left(a_i a_{ij}^{\bar{IV}} + \bar{D}_i D_{ij}^{\bar{IV}} + \bar{F}_i F_{ij}^{\bar{IV}} + \bar{G}_i G_{ij}^{\bar{IV}} \right) = 0 \qquad \text{(II-2.36d)}$$

$$2C_o + \sum_{i=1}^{\infty} \left(a_i a_i^{\bar{V}} + \bar{F}_i F_i^{\bar{V}} + \bar{G}_i G_i^{\bar{V}} \right) = 0 \qquad \text{(II-2.36e)}$$

where

$$a_{ij}^{I} = 2 \lambda_{i,o} J_1(\lambda_{i,o}) A_{ij} \lambda_{j,1}^2 \qquad \text{(II-2.37a)}$$

$$F_j^{I} = \lambda_{j,1}^2 \coth(\lambda_{j,1} L) J_o(\lambda_{j,1}) \qquad \text{(II-2.37b)}$$

$$G_j^{I} = \lambda_{j,1}^2 \tanh(\lambda_{j,1} L) J_o(\lambda_{j,1}) \qquad \text{(II-2.37c)}$$

$$a_{ij}^{\bar{II}} = -2 J_1(\lambda_{i,o}) \frac{\lambda_{i,o} \lambda_{j,1}^2}{\lambda_{i,o}^2 - \lambda_{j,1}^2} \qquad \text{(II-2.37d)}$$

$$D_{ij}^{II} = 4(-1)^i \frac{I_1(\alpha_i)}{I_o(\alpha_i)} \frac{\alpha_i \lambda_{j,1}^4}{(\alpha_i^2 + \lambda_{j,1}^2)^2} \qquad \text{(II-2.37e)}$$

$$F_j^{\bar{II}} = G_j^{II} = \lambda_{j,1}^3 J_o(\lambda_{j,1}) \qquad \text{(II-2.37f,g)}$$

$$D_j^{III} = \left[2 + \alpha_j \frac{I_1(\alpha_j)}{I_0(\alpha_j)} - \alpha_j \frac{I_0(\alpha_j)}{I_1(\alpha_j)}\right](-1)^j \qquad \text{(II-2.37h)}$$

$$F_{ij}^{III} = \frac{2}{L^2} \frac{\lambda_{i,1} J_0(\lambda_{i,1})}{\alpha_j^2 + \lambda_{i,1}^2} \left[L \lambda_{i,1} \coth(\lambda_{i,1} L) + \frac{\alpha_j^2 - \lambda_{i,1}^2}{\alpha_j^2 + \lambda_{i,1}^2}\right] \qquad \text{(II-2.37i)}$$

$$G_{ij}^{III} = \frac{2}{L} \frac{\lambda_{i,1}^2 J_0(\lambda_{i,1})}{\alpha_j^2 + \lambda_{i,1}^2} \tanh(\lambda_{i,1} L) \qquad \text{(II-2.37j)}$$

$$a_{ij}^{IV} = \delta_{ij} \frac{J_1(\lambda_{j,0})}{\lambda_{j,0}} - \frac{2}{\lambda_{j,0}} \qquad \text{(II-2.37k)}$$

$$D_{ij}^{IV} = 2(-1)^{i+1} \left[\frac{1}{\alpha_i^2 + \lambda_{j,0}^2} - \frac{1}{I_0(\alpha_i)\lambda_{j,0}^2}\right] \qquad \text{(II-2.37l)}$$

$$F_{ij}^{IV} = 2 \left\{ \frac{1}{L} \coth(\lambda_{i,1} L) \left[\frac{J_0(\lambda_{i,1})}{\lambda_{j,0}^2 - \lambda_{i,1}^2} - \frac{1}{\lambda_{j,0}^2}\right] + \left[\lambda_{i,1} \coth(\lambda_{i,1} L) + \frac{1}{L}\right] \lambda_{i,1} J_0(\lambda_{i,1}) B_{ij} \right\} \qquad \text{(II-2.37m)}$$

$$G_{ij}^{IV} = 2 \tanh(\lambda_{i,1} L) \lambda_{i,1}^2 J_0(\lambda_{i,1}) B_{ij} \qquad \text{(II-2.37n)}$$

$$a_i^{V} = 2 \frac{J_1(\lambda_{i,0})}{\lambda_{i,0}} \qquad \text{(II-2.37o)}$$

$$F_i^{V} = \pm \left[\coth(\lambda_{i,1} L) - \frac{1}{L \lambda_{i,1}}\right] J_0(\lambda_{i,1}) \qquad \text{(II-2.37p)}$$

$$G_i^{V} = \pm \tanh(\lambda_{i,1} L) J_0(\lambda_{i,1}) \qquad \text{(II-2.37q)}$$

$$C_{oj} = -\frac{4}{\lambda_{j,0}^2} \left(1 - \frac{4}{\lambda_{j,0}^2}\right) \qquad \text{(II-2.37r)}$$

The unknown constant coefficients in (II-2.36) can be evaluated numerically to any degree of accuracy by increasing the number of equations utilized.

II-3. Numerical results

Computations were performed on an AMDAHL 470/V6 computer. One first evaluates the coefficients C_0, a_n, D_n, F_n and G_n by solving successively larger truncations of (II-2.36). Truncation after N terms requires a solution of (4N+1) linear algebraic equations which yield the first N values of each set of coefficients and the constant Co. Convergence of the results was tested by comparing the values of the volumetric flow rate Q, the constant Co and the centerline velocity at the pore exit for various values of the aspect ratio L, and the number of coefficients N (Fig. II-2(a),(b),(c)). Q was calculated by integrating the axial velocity at the pore exit, while the centerline velocity is simply the sum of the a_n coefficients obtained from the solution of (II-2.36). Figure II-2 shows that for $L \sim O(1)$ the results change by less than 1 percent as N increases from 20 to 100, and that the convergence of these results deteriorates as L approaches zero.

Values of the stream function, ψ, were computed next, for increasing value of N until they did not change in the first three significant figures. For L=1, the value of the stream function was calculated from equations (II-2.6) for the inner region and (II-2.16) for the outer region, using a grid of 10x10 points in each region, from which streamlines were drawn by interpolation (Fig.II-3). The double integrals in (II-2.16) were calculated, first, by analytically integrating the inner integrals and then

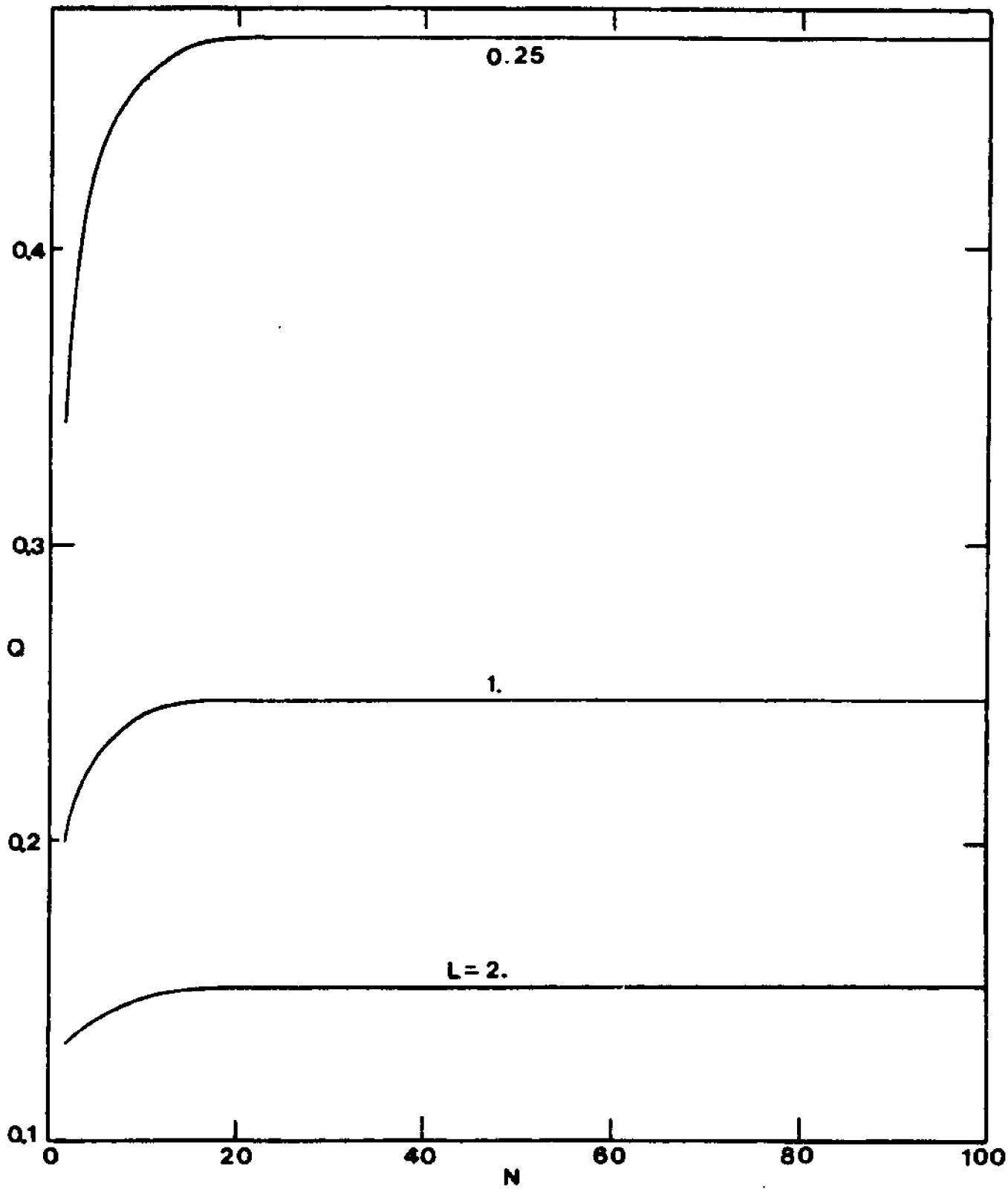

Figure II-2(a). Convergence test for the volumetric flow rate Q.

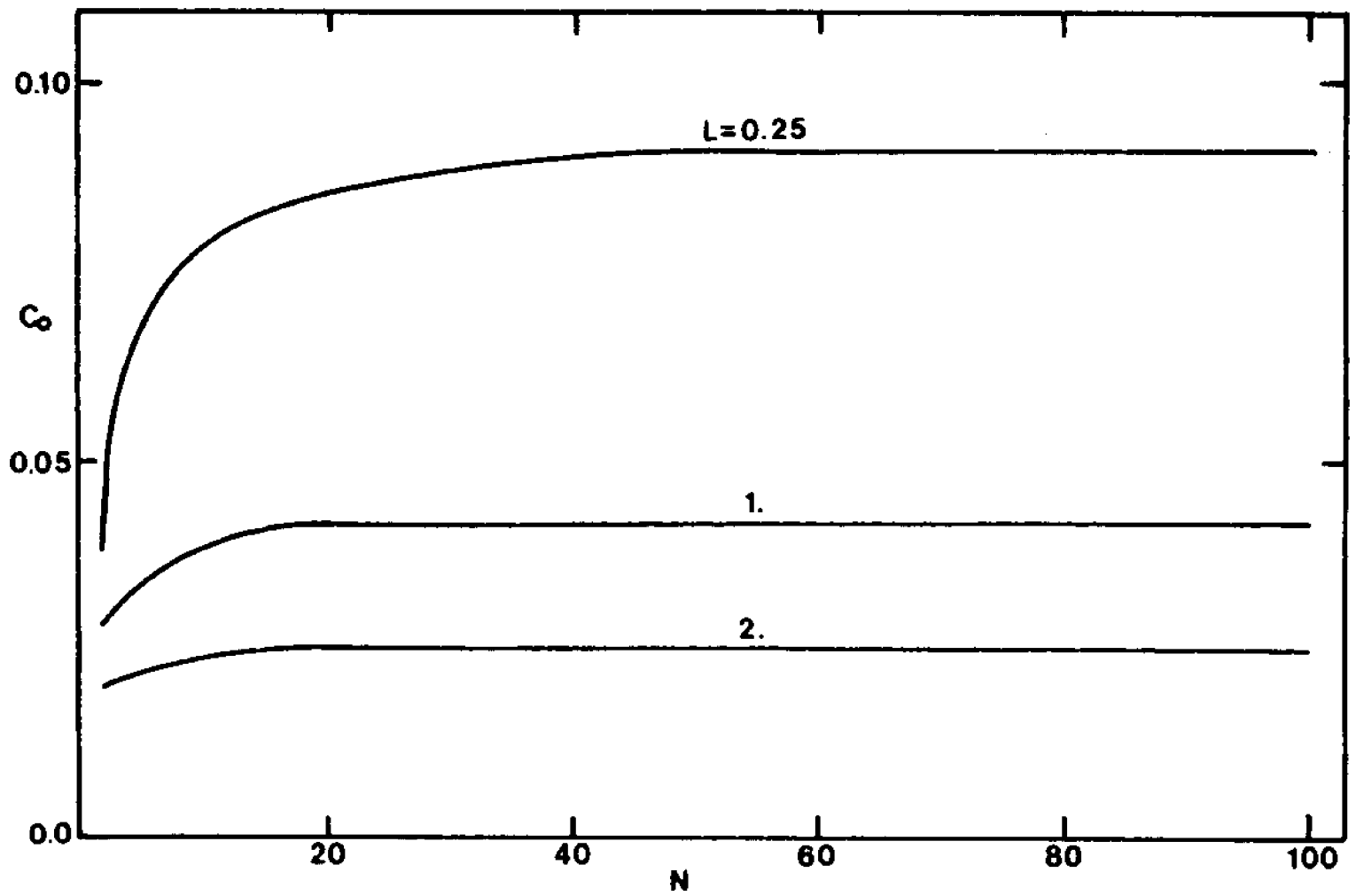

Figure II-2(b). Convergence test for the constant C_o.

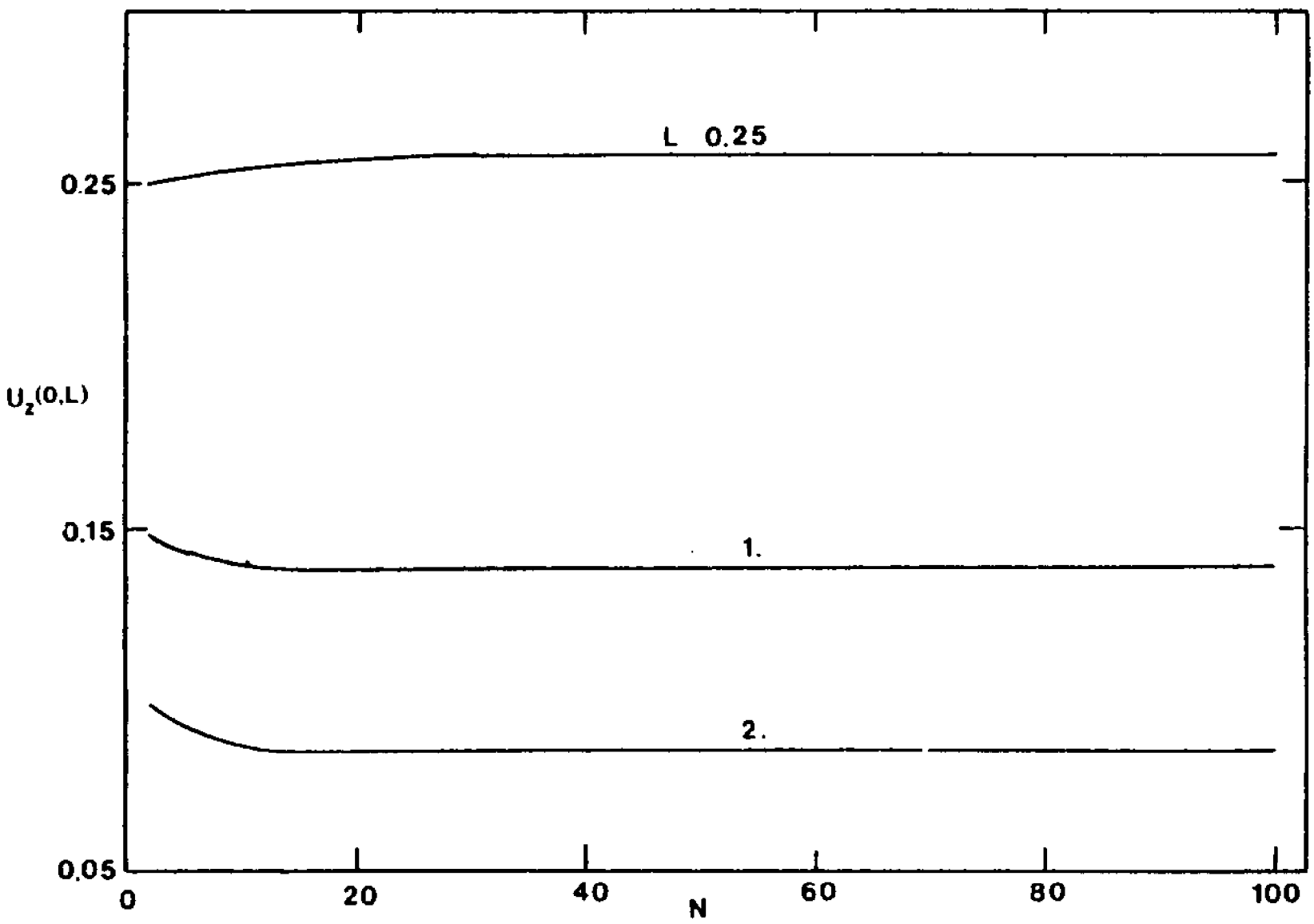

Figure II-2(c). Convergence test for the exit centerline velocity $U_z(0,L)$.

using numerical integration to evaluate the remaining improper integrals. The pressure field in the inner region was calculated from (II-2.26) using a grid of 10x10 points The pressure field in the outer region was computed from (II-2.25) using a similar grid except in the local region near the edge of the orifice, $0.8 \leq Z \leq 1.2$ and $0.8 \leq R \leq 2.0$, where a finer grid of 40x120 points was used. The integration in (II-2.25) was performed in a similar manner to that described for the calculation of the stream function from equation (II-2.16). Lines of constant pressure were drawn by interpolation and are shown in figure II-4. In figure II-5 the pressure field near the edge of the orifice is compared to the locally valid two-dimensional solution obtained by Weinbaum (1968). Qualitatively the two fields exhibit similar behaviour with increasing resemblance as the length scale near the edge of the orifice is further magnified.

The streamline pattern shown in figure II-3 for L=1. is similar in the far field to the exact solution for the flow through a circular hole in a plane wall (Sampson, 1891), while inside the pore the axial velocity approaches Poiseuille profile with less than 1.5 percent deviation after a short entrance distance equal to half the pore radius. The pressure field (Fig. II-4) is also compatible with the far field behaviour exhibited in Sampson's solution and approaches the linear axial pressure gradient behaviour associated with Poiseuille flow inside the pore.

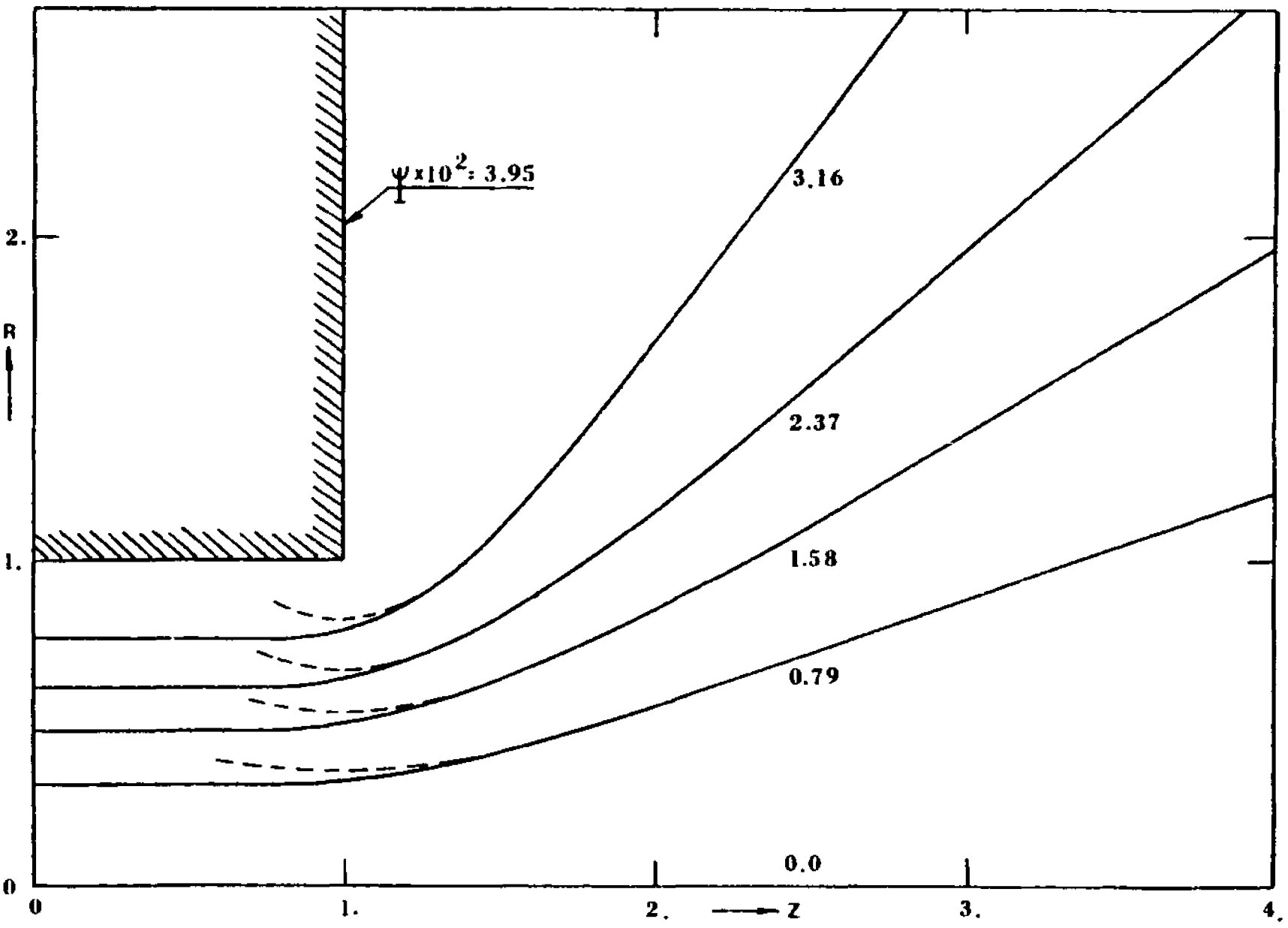

Figure II-3. Streamline pattern for the flow through a pore of finite length with L=1. ----- Sampson's solution for the flow through a zero thickness orifice (1891).

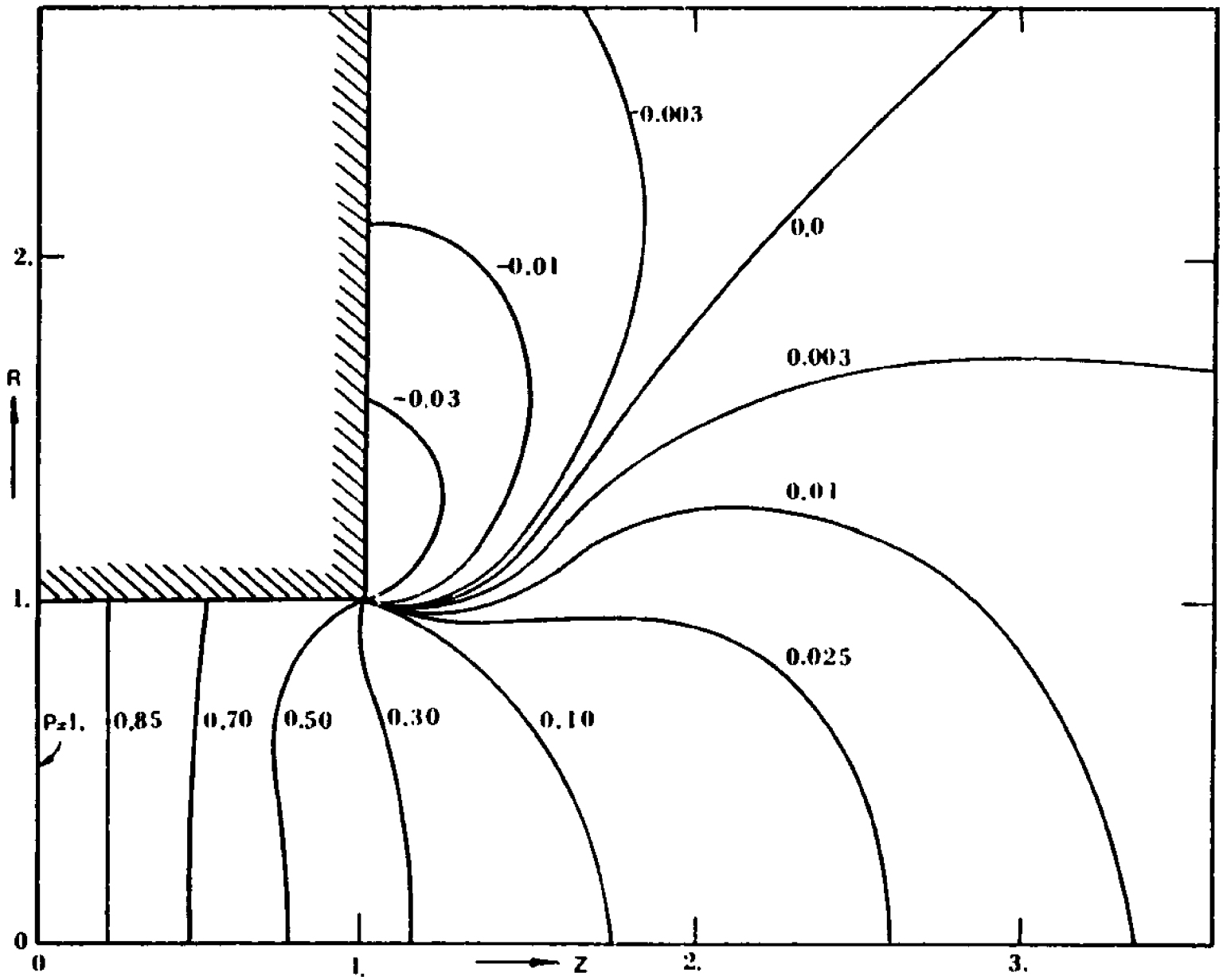

Figure II-4. Pressure field for the flow through a pore of finite length with L=1.

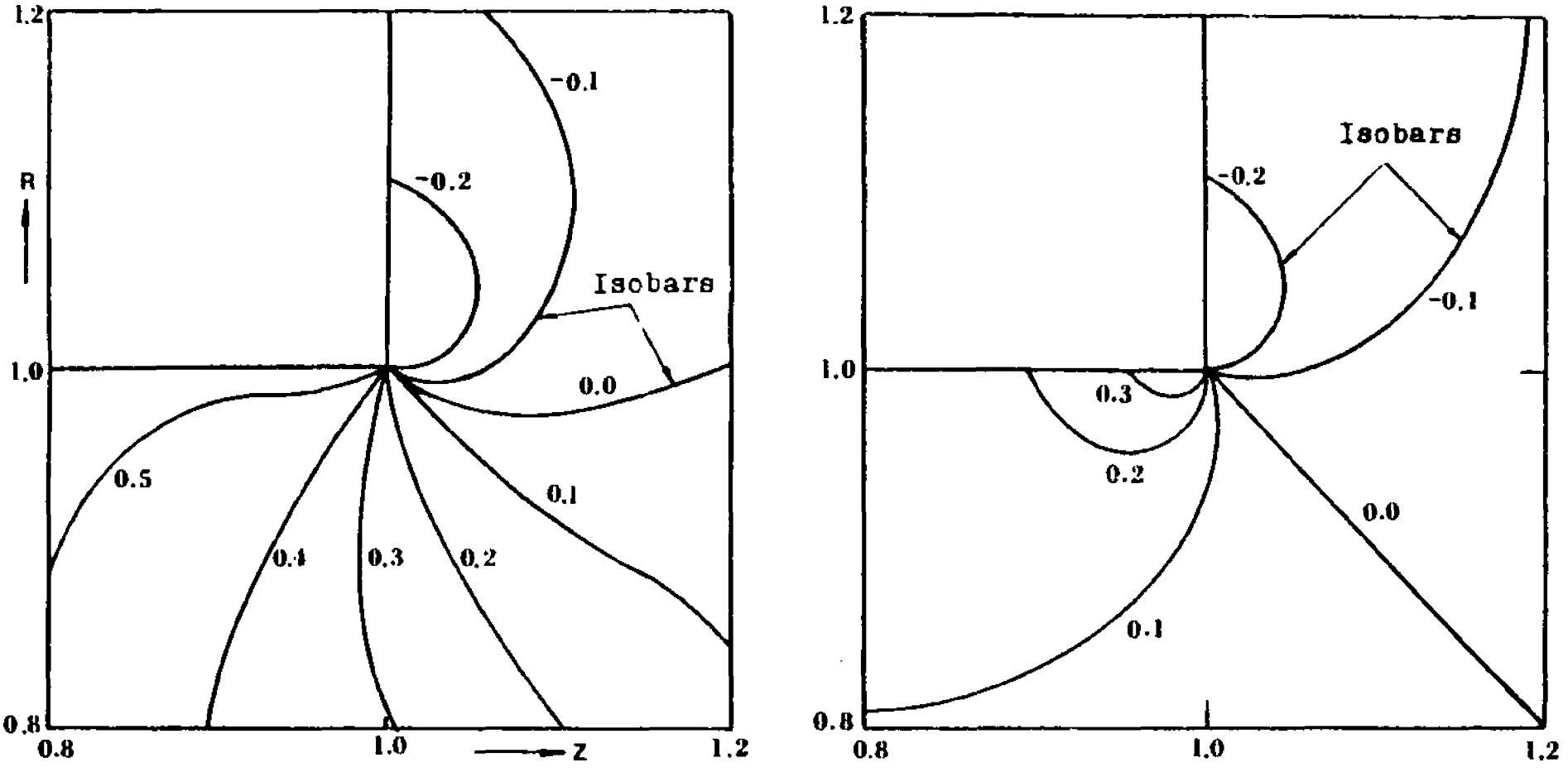

Figure II-5. Comparison between (a) the pressure field near the edge of the orifice (L=1) and (b) the locally valid two-dimensional pressure field in the vicinity of trailing edge (Weinbaum, 1968)

Computations were carried out for various values of L between 0.25 and 2.0 . When $L > \frac{1}{2}$ the flow inside the pore approaches Poiseuille flow in the manner described above. Furthermore, if Poiseuille flow is established inside the pore the streamline pattern must remain similar for all values of $L > \frac{1}{2}$ including the limiting case as $L \to \infty$. Hence, for $L > \frac{1}{2}$ the velocity profile at the exit of the pore is unchanged. Figure II-6 shows the radial and axial velocity components at the pore exit in comparison to Poiseuille and Sampson profiles. An interesting result from this comparison is that the axial velocity at the exit of the pore can be computed from the arithmetic average of Poiseuille and Sampson profiles to four significant digits.

The volumetric flow rate was calculated directly from the value of the stream function on the boundary inside the pore. In general, one can express the relations between the pressure drop across the pore $\Delta P'$, and the volumetric flow rate Q', as follows

$$\Delta P' = \Pi(L) \frac{Q'\mu}{a^3} \qquad \text{(II-3.1)}$$

where P' and Q' are dimensional variables, μ is the dynamic viscosity, a the pore radius and $\Pi(L)$ is a function of the aspect ratio L. For L=0. Sampson obtained the result

$$\Pi(0) = 3. \qquad \text{(II-3.2)}$$

For other values of L, $\Pi(L)$ is shown in figure II-7.

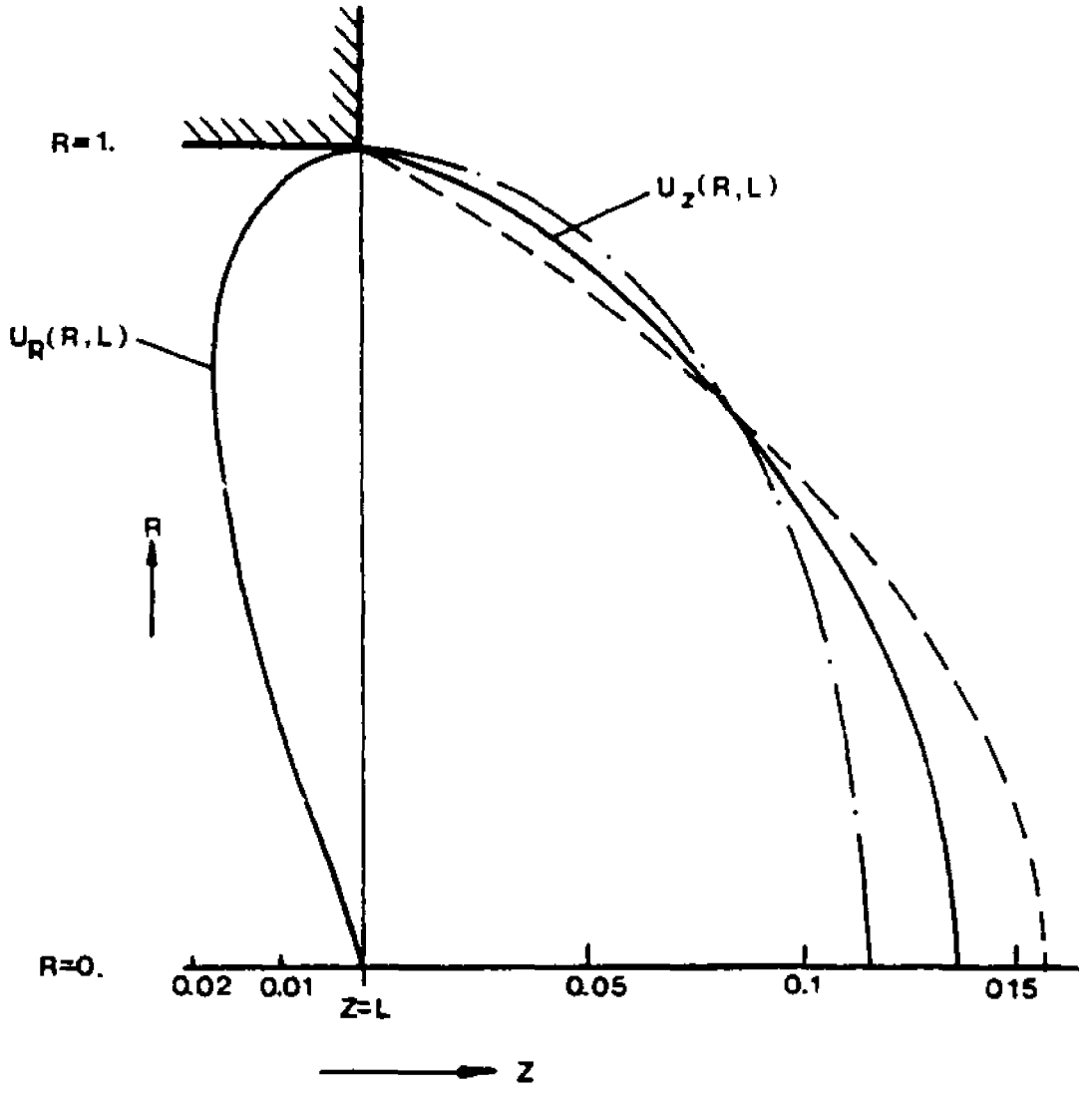

Figure II-6. Radial and axial velocity profiles at the pore exit (L=1.).- - - - Poiseuille profile;— · —· velocity profile at the opening of a zero thickness orifice (Sampson, 1891).

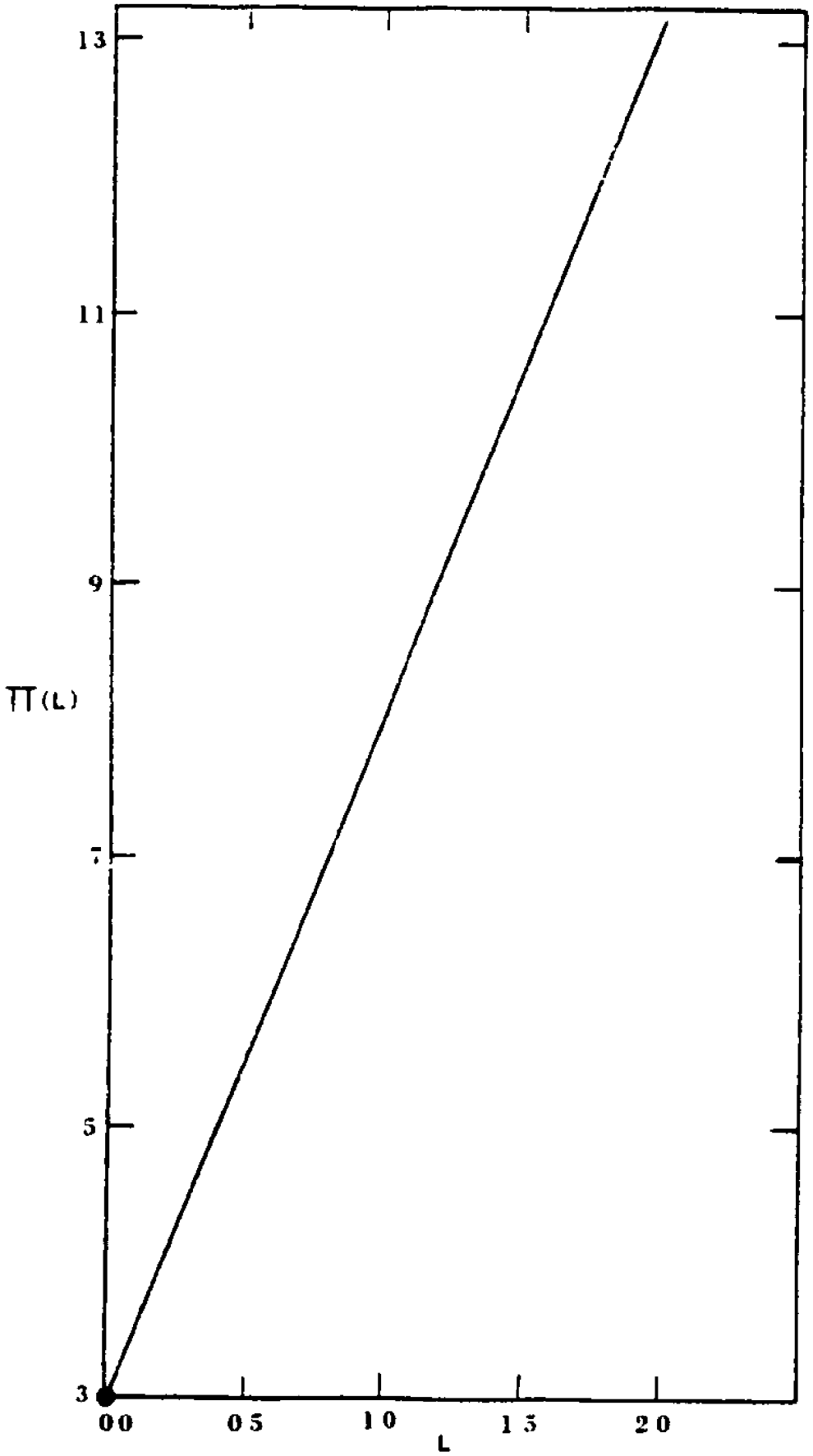

Figure II-7. Behaviour of the function $\Pi(L)$.
● Sampson (1891).

Clearly, the behaviour suggests linear relations between the pressure drop and the aspect ratio. A simple approximate expression for the pressure drop can be obtained by assuming Poiseuille flow throughout the pore and Sampson's solution outside. Then

$$\Pi(L) = \frac{16L}{\pi} + 3 \qquad \text{(II-3.3)}$$

The calculated values of $\Pi(L)$ were compared with equation (II-3.3) and are shown in table II-1. The good agreement between the exact and the approximate value is not surprising since the actual flow field deviates from the assumed one only in the vicinity of the pore opening and even in this region the local axial velocity profile does not depart significantly from the assumed profile.

Table II-1. Comparison of approximate expression (II-3.3) with the exact solution for $\Pi(L)$.

aspect ratio L	$\Pi(L)$	
	exact	equation (II-3.3)
0.0	3.00*	3.00
0.25	4.25	4.27
0.50	5.51	5.55
0.75	6.79	6.82
1.00	8.06	8.09
1.25	9.33	9.37
1.50	10.6	10.6
2.00	13.2	13.2

* Sampson (1891)

II-4. Concluding remarks

The present solution for the flow through a finite length pore suggest two general conclusions. First, the entrance effects are significant only near the pore opening, and decay to within 1.5 percent of a Poiseuille profile at a distance of half the pore radius when $L > \frac{1}{2}$. Secondly, the pressure drop across an orifice of finite length can be closely approximated (less than 1 percent error) by equations (II-3.1) and (II-3.3) which do not account for the upstream influence across the pore opening.

The method of solution used in the present problem can be easily applied to problems with boundaries that cannot be defined by a natural co-ordinate system. In particular, the study of filtration through nuclepore filters is simply modeled by a periodic distribution of equally spaced pores with an outer boundary which is a cylindrical volume coaxial with the pore. Furthermore, by combining the procedure outlined in this chapter with the collocation technique it is possible to study the motion of a sphere near boundaries of more complex shapes taking account of particle wall entrance effects.

Chapter III of the thesis contains an application of this method to the problem of the axisymmetric motion of a sphere towards an orifice and towards a disk.

Appendix

This appendix contains a detailed description of the analytic evaluation of the integrals in equations (II-2.31a,b). Substitution of a*(R) and b*(R) from (II-2.30) into (II-2.31) results in triple integrals of which the inner and the outer are definite integrals that can be easily evaluated leaving improper integrals of the form

$$A_{kn} = \int_0^\infty \frac{\omega J_1(\omega) J_0(\omega)}{(\omega^2 - \lambda_{n,1}^2)(\omega^2 - \lambda_{k,0}^2)} d\omega \qquad \text{(II-A-1)}$$

and

$$B_{kn} = A_{ak} - \frac{1}{\lambda_{k,0}^2} \int_0^\infty \frac{\omega J_1(\omega)}{\omega^2 - \lambda_{n,1}^2} d\omega \qquad \text{(II-A-2)}$$

in (II-2.31a) and (II-2.31b) respectively.

The integral in (II-A-2) is given in Oberhettinger (1972):

$$\int_0^\infty \frac{\omega J_1(\omega)}{\omega^2 - \lambda_{n,1}^2} d\omega = \frac{\pi}{2} H_{-1}(\lambda_{n,1}) \qquad \text{(II-A-3)}$$

where H_ν is the Struve function of order ν.

The recurrence relations

$$H_{\nu-1}(z) + H_{\nu+1}(z) = \frac{2\nu}{z} H_\nu(z) + \frac{(z/2)^\nu}{\sqrt{\pi}\,\Gamma(\nu+1/2)} \qquad \text{(II-A-4)}$$

are used in (II-A-3) to replace the right hand side with a Struve function of positive order. Then

$$\int_0^\infty \frac{\omega J_1(\omega)}{\omega^2 - \lambda_{n,1}^2} d\omega = 1 - \frac{\pi}{2} H_1(\lambda_{n,1}) \qquad \text{(II-A-5)}$$

To evaluate A_{kn} we write

$$A_{kn} = \frac{1}{\lambda_{k,0}^2 - \lambda_{n,1}^2} \left[S(\lambda_{n,1}) - S(\lambda_{k,0}) \right] \qquad \text{(II-A-6)}$$

where

$$S(t) = \int_0^\infty \frac{\omega J_0(\omega) J_1(\omega)}{t^2 - \omega^2} \, d\omega \qquad \text{(II-A-7)}$$

and t must be a root of J_0 or J_1. Furthermore, S(t) can be written as follows

$$S(t) = \lim_{a \to 1} \frac{d}{da} \int_0^\infty \frac{J_0(\omega) J_0(\omega a)}{\omega^2 - t^2} \, d\omega \qquad \text{(II-A-8)}$$

From the addition theorem one can obtain the equation

$$J_0(\omega) J_0(\omega a) = \frac{1}{\pi} \int_0^\pi J_0(\omega \sqrt{1 + a^2 - 2a\cos\theta}) \, d\theta \qquad \text{(II-A-9)}$$

Substitution of (II-A-9) into (II-A-8) gives rise to an outer integral of the form given in Oberhettinger (1972), which can be evaluated. Differentiation with respect to a and setting a=1 yields

$$S(t) = \frac{1}{2} \int_0^\pi \left[H_1 \left(2t \sin\frac{\theta}{2} - \frac{2}{\pi} \right) \right] \sin\frac{\theta}{2} \, d\theta \qquad \text{(II-A-10)}$$

or with the substitution $\mu = \cos\frac{\theta}{2}$ it becomes

$$S(t) = \int_0^1 H_1 \left(2t \sqrt{1 - \mu^2} \right) d\mu - \frac{2}{\pi} \qquad \text{(II-A-11)}$$

The integral in (II-A-11) can be determined by making use of the series representation of H_1 and term by term integration. Then

$$S(t) = \tfrac{16}{3}\pi^2 t^2 \, {}_2F_3\,(2,1;3/2,5/2,5/2;-t^2) - \frac{2}{\pi} \qquad \text{(II-A-12)}$$

where ${}_2F_3$ is the generalized hypergeometric series defined by

$$ {}_pF_q\,(\alpha_1,\alpha_2,\cdots,\alpha_p;\beta_1,\beta_2,\cdots\beta_q;z) = \sum_{k=0}^{\infty} \frac{(\alpha_1)_k\,(\alpha_2)_k\cdots(\alpha_p)_k\; z^k}{(\beta_1)_k\,(\beta_2)_k\cdots(\beta_p)_k\; k!} \qquad \text{(II-A-13a)}$$

where

$$(a)_k = \frac{\Gamma(a+k)}{\Gamma(a)} \qquad \text{(II-A-13b)}$$

The numerical evaluation of S(t), can be accomplished by summing the series in (II-A-13) or numerically integrating (II-A-11). The latter was found to be more efficient. The computation of H_1 in (II-A-11) was made possible by an expansion in a series of Chebyshev polynomials given by Luke (1969). Although the integration is numerical, it does not prolong the overall computation time because S(t) is independent of the characteristic lengths in the problem and therefore can be performed once for all possible values of L and N.

CHAPTER III

A STRONG INTERACTION THEORY FOR THE AXISYMMETRIC CREEPING MOTION OF A SPHERE TOWARDS FINITE PLANAR BOUNDARIES AND ORIFICES.

III-1. Introduction.

It is well recognized that the creeping motion of a spherical particle at finite distances from a boundary or an orifice can require a very substantial correction to Stokes' law for the resistance of a sphere moving in an unbounded fluid. These corrections are particularly important when the sphere-wall spacing is of the order of five sphere diameters or less where weak interaction method of reflection theory breaks down (Ganatos, Weinbaum and Pfeffer, 1980). All previous exact solutions for bounded flows of a sphere have involved infinite planar or cylindrical surfaces (Haberman and Sayre, 1958; Brenner, 1961; Goldman, Cox and Brenner, 1967). In section III-2 of this chapter we shall consider a common discontinuous infinite planar boundary, an orifice, while in section III-3 we shall consider a discontinuous finite planar boundary, a circular disk of arbitrary size. Both problems are of intrinsic mathematical interest because of their role in the theory of mixed-boundary value problems. The problems are further complicated by the absence of a natural co-ordinate system which can be used to satisfy the no-slip boundary conditions simultaneously on the discontinuous planar boundary and on the sphere. The creeping motion of a sphere near an infinite planar boundary, on the other hand, can be treated as a special case of the spherical bipolar co-ordinate system in which the infinite plane is taken as a sphere of infinitely large radius. The use of this

co-ordinate system allowed Brenner (1961) and Goldman, Cox and Brenner (1967a,b) to obtain exact solutions for the motion of a sphere perpendicular to an infinite plane wall and parallel to it.

The method of solution used to treat the problems mentioned above is based on the general approach introduced in chapter II. In each case the flow field is divided into two simply bounded regions with the interface at the plane of the orifice or the disk. Therefore, the mathematical formulation presented in this chapter is valid only when the sphere does not penetrate this interface. Some comments on the extension of the present theory to more complex geometries are articulated in chapter V.

III-2. Motion of a sphere towards an orifice.

The motion of a sphere approaching an orifice is of interest in a variety of biological and non-biological phenomena. Some biological applications are described in chapter I and the introduction of chapter II. A non-biological application is the nuclepore filter. All existing theoretical studies of the nuclepore filter have neglected the no-slip boundary conditions on the surface of the particle and hence have omitted sphere-orifice interaction effects. Another application of interest is the operation of a ball valve at low Reynolds number.

To theoretically treat the motion of a sphere towards an orifice the method used in chapter II is utilized. The flow field is divided into two simply bounded regions: the half space containing the sphere bounded by the orifice wall, and the remaining infinite half space. This partitioning of the flow field establishes well defined regions in which the solution for the velocity distribution can be obtained in terms of the unknown velocity profile at the orifice opening. Different stream function representations are chosen for each region and are analytically matched at the orifice opening to secure continuity of the kinematic and dynamic fields. The no-slip boundary conditions on the surface of the sphere can be satisfied by making use of the collocation technique (Ganatos, Pfeffer and Weinbaum, 1978). A successful application of the collocation technique depends primarily on the feasibility of representing

the disturbances generated by the sphere and felt on the confining boundary by a suitable integral transform. The inversion of this integral transform, which can be mathematically difficult, has to be performed analytically in order to reduce computation time to acceptable limits.

The combined analytical-numerical solution procedure used in this problem is an important extension of the collocation theory first developed by Gluckman, Pfeffer and Weinbaum (1971) for unbounded axisymmetric multi-sphere Stokes flow. The technique has also been applied to axisymmetric flows with infinite cylindrical boundaries (Leichtberg, Pfeffer and Weinbaum, 1976) for the coaxial creeping motion of finite clusters of spheres in a tube, and recently extended to fully three-dimensional bounded motion (Ganatos, Weinbaum and Pfeffer, 1980a,b) for the arbitrary motion of a sphere between plane parallel boundaries. The method of solution used in the present study is the first to incorporate the collocation technique in a partitioned flow field with discontinuous planar boundaries.

In view of the linearity of the governing differential equations and the boundary conditions, the axisymmetric motion of a neutrally buoyant sphere towards an orifice can be decomposed into two separate contributions: (i) a translational motion of a sphere in quiescent fluid, (ii) flow through an orifice past a stationary sphere. This problem is presented in 5 subsections. Subsection III-2.1 contains the mathematical formulation of the

problem. In subsection III-2.2 solutions for the motion of a sphere in a quiescent fluid are presented. The case of flow through an orifice past a stationary sphere is described in subsection III-2.3. In subsection III-2.4 results for the pressure drop across the orifice are presented. Finally, in subsection III-2.5 the two cases are superposed to determine the motion of a neutrally buoyant sphere towards the orifice.

III-2.1 Mathematical formulation.

The flow field considered consists of a solid sphere of radius a' moving axially with an instantaneuos velocity V' in viscous fluid towards an orifice of radius b' in a wall of zero thickness whose distance from the sphere is d'. The origin of co-ordinates is chosen at the sphere center. Before presenting the equations of motion it is convenient to non-dimensionalize the co-ordinates (unprimed) in terms of the dimensional co-ordinates (primed) as follows (see figure III-1):

$$R = \frac{R'}{b'}, \qquad Z = \frac{Z'}{b'} \qquad \text{(III-2.1a,b)}$$

such that the dimensionless sphere radius and its distance from the orifice are respectively

$$a = \frac{a'}{b'}, \qquad d = \frac{d'}{b'} \qquad \text{(III-2.2a,b)}$$

The stream function ψ', the drag force F' and the

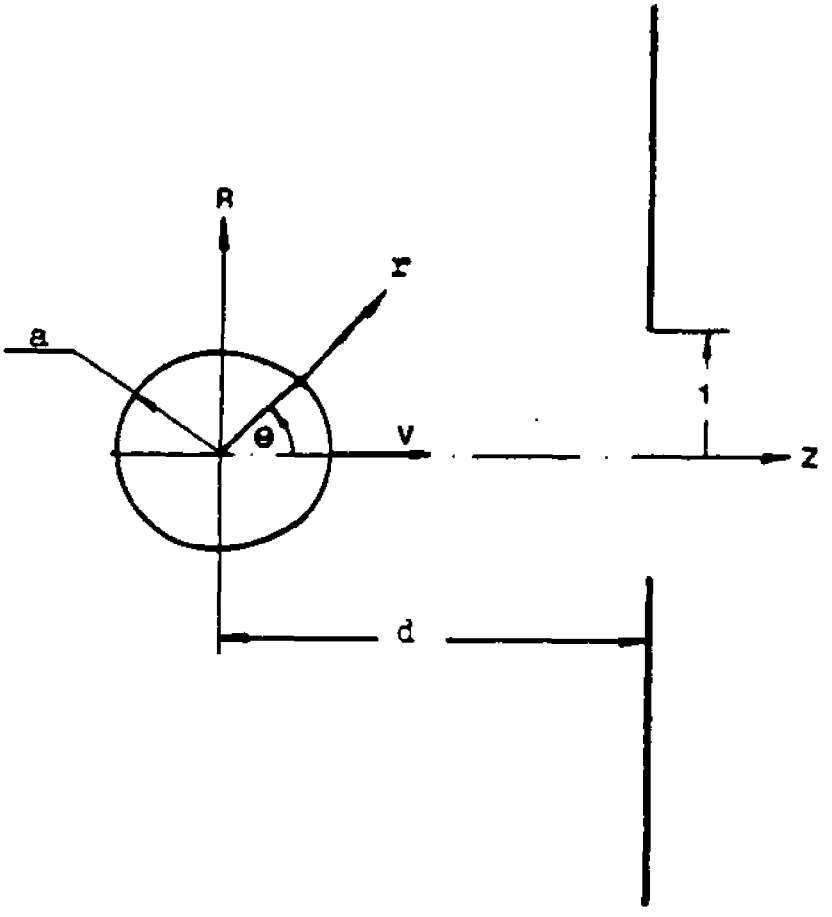

Figure III-1. Geometry for the problem of a sphere translating axisymmetrically towards an orifice.

pressure P' are expressed in dimensionless form, using the fluid density ρ, the kinematic viscosity ν and the characteristic length b' as follows:

$$\Psi = \frac{\Psi'}{b\nu} \qquad P = \frac{P' b^2}{\rho \nu^2} \qquad F = \frac{F'}{\rho \nu^2} \qquad \text{(III-2.3a,b,c)}$$

The proposed theory is valid up to the point where the sphere is tangent to the plane of the orifice. The governing equations for the fluid motion are:

$$\nabla^2 \vec{u} = \nabla P \qquad \text{(III-2.4a)}$$

$$\nabla \cdot \vec{u} = 0 \qquad \text{(III-2.4b)}$$

where ∇ is the gradient operator in dimensionless co-ordinates and $\vec{u}$ is the dimensionless fluid velocity. Due to the axisymmetric nature of the flow, the stream function can be introduced and is given in cylindrical co-ordinates by

$$u_R = -\frac{1}{R}\frac{\partial \Psi}{\partial Z} \qquad \text{(III-2.5a)}$$

$$u_Z = \frac{1}{R}\frac{\partial \Psi}{\partial R} \qquad \text{(III-2.5b)}$$

where u_R and u_Z are the radial and axial velocity components respectively. Taking the curl of (III-2.4a) using the definition of the stream function (III-2.5), one obtains the the fourth order equation:

$$D^2(D^2\Psi) = 0 \qquad \text{(III-2.6)}$$

where D^2 is the generalized axisymmetric Stokesian operator given by

$$D^2 = \frac{\partial^2}{\partial R^2} - \frac{1}{R}\frac{\partial}{\partial R} + \frac{\partial^2}{\partial Z^2} \qquad \text{(III-2.7)}$$

As discussed in subsection III-2.1, the flow field is partitioned into two regions, the half space containing the sphere $Z \leq d$ and the infinite half space $Z \geq d$. The essential mathematical problem is to kinematically and dynamically match the solution in each region at the orifice opening.

The stream function for the region $Z \leq d$ is linearly composed of two parts

$$\Psi^I = \Psi_w + \Psi_s \qquad \text{(III-2.8)}$$

Here Ψ_w is a solution of (III-2.6) in cylindrical coordinates that represents the disturbances generated by the orifice and the wall approaching the plane Z=d from the left which yields finite velocities everywhere for $Z \leq d$. Ψ_w is given by the Fourier-Bessel integral

$$\Psi_w = \int_0^\infty R J_1(\omega R)\left[A_1(\omega) + Z B_1(\omega)\right] e^{\omega Z} d\omega, \quad (Z \leq d) \qquad \text{(III-2.9)}$$

where $A_1(\omega)$ and $B_1(\omega)$ are unknown functions of ω and J_1 is the ordinary Bessel function of the first kind of order one.

The second part of Ψ^I, denoted by Ψ_s, is an

infinite series representing the disturbance generated by the sphere. Ψ_s is given by all the simply separable solutions of (III-2.6) in spherical co-ordinates which yield finite velocity everywhere. This series is given in Sampson (1891) as

$$\Psi_s = \sum_{n=2}^{\infty} \left(B_n r^{-n+1} + D_n r^{-n+3} \right) I_n(\xi), \quad (z \geq d) \quad \text{(III-2.10)}$$

Here r and Θ are the spherical co-ordinates shown in figure III-1, $\xi = \cos\Theta$ and I_n is the Gegenbauer function of the first kind of order n and degree -1/2. B_n and D_n are unknown constant coefficients to be determined by satisfying the no-slip boundary conditions on the sphere.

For the infinite half space $Z \geq d$, it is sufficient to represent all disturbances generated at the plane Z=d by a Fourier-Bessel integral of the form given by (III-2.9) which yields finite velocity as Z approaches infinity.

$$\Psi^{II} = \int_0^{\infty} R J_1(\omega R) \left[A_2(\omega) + z B_2(\omega) \right] e^{-\omega z} d\omega, \quad (z \geq d) \quad \text{(III-2.11)}$$

Here $A_2(\omega)$ and $B_2(\omega)$ are unknown functions of ω .

To help the reader follow the mathematical development, a brief conceptual summary of the solution procedure to determine the unknown functions and coefficients is given. In each region the no-slip boundary conditions are first satisfied along the orifice wall. This permits the unknown functions $A_1(\omega)$ and $B_1(\omega)$ to be determined in terms

of the spherical coefficients B_n and D_n and the unknown velocity at the orifice opening. Similarly, $A_2(\omega)$ and $B_2(\omega)$ can be determined in terms of the unknown velocity at the orifice. Then, by matching the stress tensor at the opening of the orifice, the unknown orifice velocity can be obtained in terms of the spherical coefficients. This matching assures that the disturbances produced by the sphere for all values of B_n and D_n are cancelled along the boundary Z=d approaching the orifice wall from both left and right. Finally, the cancellation of the disturbances generated by the orifice wall, on the surface of the sphere will be accomplished by applying the collocation method. The solution of the collocation matrix provides numerical values for the coefficients B_n and D_n.

In order to apply the no-slip boundary conditions along the wall at the plane of the orifice it is necessary to write the spherical disturbance equation (III-2.8) in cylindrical co-ordinates. Therefore, the spherical co-ordinate system (r,θ) has to be related to the cylindrical co-ordinate system (R,Z). From figure III-1, the co-ordinate transformation is given by

$$r = (R^2+Z^2)^{1/2}, \quad \theta = \cos^{-1}\left[Z\,(R^2+Z^2)^{-1/2}\right] \qquad \text{(III-2.12a,b)}$$

Differentiation of (III-2.8) according to (III-2.5), utilizing the properties of the Gegenbauer and Legendre polynomials and the chain rule, yields the ex-

pressions for the radial and axial velocity components for the half space Z ≤ d

$$u_R^I = -\frac{1}{R}\frac{\partial \varphi^I}{\partial z} = -\int_0^\infty k_1'(\omega,z)\,\omega J_1(\omega R)\,d\omega + \sum_{n=2}^{\infty}\left[B_n B_n'(R,z) + D_n D_n'(R,z)\right] \qquad \text{(III-2.13a)}$$

$$u_z^I = \frac{1}{R}\frac{\partial \varphi^I}{\partial R} = \int_0^\infty k_1''(\omega,z)\,\omega J_0(\omega R)\,d\omega + \sum_{n=2}^{\infty}\left[B_n B_n''(R,z) + D_n D_n''(R,z)\right] \qquad \text{(III-2.13b)}$$

where

$$k_1'(\omega,z) = \left[A_1(\omega) + B_1(\omega)\left(\frac{1}{\omega} + z\right)\right] e^{\omega z} \qquad \text{(III-2.14a)}$$

$$B_n'(R,z) = \frac{n+1}{(R^2+z^2)^{\frac{n}{2}}}\,\frac{1}{R}\,I_n\left(\frac{z}{\sqrt{R^2+z^2}}\right) \qquad \text{(III-2.14b)}$$

$$D_n'(R,z) = \frac{n+1}{(R^2+z^2)^{\frac{n-2}{2}}}\,\frac{1}{R}\,I_{n+1}\left(\frac{z}{\sqrt{R^2+z^2}}\right) - \frac{2}{(R^2+z^2)^{\frac{n-1}{2}}}\,\frac{z}{R}\,I_n\left(\frac{z}{\sqrt{R^2+z^2}}\right) \qquad \text{(III-2.14c)}$$

$$k_1''(\omega,z) = \left[A_1(\omega) + z\,B_1(\omega)\right] e^{\omega z} \qquad \text{(III-2.14d)}$$

$$B_n''(R,z) = \frac{1}{(R^2+z^2)^{\frac{n+1}{2}}}\,P_n\left(\frac{z}{\sqrt{R^2+z^2}}\right) \qquad \text{(III-2.14e)}$$

$$D_n''(R,z) = \frac{2}{(R^2+z^2)^{\frac{n-1}{2}}}\,I_n\left(\frac{z}{\sqrt{R^2+z^2}}\right) + \frac{1}{(R^2+z^2)^{\frac{n-1}{2}}}\,P_n\left(\frac{z}{\sqrt{R^2+z^2}}\right) \qquad \text{(III-2.14f)}$$

and P_n are Legendre polynomials of order n. Similarly, for

the region $Z \gg d$, the velocity components are obtained by differentiation of (III-2.11) and are given by

$$u_R^{II} = -\frac{1}{R}\frac{\partial \psi^{II}}{\partial z} = -\int_0^\infty k_2'(\omega, z)\, \omega\, J_1(\omega R)\, d\omega \,, \quad (z \gg d) \qquad \text{(III-2.15a)}$$

$$u_z^{II} = \frac{1}{R}\frac{\partial \psi^{II}}{\partial R} = \int_0^\infty k_2''(\omega, z)\, \omega\, J_0(\omega R)\, d\omega \,, \quad (z \gg d) \qquad \text{(III-2.15b)}$$

where

$$k_2'(\omega, z) = -\left[A_2(\omega) - B_2(\omega)\left(\frac{1}{\omega} - z\right)\right] e^{-\omega z} \qquad \text{(III-2.16a)}$$

$$k_2''(\omega, z) = \left[A_2(\omega) + z B_2(\omega)\right] e^{-\omega z} \qquad \text{(III-2.16b)}$$

The no-slip boundary conditions along the wall of the orifice can now be applied provided the velocity at the orifice is prescribed. This velocity can be defined as follows

$$\vec{u}(R, d) = \frac{1}{R}\left[f(R)\hat{z} - g(R)\hat{r}\right] \qquad 0 \le R \le 1 \qquad \text{(III-2.17)}$$

where $f(R)/R$ and $-g(R)/R$ are the unknown radial and axial velocity components at the opening, respectively. From the definition (III-2.17) the no-slip boundary conditions on the orifice wall are

$$u_z(R, d) = F(R) = \begin{cases} 0 & R > 1 \\ \dfrac{f(R)}{R} & 0 \le R < 1 \end{cases} \qquad \text{(III-2.18a)}$$

$$u_R(R, d) = G(R) = \begin{cases} 0 & R > 1 \\ -\dfrac{g(R)}{R} & 0 \le R \le 1 \end{cases} \qquad \text{(III-2.18b)}$$

In addition, the shear stress has to be matched along the interface between the two regions; this dynamic boundary condition is

$$\tau_{ij}^{I}(R,d) = \tau_{ij}^{II}(R,d) \qquad 0 \le R \le 1 \qquad \text{(III-2.19)}$$

where τ_{ij} is the stress tensor.

Following the solution summary given previously, one needs to determine the Fourier coefficients $A_i(\omega)$, $B_i(\omega)$ i=1,2. Application of the kinematic boundary conditions (III-2.18) along the wall in the half space containing the sphere results in:

$$\int_0^\infty k_1'(\omega,d)\,\omega J_1(\omega R)\,d\omega = \sum_{n=2}^{\infty}\left[B_n B_n'(R,d) + D_n D_n'(R,d)\right] - G(R) \qquad \text{(III-2.20a)}$$

$$\int_0^\infty k_1''(\omega,d)\,\omega J_0(\omega R)\,d\omega = -\sum_{n=2}^{\infty}\left[B_n B_n''(R,d) + D_n D_n''(R,d)\right] + F(R) \qquad \text{(III-2.20b)}$$

The right hand side in (III-2.20) represents the disturbance generated by the sphere and the orifice opening which must be cancelled on the orifice wall. The unknown functions $K_1'(\omega,d)$ and $K_1''(\omega,d)$ in (III-2.20) are simply Hankel transforms of these disturbances. Inversion of these equations gives

$$K_1'(\omega,d) = \int_0^\infty \sum_{n=2}^{\infty}\left[B_n B_n'(t,d) + D_n D_n'(t,d)\right] t\,J_1(\omega t)\,dt + \int_0^\infty g(t)\,J_1(\omega t)\,dt \qquad \text{(III-2.21a)}$$

$$K_1''(\omega,d) = -\int_0^\infty \sum_{n=2}^{\infty} [B_n B_n''(t,d) + D_n D_n''(t,d)]\, t J_0(\omega t)\, dt$$

$$+ \int_0^1 f(t) J_0(\omega t)\, dt \qquad \text{(III-2.21b)}$$

The integrals in (III-2.21) can be performed analytically by making use of the result given by Erdelyi (1954, vol. 2, p.45)

$$\int_0^\infty \frac{x}{(a^2+x^2)^{\mu/2}} P_{\mu-1}^{\nu}\left(\frac{a}{\sqrt{a^2+x^2}}\right) J_\nu(xy)\, dx = \frac{y^{\mu-2} e^{-ay}}{\Gamma(\mu+\nu)} \qquad \text{(III-2.22)}$$

$$(\mathrm{Re}\,\nu > -1,\ \mathrm{Re}\,\mu > 1/2)$$

the Legendre polynomial representation of the Gegenbauer function given by

$$I_n(x) = \frac{P_{n-2}(x) - P_n(x)}{2n-1} \qquad \text{(III-2.23)}$$

and the recurrence relation for Legendre polynomials. Thus, one can show that

$$\int_0^\infty \frac{1}{(t^2+d^2)^{\frac{n}{2}}} I_{n+1}\left(\frac{d}{\sqrt{t^2+d^2}}\right) J_1(\omega t)\, dt = \frac{\omega^{n-1}}{(n+1)!} e^{-\omega d} \qquad \text{(III-2.24a)}$$

$$\int_0^\infty \frac{1}{(t^2+d^2)^{\frac{n-2}{2}}} I_{n+1}\left(\frac{d}{\sqrt{t^2+d^2}}\right) J_1(\omega t)\, dt = \frac{\omega^{n-3}}{(n+1)!} [(2n-1)\omega d - n(n-2)] e^{-\omega d} \qquad \text{(III-2.24b)}$$

$$\int_0^\infty \frac{t}{(t^2+d^2)^{\frac{n+1}{2}}} P_n\left(\frac{d}{\sqrt{t^2+d^2}}\right) J_0(\omega t)\, dt = \frac{\omega^{n-1}}{(n)!} e^{-\omega d} \qquad \text{(III-2.24c)}$$

$$\int_0^\infty \frac{t}{(t^2+d^2)^{\frac{n-1}{2}}} P_n\left(\frac{d}{\sqrt{t^2+d^2}}\right) J_0(\omega t)\, dt$$

$$= \frac{\omega^{n-3}}{(n)!}\left[(2n-1)\omega d - (n-1)^2\right] e^{-\omega d} \qquad \text{(III-2.24d)}$$

$$\int_0^\infty \frac{t}{(t^2+d^2)^{\frac{n-1}{2}}} I_n\left(\frac{d}{\sqrt{t^2+d^2}}\right) J_0(\omega t)\, dt$$

$$= \frac{\omega^{n-3}}{(n)!}\left[(n-1) - \omega d\right] e^{-\omega d} \qquad \text{(III-2.24e)}$$

Utilizing these results in equation (III-2.21) gives

$$K_1'(\omega,d) = \sum_{n=2}^{\infty}\left[B_n B_n^*(\omega,d) + D_n D_n^*(\omega,d)\right] + \int_0^{'} g(t) J_1(\omega t)\, dt \qquad \text{(III-2.25a)}$$

$$K_1''(\omega,d) = \sum_{n=2}^{\infty}\left[B_n B_n^{**}(\omega,d) + D_n D_n^{**}(\omega,d)\right] + \int_0^{'} f(t) J_0(\omega t)\, dt \qquad \text{(III-2.25b)}$$

where

$$B_n^*(\omega,d) = \int_0^\infty B_n'(t,d)\, t J_1(\omega t)\, dt = \frac{\omega^{n-1}}{n!} e^{-\omega d} \qquad \text{(III-2.26a)}$$

$$D_n^*(\omega,d) = \int_0^\infty D_n'(t,d)\, t J_1(\omega t)\, dt = \frac{\omega^{n-3}}{n!}\left[(2n-3)\omega d - (n-2)n\right] e^{-\omega d} \qquad \text{(III-2.26b)}$$

$$B_n^{**}(\omega,d) = \int_0^\infty B_n''(t,d)\, t J_0(\omega t)\, dt = \frac{\omega^{n-1}}{n!} e^{-\omega d} \qquad \text{(III-2.26c)}$$

$$D_n^{**}(\omega,d) = \int_0^\infty D_n''(t,d)\, t J_0(\omega t)\, dt = \frac{\omega^{n-3}}{n!}\left[(2n-3)\omega d - (n-1)(n-3)\right] e^{-\omega d} \qquad \text{(III-2.26d)}$$

The functions K_1' and K_1'' in equations (III-2.25), evaluated at Z=d, are expressed in terms of the unknown coefficients B_n and D_n in the spherical solution, and the unknown velocity components f and g at the opening. To obtain the expression for the velocity field, the Fourier functions $A_1(\omega)$ and $B_1(\omega)$ in the expression for K_1' and K_1'' must be determined. This is accomplished by evaluating (III-2.14a) and (III-2.14d) at Z=d and equating with (III-2.25). The resulting equations are then solved for $A_1(\omega)$ and $B_1(\omega)$ (see appendix), which are substituted back into (III-2.14) yielding

$$K_1'(\omega,\bar{z}) = -\left\{[\omega(d-\bar{z})-1]\int_0^1 g(t)J_1(\omega t)dt - \omega(d-\bar{z})\int_0^1 f(t)J_0(\omega t)dt\right\}e^{-\omega(d-\bar{z})}$$
$$+\sum_{n=2}^{\infty} B_n\left\{[1-\omega(d-\bar{z})]B_n^*(\omega,d) - \omega(d-\bar{z})B_n^{**}(\omega,d)\right\}e^{-\omega(d-\bar{z})}$$
$$+\sum_{n=2}^{\infty} D_n\left\{[1-\omega(d-\bar{z})]D_n^*(\omega,d) - \omega(d-\bar{z})D_n^{**}(\omega,d)\right\}e^{-\omega(d-\bar{z})} \qquad \text{(III-2.27a)}$$

$$K_1''(\omega,\bar{z}) = \left\{[1+\omega(d-\bar{z})]\int_0^1 f(t)J_0(\omega t)dt - \omega(d-\bar{z})\int_0^1 g(t)J_1(\omega t)dt\right\}e^{-\omega(d-\bar{z})}$$
$$+\sum_{n=2}^{\infty} B_n\left\{-\omega(d-\bar{z})B_n^*(\omega,d) - [1+\omega(d-\bar{z})]B_n^{**}(\omega,d)\right\}e^{-\omega(d-\bar{z})}$$
$$+\sum_{n=2}^{\infty} D_n\left\{-\omega(d-\bar{z})D_n^*(\omega,d) - [1+\omega(d-\bar{z})]D_n^{**}(\omega,d)\right\}e^{-\omega(d-\bar{z})} \qquad \text{(III-2.27b)}$$

Substituting (III-2.27) into (III-2.13) and integrating the series provides the expressions for the radial and axial velocity components

$$u_R^I = \int_0^\infty \Big\{ [\omega(d-z)-1] \int_0^1 g(t) J_1(\omega t)\, dt$$

$$- \omega(d-z) \int_0^1 f(t) J_0(\omega t)\, dt \Big\} \omega J_1(\omega R)\, e^{-\omega(d-z)}\, d\omega$$

$$+ \sum_{n=2}^{\infty} [B_n \beta_n'(R,z) + D_n \delta_n'(R,z)] \qquad \text{(III-2.28a)}$$

$$u_z^I = \int_0^\infty \Big\{ [1+\omega(d-z)] \int_0^1 f(t) J_0(\omega t)\, dt$$

$$- \omega(d-z) \int_0^1 g(t) J_1(\omega t)\, dt \Big\} \omega J_0(\omega R)\, e^{-\omega(d-z)}\, d\omega$$

$$+ \sum_{n=2}^{\infty} [B_n \beta_n''(R,z) + D_n \delta_n''(R,z)] \qquad \text{(III-2.28b)}$$

where

$$\beta_n'(R,z) = B_n'(R,z) - B_n'(R,2d-z)$$

$$+ 2(d-z)(n+1) B_{n+1}'(R,2d-z) \qquad \text{(III-2.29a)}$$

$$\delta_n'(R,z) = D_n'(R,z) - D_n'(R,2d-z) - \frac{2}{n}(n-1)(n-3)(d-z) B_{n-1}'(R,2d-z)$$

$$+ 2(2n-3)d(d-z) B_n'(R,2d-z) \qquad \text{(III-2.29b)}$$

$$\beta_n''(R,z) = B_n''(R,z) - B_n''(R,2d-z)$$

$$- 2(d-z)(n+1) B_{n+1}''(R,2d-z) \qquad \text{(III-2.29c)}$$

$$\delta_n''(R,z) = D_n''(R,z) - D_n''(R,2d-z) + 2(n-2)(d-z) B_{n-1}''(R,2d-z)$$

$$- 2(2n-3)d(d-z) B_n''(R,2d-z) \qquad \text{(III-2.29d)}$$

Although the velocities in (III-2.28) are still expressed in terms of the unknown spherical coefficients B_n and D_n, and the two unknown functions f and g, they do vanish on the wall of the orifice and can properly represent any arbitrary disturbance at the opening.

Following a similar procedure, the no-slip boundary conditions (III-2.18) can be satisfied in the infinite half space $Z \geq d$ and the Fourier coefficients $A_2(\omega)$ and $B_2(\omega)$ expressed in terms of the unknown functions f and g for the velocity at the orifice plane. These expressions are given in equations (III-A-3,4) in the appendix. Substituting these results in equations (III-2.16a,b), one obtains

$$\omega^{-1} K_2'(\omega, z) = \left\{ -(z-d) \int_0^1 f(t) J_0(\omega t)\, dt + \frac{1}{\omega}\left[1-\omega(z-d)\right] \int_0^1 g(t) J_1(\omega t)\, dt \right\} e^{-\omega(z-d)} \qquad \text{(III-2.30a)}$$

$$\omega^{-1} K_2''(\omega, z) = \left\{ \frac{1}{\omega}\left[1+\omega(z-d)\right] \int_0^1 f(t) J_0(\omega t)\, dt + (z-d) \int_0^1 g(t) J_1(\omega t)\, dt \right\} e^{-\omega(z-d)} \qquad \text{(III-2.30b)}$$

Equations (III-2.30) together with (III-2.15) provide the solution for the velocity field in the region $Z \geq d$, in terms of the yet unknown velocity at the orifice opening.

The solution obtained for each region, is capable of cancelling all disturbances on the confining wall.

Furthermore, the two solutions are matched kinematically at the opening since they satisfy the same velocity conditions at Z=d. However, the solutions have been obtained without accounting for the compatibility of the shear stress and the pressure field across the plane of the opening. A unique solution for f and g can, therefore, be obtained by matching the stress tensor at the interface between the two regions. As shown in chapter II, the dynamic condition of matching the shear stress (III-2.19) can be replaced by matching the pressure and its gradient at Z=d. Namely

$$P^{I}(R,d) = P^{II}(R,d) \qquad \text{(III-2.31a)}$$

$$\frac{\partial P^{I}}{\partial Z}(R,d) = \frac{\partial P^{II}}{\partial Z}(R,d) \qquad \text{(III-2.31b)}$$

The general expression for the pressure field in each region can be determined by integrating the creeping motion equations (III-2.4) with the appropriate stream function representation. For the half space containing the sphere the resulting equation is

$$P^{I}(R,Z) = 2\int_{0}^{\infty} \omega J_0(\omega R)\, B_1(\omega)\, e^{\omega Z}\, d\omega + 2\sum_{n=2}^{\infty} D_n \frac{2n-3}{n} r^{-n} P_{n-1}(\xi) + P_{-\infty} \qquad \text{(III-2.32)}$$

and for the infinite half space $Z \geq d$:

$$P^{II}(R,Z) = 2\int_0^\infty \omega J_0(\omega R)\, B_2(\omega)\, e^{-\omega Z} d\omega + P_\infty \qquad \text{(III-2.33)}$$

where $P_{-\infty}$ and P_∞ are the uniform pressures prescribed at $Z \to -\infty$ and $Z \to \infty$ respectively.

Introducing $B_1(\omega)$ and $B_2(\omega)$ (given in the appendix) into equations (III-2.32) and (III-2.33), the pressure matching conditions (III-2.31a,b) yield the relations

$$\int_0^\infty \omega^2 J_0(\omega R)\left[\int_0^1 f(t) J_0(\omega t)\, dt\right] d\omega = F^*(R) \qquad 0 \le R \le 1 \qquad \text{(III-2.34a)}$$

$$\int_0^\infty \omega^3 J_0(\omega R)\left[\int_0^1 g(t) J_1(\omega t)\, dt\right] d\omega = G^*(R) \qquad 0 \le R \le 1 \qquad \text{(III-2.34b)}$$

where

$$F^*(R) = \frac{1}{2}\int_0^\infty \left\{ \sum_{n=2}^\infty B_n \left[B_n^*(\omega,d) + B_n^{**}(\omega,d)\right] + D_n\left[D_n^*(\omega,d) + D_n^{**}(\omega,d)\right]\right\} \omega^2 J_0(\omega R)\, d\omega + \frac{1}{2}\sum_{n=2}^\infty D_n \frac{2n-3}{n} B_{n-1}''(R,d) + \frac{\Delta P}{4} \qquad \text{(III-2.35a)}$$

$$G^*(R) = -\frac{1}{2}\int_0^\infty \left\{ \sum_{n=2}^\infty B_n \left[B_n^*(\omega,d) + B_n^{**}(\omega,d)\right] + D_n\left[D_n^*(\omega,d) + D_n^{**}(\omega,d)\right]\right\} \omega^3 J_0(\omega R)\, d\omega + \frac{1}{2}\sum_{n=2}^\infty D_n (2n-3) B_n''(R,d) \qquad \text{(III-2.35b)}$$

and ΔP is the pressure drop across the orifice defined by

$$\Delta P = P_{-\infty} - P_{\infty} \geq 0 \qquad \text{(III-2.36)}$$

The integral equations (III-2.34) can be solved for the f and g functions as follows. Defining the new functions

$$f^*(\omega) = \omega \int_0^1 f(t) J_0(\omega t)\, dt \qquad \text{(III-2.37a)}$$

$$g^*(\omega) = \omega^2 \int_0^1 g(t) J_1(\omega t)\, dt \qquad \text{(III-2.37b)}$$

and realizing that

$$\int_0^\infty \begin{Bmatrix} f^*(\omega) \\ g^*(\omega) \end{Bmatrix} J_0(\omega R)\, d\omega = 0 \qquad \text{for } R > 1 \quad \text{(III-2.38a,b)}$$

one obtains two sets of dual integral equations. With the definition (III-2.37), equations (III-2.34a) and (III-2.38a) comprise the set for $f^*(\omega)$, while (III-2.34b) and (III-2.38b) define the second set for $g^*(\omega)$.

The solution for a dual integral equation of this form is given by Tranter (1951)

$$\begin{Bmatrix} f^*(\omega) \\ g^*(\omega) \end{Bmatrix} = \frac{2}{\pi} \int_0^1 dt \sin \omega t \int_0^t ds \, \frac{s}{\sqrt{t^2 - s^2}} \begin{Bmatrix} F^*(s) \\ G^*(s) \end{Bmatrix} \qquad \text{(III-2.39)}$$

The functions F* and G* are substituted from (III-2.35) into (III-2.39), where B_n'' is replaced by its integral transform given in (III-2.26). The resulting right hand side of (III-2.39) consists of triple integral expressions of which two integrals can be performed analytically. The middle integral is evaluated first using the result (Erdelyi, 1954, vol.2, p. 7)

$$\int_0^t \frac{s}{\sqrt{t^2-s^2}} J_0(\xi s)\,ds = \frac{1}{\xi}\sin t\xi \qquad \text{(III-2.40)}$$

Then, the improper inner integral is determined using the basic relations (Erdelyi, 1954, vol. 1, p. 152)

$$\int_0^\infty \sin\xi t\; \xi^{n-1} e^{-\xi d}\,d\xi = \frac{\Gamma(n)}{(d^2+t^2)^{n/2}} \sin\left[n\tan^{-1}\frac{t}{d}\right] \qquad \text{(III-2.41)}$$

$$\text{Re } n > -1,\quad \text{Re } d > |\text{Im } t|$$

The resulting expressions for f* and g* are

$$f^*(\omega) = \frac{\Delta P}{2\pi\omega}\left(\frac{\sin\omega}{\omega} - \cos\omega\right) + \sum_{n=2}^{\infty}\left\{B_n F_{n+1}(\omega,d) + D_n\left[\frac{2n-3}{n}F_n(\omega,d) - \frac{n-3}{n}F_{n-1}(\omega,d)\right]\right\} \qquad \text{(III-2.42a)}$$

$$g^*(\omega) = -\sum_{n=2}^{\infty}\left\{B_n(n+1)F_{n+2}(\omega,d) + D_n\left[(2n-3)d\,F_{n+1}(\omega,d) - (n-2)F_n(\omega,d)\right]\right\} \qquad \text{(III-2.42b)}$$

where $F_n(\omega,d)$ is the remaining outer integral given by

$$F_n(\omega,d) = \frac{2}{\pi}\int_0^1 \sin\omega t \; \frac{\sin\left(n\tan^{-1}\frac{t}{d}\right)}{(t^2+d^2)^{n/2}}\, dt \qquad \text{(III-2.43)}$$

Equations (III-2.42) and (III-2.43) provide the solutions for f* and g* in terms of the unknown spherical coefficients B_n and D_n. Utilizing these results and the definition of f* and g* given by (III-2.37), one can determine the functions f and g using Hankel inversion formulae. One can also substitute the f* and g* functions directly into (III-2.28) to obtain the expression for the velocity field in the region $Z \leq d$ in terms of the unknown spherical coefficients. After considerable algebraic manipulation this result is:

$$u_R^I = \sum_{n=2}^{\infty} \left\{ B_n \left[\beta_n'(R,Z) + \frac{2}{\pi}\int_0^1 \beta_n^*(R,Z,t)\,dt\right] + D_n \left[\delta_n'(R,Z) + \frac{2}{\pi}\int_0^1 \delta_n^*(R,Z,t)\,dt\right]\right\} - \frac{\Delta P}{2\pi}(Z-d)\,H'(R,X) \qquad \text{(III-2.45a)}$$

$$u_Z^I = \sum_{n=2}^{\infty} \left\{ B_n \left[\beta_n''(R,Z) + \frac{2}{\pi}\int_0^1 \beta_n^{**}(R,Z,t)\,dt\right] + D_n \left[\delta_n''(R,Z) + \frac{2}{\pi}\int_0^1 \delta_n^{**}(R,Z,t)\,dt\right]\right\} + \frac{\Delta P}{2\pi}H''(R,X) \qquad \text{(III-2.45b)}$$

where

$$X = Z-d \qquad \text{(III-2.46a)}$$

$$\beta_n^*(R,Z,t) = (n+1)\,S_{n+2}(t,d)\,[K_1^{-1}(R,X,t) - X K_1^0(R,X,t)]$$

$$- X S_{n+1}(t,d)\,K_1^1(R,X,t) \qquad \text{(III-2.46b)}$$

$$\delta_n^*(R,Z,t) = K_1^{-1}(R,X,t)\,[(2n-3)d\,S_{n+1}(t,d) - (n-2)S_n(t,d)]$$

$$+ K_1^0(R,X,t)\,[X(n-2)S_n(t,d) - X(2n-3)d\,S_{n+1}(t,d)]$$

$$+ \frac{X}{n} K_1^1(R,X,t)\,[(n-3)S_{n-1}(t,d) - (2n-3)d\,S_n(t,d)] \qquad \text{(III-2.46c)}$$

$$H^1(R,X) = \int_0^\infty \left(\frac{\sin\omega}{\omega} - \cos\omega\right) J_1(\omega R)\,e^{-\omega X}\,d\omega \qquad \text{(III-2.46d)}$$

$$\beta_n^{**}(R,Z,t) = S_{n+1}(t,d)\,[K_0^0(R,X,t) + X K_0^1(R,X,t)]$$

$$+ X(n+1)S_{n+2}(t,d)\,K_0^0(R,X,t) \qquad \text{(III-2.46e)}$$

$$\delta_n^{**}(R,Z,t) = [K_0^0(R,X,t) + X K_0^1(R,X,t)]\left[\frac{2n-3}{n} d\,S_n(t,d) - \frac{n-3}{n} S_{n-1}(t,d)\right]$$

$$+ K_0^0(R,X,t)\,X\,[(2n-3)d\,S_{n+1}(t,d) - (n-2)S_n(t,d)] \qquad \text{(III-2.46f)}$$

$$H^{11}(R,X) = \int_0^\infty \left(\frac{1}{\omega} + X\right)\left(\frac{\sin\omega}{\omega} - \cos\omega\right) J_0(\omega R)\,e^{-\omega X}\,d\omega \qquad \text{(III-2.45g)}$$

and

$$S_n(t,d) = (d^2+t^2)^{-\frac{n}{2}} \sin\left(n \tan^{-1}\frac{t}{d}\right) \qquad \text{(III-2.47a)}$$

$$K_\nu^\mu(R,X,t) = \int_0^\infty \omega^\mu J_\nu(\omega R)\,e^{-\omega X} \sin\omega t\,d\omega \qquad \text{(III-2.47b)}$$

The integrals K_ν^μ in (III-2.46) can be evaluated analytically by making use of the basic result (Erdelyi, 1954, vol. 1, p.101)

$$K_1^{-1}(R,x,t) = \frac{t}{R}(1-h) \qquad \text{(III-2.48a)}$$

where h is a positive root of the algebraic equation

$$t^2 = \frac{R^2}{1-h^2} - \frac{x^2}{h^2} \qquad \text{(III-2.48b)}$$

Hence, it can be easily shown that

$$K_1^0(R,x,t) = \frac{x(t^2-h^2)}{Rh\sigma} \qquad \text{(III-2.48c)}$$

$$K_1^1(R,x,t) = \frac{t^2-h^2}{Rh\sigma}\left[\frac{x^2}{\sigma}(t^2-h^2)\left(\frac{4}{\sigma}+\frac{1}{h^2}\right)+\frac{4x^2}{\sigma}-1\right] \qquad \text{(III-2.48d)}$$

$$K_0^0(R,x,t) = \frac{h}{\sigma} \qquad \text{(III-2.48e)}$$

$$K_0^1(R,x,t) = \frac{x}{\sigma^2}\left[\frac{4h}{\sigma}(t^2-h^2)-(t^2-3h^2)\right] \qquad \text{(III-2.48f)}$$

where

$$\sigma = \left[(t^2-R^2-x^2)^2+4x^2t^2\right]^{1/2} \qquad \text{(III-2.49)}$$

and

$$H^1(R,x) = \frac{h_1(1-h_1^2)}{R\sigma_1} \qquad \text{(III-2.50a)}$$

$$H^{11}(R,x) = \int_0^1 \frac{t}{\sigma}\left[h-\frac{x^2(t^2-3h^2)}{h\sigma}+\frac{4hx^2(t^2-h^2)}{\sigma^2}\right]dt \qquad \text{(III-2.50b)}$$

where h_1 and σ_1 are defined by (III-2.48b) and (III-2.49) with t=1.

The solution for the velocity field (III-2.45) both satisfies the no-slip boundary conditions on the orifice wall and provides an exact solution for the velocity at the orifice opening. This solution still incorporates the unknown spherical coefficients B_n and D_n which must be determined from the remaining no-slip boundary conditions on the surface of the sphere. The definite integrals in (III-2.45) must be performed numerically and special consideration given to the limit as t approaches zero. For t=0, the functions K^{μ}_{ν} given in (III-2.48) and (III-2.49), and the integral in (III-2.50b) should be determined by L'Hospital's rule or from their Taylor series approximation for small values of t.

On the surface of the sphere, the solution must satisfy the following no-slip boundary conditions

$$u_R^I = 0, \quad u_z^I = V \qquad \text{(III-2.51a,b)}$$

where V is the translatory sphere velocity shown in figure III-1. Application of these boundary conditions on the surface of the sphere, r=a, is accomplished by utilizing the collocation technique.

To satisfy the boundary conditions (III-2.51) exactly on the surface r=a would require the solution of the entire infinite array of the unknown coefficients B_n

and D_n. Instead, the collocation technique satisfies the boundary conditions at a finite number of discrete points on the sphere's generating arc and truncates the infinite series into a finite one. The two sets of unknown coefficients in each term of the series in (III-2.45) permit one to satisfy the exact no-slip boundary conditions at one discrete point on the sphere surface. Thus, if the spherical boundary is approximated by satisfying conditions (III-2.51) at M discrete points on its generating arc, the infinite series in (III-2.45) is truncated after M terms resulting in a set of 2M simultaneous linear algebraic equations which can be solved for the 2M B_n and D_n unknown coefficients by any standard matrix reduction technique. The accuracy of the truncation technique can be improved by increasing the order of truncation M. Clearly, as $M\to\infty$ the truncation error vanishes and the overall accuracy of the solution depends only on the accuracy of the numerical integration required in evaluating the matrix elements.

The force exerted by the fluid on the sphere is shown in Happel and Brenner (1965, p. 115) to be

$$F = \pi \int_0^{\pi} r^2 \sin^3\theta \frac{\partial}{\partial r}\left[\frac{D^2\Psi}{r^2\sin^2\theta}\right] r\,d\theta \qquad \text{(III-2.52)}$$

Application of this operator and the orthogonality properties of the Gegenbauer function to (III-2.8)-(III-2.10) results in the simple relation

$$F = 4\pi D_2 \qquad \text{(III-2.53)}$$

The drag force can be expressed in terms of two drag correction factors $\lambda^{(V)}$ and $\lambda^{(U_o)}$. $\lambda^{(V)}$ describes the case of a sphere translating with velocity V towards the orifice along its centerline in a quiescent fluid ($\Delta P=0$), and $\lambda^{(U_o)}$ describes the flow through an orifice past a stationary sphere (V=0)

For a sphere moving with velocity V, the drag force can be written as

$$F = 4\pi D_2^{(V)} = 6\pi a V \lambda^{(V)} \qquad \text{(III-2.54a)}$$

and hence

$$\lambda^{(V)} = \frac{D_2^{(V)}}{1.5 a V} \qquad \text{(III-2.54b)}$$

Here $\lambda^{(V)}$ represents the ratio of the drag force acting on the sphere in the presence of the confining boundary to the force exhibited under the same conditions in unbounded fluid.

In the case of flow past a stationary sphere, the drag force is given by

$$F = 4\pi D_2^{(U_o)} = 6\pi a U_o \lambda^{(U_o)} \qquad \text{(III-2.55a)}$$

and hence

$$\lambda^{(U_o)} = \frac{D_2^{(U_o)}}{1.5 a U_o} \qquad \text{(III-2.55b)}$$

where U_o is the centerline fluid velocity in the plane of

the orifice in the absence of the sphere and $\lambda^{(U_0)}$ represents the ratio of F to the drag force acting on a stationary sphere in an infinite fluid of uniform velocity U_0.

In the general case, when both the fluid and the sphere are in motion, the linearity of the equations allows one to write the net drag force as the sum of the forces discussed above, i.e.

$$F = 4\pi D_2 = 4\pi \left[D_2^{(V)} + D_2^{(U_0)} \right] \qquad \text{(III-2.56a)}$$

or

$$F = 6\pi a \left[V \lambda^{(V)} + U_0 \lambda^{(U_0)} \right] \qquad \text{(III-2.56b)}$$

III-2.2 Solution for the axisymmetric motion of a sphere towards an orifice in quiescent fluid.

The solutions for the motion of a sphere towards an orifice through an otherwise quiescent fluid, will be presented in this subsection together with a detailed description of the convergence characteristics of the collocation technique. The results obtained by the present method for the limiting case $a \to \infty$ will be compared with the exact solution of Brenner (1961) for translation of a sphere perpendicular to a plane wall.

The system of linear algebraic equations to be solved for B_n and D_n, is constructed from equations (III-2.45) and the boundary conditions (III-2.51) with $\Delta P=0$. When the sphere is moving towards a solid wall ($b'=0, a \to \infty$) the system is easily modified by using (III-2.28) with

$f(R)=0$ and $g(R)=0$.

In general, there are many schemes which may be used to select the boundary points on the surface of the sphere to satisfy the no-slip boundary conditions. Two different schemes which were successfully employed by Leichtberg, Pfeffer and Weinbaum (1976) for the problem of flow past a chain of spheres and by Leichtberg, Weinbaum, Pfeffer and Gluckman (1976) for two closely spaced adjacent spheres in a chain, will be examined in detail.

The most accurate lowest truncation solution for the drag force is obtained by using one boundary point at $\theta=\frac{\pi}{2}$ on the sphere's generating arc. This point is of great importance since it defines the projected area of the sphere normal to the direction of motion. However, an examination of the system of linear algebraic equations shows that for $\theta=\frac{\pi}{2}$ the coefficient matrix in (III-2.45) is singular. In order to overcome this difficulty, the top point $\theta=\frac{\pi}{2}$ is replaced by two closely spaced points $\theta=\frac{\pi}{2}\pm\delta$ where the optimum value of δ is determined by considering a set of solutions for various sphere to pore spacings in which the boundary conditions are satisfied only at the top two points for decreasing value of δ . Furthermore, in order to examine the dependence of δ on the ratio of sphere to pore diameter the solutions are computed for three different values of a. Consequently, the largest value of δ for which convergence to five significant figures is obtained was selected. These solutions are presented in tables

III-1(a),(b),(c). The parameter α used in the table is given in terms of the ratio of the dimensionless sphere radius a to the dimensionless distance d by the relationship $\alpha=\cosh^{-1}(\frac{d}{a})$. Table III-1 indicates that the rate of convergence of the drag correction factor $\lambda^{(\nu)}$ is reduced greatly with decreasing α and when b'=0. Convergence to five significant figures for all spacings and sphere radii is achieved when $\delta \leq 0.01^{\circ}$. Therefore δ is chosen as 0.01°.

Additional boundary points are selected as mirror-image pairs about the cross section $\theta=\frac{\pi}{2}$ in order to maintain the geometrical symmetry of the boundary about this plane. In the first scheme tested the boundary points were selected by dividing the half arc into equal segments. That is, for an even order of truncation M, the boundary points are defined by $\theta_i=\frac{180^{\circ}}{M}i$ where $i=1,2,\ldots,(M-1)$ with the point at $\theta=90^{\circ}$ replaced by the doublet 89.99° and 90.01°. Using this scheme, solutions for $\lambda^{(\nu)}$ were obtained for the case of a sphere approaching a solid plane wall (b'=0) for various spacing parameter α, by increasing M until convergence to five significant digits is achieved. The results, presented in table III-2, are compared with the exact solution of Brenner (1961) and are found to be in perfect agreement for the desired accuracy. The rate of convergence is rapid for large values of α and monotonically deteriorates as the distance between the sphere and the wall decreases.

A second scheme for selecting the boundary points, tested for the same flow conditions, includes the points $\theta=0$

Table III-1. Drag correction factor for a sphere translating axisymmetrically towards an orifice in quiescent fluid. M=2. Convergence test for δ.

(a) a=1.0

δ	$\alpha = 0.5$ $\frac{d}{a} = 1.13$	$\alpha = 1.0$ $\frac{d}{a} = 1.54$	$\alpha = 2.0$ $\frac{d}{a} = 3.76$	$\alpha = 3.0$ $\frac{d}{a} = 10.1$
10°	-2.2272	-1.9432	-1.3862	-1.1247
1°	-2.2160	-1.9353	-1.3855	-1.1246
0.1°	-2.2159	-1.9353	-1.3855	-1.1246
0.01°	-2.2159	-1.9353	-1.3855	-1.1246

(b) a=10.

δ	$\alpha = 0.5$ $\frac{d}{a} = 1.13$	$\alpha = 1.0$ $\frac{d}{a} = 1.54$	$\alpha = 2.0$ $\frac{d}{a} = 3.76$	$\alpha = 3.0$ $\frac{d}{a} = 10.1$
10°	-3.5647	-2.5239	-1.4038	-1.1249
1°	-3.4857	-2.4988	-1.4030	-1.1249
0.1°	-3.4849	-2.4986	-1.4030	-1.1249
0.01°	-3.4849	-2.4986	-1.4030	-1.1249

Table III-1. Cont.

(c) $\underline{a \to \infty,\ b'=0}$.

δ	$\kappa = 0.5$ $\frac{d}{a} = 1.13$	$\kappa = 1.0$ $\frac{d}{a} = 1.54$	$\kappa = 2.0$ $\frac{d}{a} = 3.76$	$\kappa = 3.0$ $\frac{d}{a} = 10.1$
10°	-3.5674	-2.5251	-1.4039	-1.1249
1°	-3.4885	-2.5000	-1.4030	-1.1249
0.1°	-3.4877	-2.4998	-1.4030	-1.1249
0.01°	-3.4877	-2.4997	-1.4030	-1.1249
0.001°	-3.4877	-2.4997	-1.4030	-1.1249

Table III-2. Convergence of $\lambda^{(\nu)}$ for a sphere translating perpendicular to an infinite plane wall. $b'=0$.

M	$\alpha = 0.5$ $\frac{d}{a} = 1.13$	$\alpha = 1.0$ $\frac{d}{a} = 1.54$	$\alpha = 1.5$ $\frac{d}{a} = 2.35$	$\alpha = 2.0$ $\frac{d}{a} = 3.76$	$\alpha = 2.5$ $\frac{d}{a} = 6.13$	$\alpha = 3.0$ $\frac{d}{a} = 10.1$
2	-3.4877	-2.4997	-1.7728	-1.4030	-1.2202	-1.1249
4	-6.3569	-2.9842	-1.8359	-1.4128	-1.2220	-1.1252
6	-7.8347	-3.0309	-1.8374	-1.4129	-1.2220	-1.1252
8	-8.6423	-3.0356	-1.8375	-1.4129		
10	-9.0189	-3.0360	-1.8375			
12	-9.1693	-3.0361				
14	-9.2237	-3.0361				
16	-9.2424					
18	-9.2486					
20	-9.2507					
22	-9.2514					
24	-9.2516					
26	-9.2517					
28	-9.2518					
30	-9.2518					
*	-9.2518	-3.0361	-1.8375	-1.4129	-1.2220	-1.1252

* Exact solution (Brenner, 1961)

and $\theta=\pi$. These points are of great importance when the sphere is located adjacent to the wall since they define the gap between the sphere and the plane Z=d. As in the case when $\theta=\pi/2$, the coefficient matrix (III-2.45) becomes singular when $\theta=0$ or π . A similar procedure to that used for the point $\theta=\frac{\pi}{2}$ is employed to overcome this obstacle. Using M=4 with $\theta=\delta, \frac{\pi}{2}\pm\delta, \pi-\delta$ solutions are obtained for various values of δ, α and a. The results are presented in tables III-3(a),(b),(c), indicating clearly that $\lambda^{(v)}$ converges to five significant figures for all values of α and a when $\delta \leq 0.01^{\circ}$, with the slowest convergence rate exhibited when b'=0. Selection of additional points is done in pairs as before. An even number of points M are given by $\theta_i=\frac{180^{\circ}}{M-2}(i-1)$ where $i=1,2,\ldots,(M-1)$ and the points $\theta=0,90^{\circ},180^{\circ}$ replaced by $\theta=0.01^{\circ},89.99^{\circ},90.01^{\circ},179.99^{\circ}$. Solutions obtained for a sphere moving perpendicualr to a plane wall for various spacings, are presented in table III-4 and compared with the exact solution. The solutions obtained by this method converge somewhat faster than those obtained by the previous scheme, shown in table III-2. At the distance of closest approach, $\alpha=0.5$, the use of the current scheme yields convergence to five significant digits with 24 boundary points, while the first scheme achieves the same accuracy with 28 points. In view of these tests, the second scheme provides more rapid convergence and therefore will be used to determine $\lambda^{(v)}$ for various orifice diameters.

Before presenting these results, the effect of the

Table III-3. Drag correction factor for a sphere translating axisymmetrically towards an orifice in quiescent fluid. M=4. Convergence tests for δ.

(a) a=1.0

δ	α = 0.5 $\frac{d}{a}$ =1.13	α = 1.0 $\frac{d}{a}$ =1.54	α = 2.0 $\frac{d}{a}$ =3.76	α = 3.0 $\frac{d}{a}$ =10.1
10^{o}	-2.3084	-2.0026	-1.3870	-1.1247
1^{o}	-2.3016	-1.9983	-1.3864	-1.1246
0.1^{o}	-2.3015	-1.9983	-1.3864	-1.1246
0.01^{o}	-2.3015	-1.9983	-1.3864	-1.1246

(b) a=10.

δ	α = 0.5 $\frac{d}{a}$ =1.13	α = 1.0 $\frac{d}{a}$ =1.54	α = 2.0 $\frac{d}{a}$ =3.76	α = 3.0 $\frac{d}{a}$ =10.1
10^{o}	-3.5654	-2.5240	-1.4038	-1.1249
1^{o}	-3.4866	-2.4990	-1.4030	-1.1249
0.1^{o}	-3.4859	-2.4987	-1.4030	-1.1249
0.01^{o}	-3.4859	-2.4987	-1.4030	-1.1249

Table III-3. Cont.

(c) $a \to \infty$, $b' = 0$.

δ	$\alpha = 0.5$ $\frac{d}{a} = 1.13$	$\alpha = 1.0$ $\frac{d}{a} = 1.54$	$\alpha = 2.0$ $\frac{d}{a} = 3.76$	$\alpha = 3.0$ $\frac{d}{a} = 10.1$
10°	-20.434	-3.1592	-1.4131	-1.1252
1°	-33.195	-3.1948	-1.4132	-1.1252
0.1°	-33.407	-3.1952	-1.4132	-1.1252
0.01°	-33.409	-3.1952	-1.4132	-1.1252
0.001°	-33.409	-3.1952	-1.4132	-1.1252

Table III-4. Convergence of $\lambda^{(v)}$ for a sphere translating perpendicular to an infinite plane wall with boundary points placed near $\theta=0,\pi$. $b'=0$.

M	$\alpha = 0.5$ $\frac{d}{a} = 1.13$	$\alpha = 1.0$ $\frac{d}{a} = 1.54$	$\alpha = 1.5$ $\frac{d}{a} = 2.35$	$\alpha = 2.0$ $\frac{d}{a} = 3.76$	$\alpha = 2.5$ $\frac{d}{a} = 6.13$	$\alpha = 3.0$ $\frac{d}{a} = 10.1$
4	-33.409	-3.1952	-1.8428	-1.4132	-1.2220	-1.1252
6	-14.902	-3.0399	-1.8374	-1.4129	-1.2220	-1.1252
8	-9.8323	-3.0360	-1.8375	-1.4129		
10	-9.3260	-3.0361	-1.8375			
12	-9.2603	-3.0361				
14	-9.2513					
16	-9.2510					
18	-9.2515					
20	-9.2517					
22	-9.2517					
24	-9.2518					
26	-9.2518					
*	-9.2518	-3.0361	-1.8375	-1.4129	-1.2220	-1.1252

* Exact solution (Brenner, 1961)

ratio of the sphere to the pore diameter on the rate of convergence is examined. Since the spherical solution in (III-2.45) must cancel the disturbance generated at the orifice opening as well, the rate of convergence is expected to deteriorate as the ratio of the sphere to orifice diameter increases. Solutions were computed for various values of a and d/a with increasing number of boundary points, starting with the minimum value of M from table III-4 which yields convergence to four significant digits. Examination of these solutions, shown in table III-5, indicates that the pore size has little effect on the rate of convergence except when a is large and the sphere is adjacent to the orifice. The slow convergence for the case a=10, $\frac{d}{a}$=1.1 is mainly due to the high velocity gradient in the gap between the sphere and the wall. This necessitates a higher concentration of boundary points. Therefore for large values of a and small values of $\frac{d}{a}$, when convergence is slow and computation time prohibitively long, the accuracy will be reduced to three significant digits.

Final results for $\lambda^{(v)}$ for various dimensionless sphere radii and sphere to wall spacings are presented in table III-6. The solutions are plotted in figure III-2 together with the exact solution for the case of motion perpendicular to an infinite plane wall, corresponding to the limiting case when $a \to \infty$. An interesting result, observed in figure III-2, is that the drag on a sphere whose diameter is smaller than that of the orifice decreases

Table III-5. Convergence of $\lambda^{(v)}$ for various sphere radii and sphere-to-orifice spacings.

$\frac{d}{a}$	M	a = 0.1	a = 0.5	a = 1.0	a = 10.
5.0	4	-1.0532	-1.2508	-1.2795	-1.2851
	6	-1.0532	-1.2509	-1.2795	-1.2851
	8	-1.0532	-1.2509	-1.2795	-1.2851
2.0	6	-1.0505	-1.3918	-1.8066	-2.1248
	8	-1.0505	-1.3919	-1.8058	-2.1248
	10	-1.0505	-1.3919	-1.8058	-2.1248
1.5	8	-1.0504	-1.3882	-2.0335	-3.1981
	10	-1.0504	-1.3882	-2.0334	-3.1983
	12	-1.0504	-1.3882	-2.0334	-3.1983
1.1	16	-1.0504	-1.3777	-2.2867	-10.593
	18	-1.0504	-1.3777	-2.2867	-10.590
	20	-1.0504	-1.3777	-2.2867	-10.566
	22				-10.543
	24				-10.527
	26				-10.517
	28				-10.512
	30				-10.511

Table III-6. Drag correction factor $\lambda^{(v)}$ for a sphere translating axisymmetrically towards an orifice for various sphere radii a and sphere-to-orifice spacings d/a.

$\frac{d}{a}$	a= 0.10	a= 0.25	a= 0.50	a= 0.75	a= 1.00	a= 2.50	a= 5.00	a= 7.50	a= 10.0
1.1	-1.0503	-1.1412	-1.3777	-1.7666	-2.2867	-5.89	-8.94	-9.99	-10.5
1.25	-1.0502	-1.1419	-1.3819	-1.7497	-2.1807	-4.0355	-4.9183	-5.1532	-5.2340
1.5	-1.0504	-1.1433	-1.3882	-1.7164	-2.0334	-2.9207	-3.1535	-3.1889	-3.1983
2.0	-1.0505	-1.1475	-1.3919	-1.6348	-1.8058	-2.0857	-2.1200	-2.1239	-2.1248
3.0	-1.0510	-1.1579	-1.3581	-1.4679	-1.5168	-1.5649	-1.5687	-1.5690	-1.5691
4.0	-1.0519	-1.1637	-1.3019	-1.3491	-1.3655	-1.3791	-1.3801	-1.3802	-1.3802
5.0	-1.0532	-1.1617	-1.2509	-1.2728	-1.2795	-1.2847	-1.2850	-1.2851	-1.2851
6.0	-1.0549	-1.1541	-1.2110	-1.2222	-1.2254	-1.2277	-1.2279	-1.2279	-1.2279
8.0	-1.0579	-1.1328	-1.1571	-1.1608	-1.1617	-1.1624	-1.1625	-1.1625	-1.1625
10.0	-1.0596	-1.1125	-1.1240	-1.1255	-1.1262	-1.1262	-1.1262	-1.1262	-1.1262

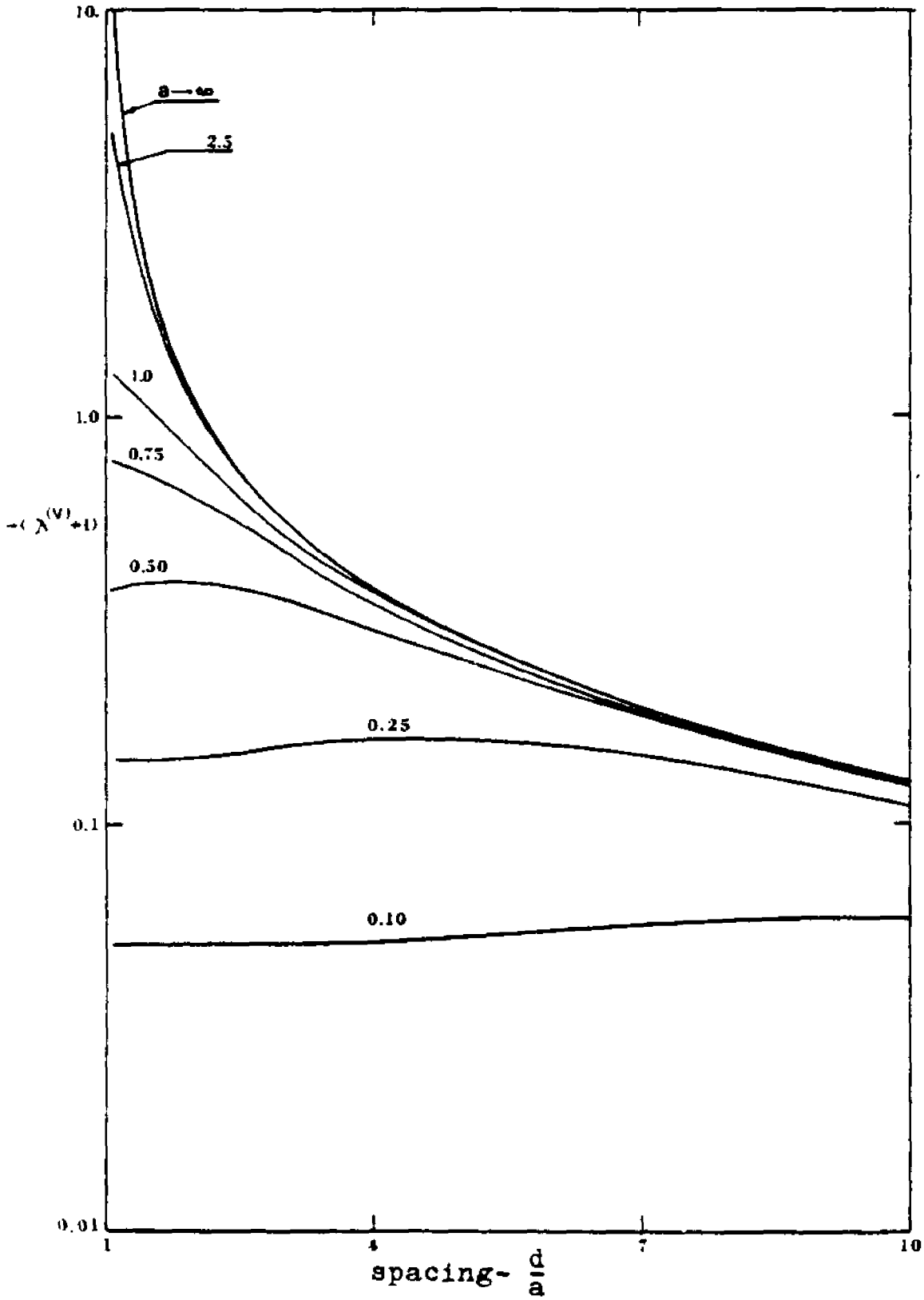

Figure III-2. Drag on a sphere translating axisymmetrically towards an orifice.

when the sphere is close to the orifice with a relative minimum value as d approaches a. This effect is due to the decrease of the effective wall interaction area that offers resistance to the motion of a "small sphere" as it approaches the opening.

III-2.3 Solution for the flow through an orifice past a stationary sphere.

The results for $\lambda^{(4)}$ for the case of flow into an orifice past a stationary sphere are obtained from the solution of the system of linear algebraic equations defined by (III-2.45) and the boundary conditions (III-2.51) with V=0.

The collocation technique is employed in a manner similar to that described in subsection III-2.3. The two schemes for selection of boundary points are tested again. Tables III-7(a),(b),(c) provide solutions for various values of δ according to the first scheme ($\theta = \frac{\pi}{2} \pm \delta$). As before δ is chosen to be 0.01°. Increasing the number of points, the convergence of the first scheme is tested for the case when a=1. These results are shown in table III-8. Based on the results in the previous subsection, solutions were not computed for small values of M when the results are far from the final converged value.

The procedure was repeated with the second collocation scheme. Convergence tests for δ are presented in tables III-9(a),(b),(c). δ is chosen as 0.01°. Finally, convergence of the solutions for a=1 and various sphere to

Table III-7. Drag correction factor for a flow through an orifice past a stationary sphere. M=2. Convergence tests for σ.

(a) a=0.5

σ	$\alpha = 0.5$ $\frac{d}{a} = 1.13$	$\alpha = 1.0$ $\frac{d}{a} = 1.54$	$\alpha = 2.0$ $\frac{d}{a} = 3.76$	$\alpha = 3.0$ $\frac{d}{a} = 10.1$
10°	0.84428	0.68626	0.25376	0.041454
1°	0.83603	0.67746	0.25129	0.041360
0.1°	0.83595	0.67737	0.25127	0.041359
0.01°	0.83595	0.67737	0.25127	0.041359

(b) a=1.0

σ	$\alpha = 0.5$ $\frac{d}{a} = 1.13$	$\alpha = 1.0$ $\frac{d}{a} = 1.54$	$\alpha = 2.0$ $\frac{d}{a} = 3.76$	$\alpha = 3.0$ $\frac{d}{a} = 10.1$
10°	0.41323	0.31117	0.077104	0.010668
1°	0.39605	0.29969	0.076037	0.010642
0.1°	0.39588	0.29958	0.076027	0.010642
0.01°	0.39588	0.29958	0.076027	0.010642

Table III-7. Cont.

(c) a=2.0

δ	α = 0.5 $\frac{d}{a}$ = 1.13	α = 1.0 $\frac{d}{a}$ = 1.54	α = 2.0 $\frac{d}{a}$ = 3.76	α = 3.0 $\frac{d}{a}$ = 10.1
10°	0.14969	0.10191	0.020210	0.0026862
1°	0.14106	0.096825	0.019905	0.0026796
0.1°	0.14098	0.096776	0.019901	0.0026796
0.01°	0.14098	0.096775	0.019901	0.0026796
0.005°	0.14098	0.096775	0.019901	0.0026796

Table III-8. Convergence of $\lambda^{(\omega)}$ for the flow through an orifice past a stationary sphere at various sphere-to-orifice spacings. a=1.0

M	$\frac{d}{a}$ = 1.1	$\frac{d}{a}$ = 1.5	$\frac{d}{a}$ = 2.0	$\frac{d}{a}$ = 5.0	$\frac{d}{a}$ = 10.0
4	---	---	---	---	0.011092
6	---	---	0.32709	0.048593	0.011094
8	---	0.48351	0.32756	0.048597	0.011094
10	---	0.48326	0.32755	0.048597	
12	---	0.48321	0.32754		
14	---	0.48320	0.32754		
16	0.64020	0.48320			
18	0.64018				
20	0.64018				

pore spacings are presented in table III-10. Comparison of the results presented in tables III-8 and III-10, shows no major difference between the two schemes. This behaviour may be explained by the fact that large fluid velocities can be generated in the gap between the sphere and the edge of the orifice rather than in the front of the sphere where the gap between the sphere and the orifice plane is smaller. Nevertheless, the second scheme is chosen in further computations for the sake of consistency per se.

The effect of the ratio of the sphere to pore diameter on the rate of convergence was tested and is presented in table III-11. Examination of these results indicates that convergence deteriorates for large values of a and small spacings. For a=10 and $\frac{d}{a}$=1.1 the solutions converge to only three significant digits with 30 boundary points.

Solutions for $\lambda^{(n)}$ for various values of a and $\frac{d}{a}$ are plotted in figure III-3 and are presented, for reference, in table III-12. Figure III-3 indicates that for a fixed pressure drop across the orifice the drag force increases with decreasing spacing for all sphere sizes and approaches a finite value when the sphere touches the plane of the pore. One notes that the drag on the sphere decreases markedly as the sphere size increases for a fixed ΔP. This is a consequence of the reduction of the volume flow through the orifice due to obstruction of the sphere. The relationship between volumetric flow rate, pressure drop and the sphere size is examined in the next subsection.

Table III-9. Drag correction factor for a flow through an orifice past a stationary sphere. M=4. Convergence tests for δ .

(a) a=0.5

δ	$\alpha = 0.5$ $\frac{d}{a} = 1.13$	$\alpha = 1.0$ $\frac{d}{a} = 1.54$	$\alpha = 2.0$ $\frac{d}{a} = 3.76$	$\alpha = 3.0$ $\frac{d}{a} = 10.1$
10°	0.88123	0.75306	0.28347	0.042460
1°	0.87685	0.75064	0.28402	0.042466
0.1°	0.87681	0.75061	0.28402	0.042466
0.01°	0.87681	0.75061	0.28402	0.042466

(b) a=1.0

δ	$\alpha = 0.5$ $\frac{d}{a} = 1.13$	$\alpha = 1.0$ $\frac{d}{a} = 1.54$	$\alpha = 2.0$ $\frac{d}{a} = 3.76$	$\alpha = 3.0$ $\frac{d}{a} = 10.1$
10°	0.63813	0.51476	0.092277	0.010945
1°	0.63939	0.52487	0.092800	0.010946
0.1°	0.63940	0.52497	0.092805	0.010946
0.01°	0.63940	0.52497	0.092805	0.010946

Table III-9. Cont.

(c) a=2.0

δ	α = 0.5 $\frac{d}{a}$ = 1.13	α = 1.0 $\frac{d}{a}$ = 1.54	α = 2.0 $\frac{d}{a}$ = 3.76	α = 3.0 $\frac{d}{a}$ = 10.1
10°	0.80126	0.40930	0.024831	0.0027570
1°	0.83023	0.45394	0.025017	0.0027574
0.1°	0.83048	0.45441	0.025019	0.0027574
0.01°	0.83048	0.45442	0.025019	0.0027574
0.005°	0.83048	0.45442	0.025019	0.0027574

Table III-10. Convergence of $\lambda^{(4)}$ for the flow through an orifice past a stationary sphere at various sphere-to-orifice spacings with boundary points at $\Theta=0,\pi$. a=1.0

M	$\frac{d}{a}$ = 1.1	$\frac{d}{a}$ = 1.5	$\frac{d}{a}$ = 2.0	$\frac{d}{a}$ = 5.0	$\frac{d}{a}$ = 10.0
4	---	---	---	---	0.011102
6	---	---	0.32639	0.048591	0.011094
8	---	0.48302	0.32756	0.048597	0.011094
10	---	0.48315	0.32754	0.048597	
12	---	0.48319	0.32754		
14	---	0.48320			
16	0.64017	0.48320			
18	0.64018				
20	0.64018				

Table III-11. Convergence of $\lambda^{(v_3)}$ for various sphere radii and sphere-to-orifice spacings.

$\frac{d}{a}$	M	a = 0.1	a = 0.5	a = 1.0	a = 10.
5.0	6	0.83796	0.16985	0.048591	0.00050765
	8	0.83796	0.16986	0.048597	0.00050774
	10	0.83796	0.16986	0.048597	0.00050774
2.0	6	1.0036	0.62755	0.32639	0.0057674
	8	1.0036	0.62719	0.32756	0.0056361
	10	1.0036	0.62720	0.32754	0.0056518
	12		0.62720	0.32754	0.0056541
	14		0.62720	0.32754	0.0056546
	16				0.0056546
1.5	8	1.0206	0.77574	0.48302	0.018657
	10	1.0206	0.77576	0.48315	0.018353
	12	1.0206	0.77576	0.48319	0.018433
	14		0.77576	0.48320	0.018465
	16			0.48320	0.018479
	18			0.48320	0.018484
1.1	16	1.0310	0.90571	0.64017	0.13261
	18	1.0310	0.90571	0.64018	0.13360
	20	1.0310	0.90571	0.64018	0.13847
	22			0.64018	0.14294
	24				0.14610
	26				0.14799
	28				0.14882
	30				0.14899

Table III-12. Drag correction factor $\lambda^{(v_o)}$ for a flow through an orifice past a stationary sphere for various sphere radii a and sphere-to-orifice spacings d/a.

$\frac{d}{a}$	a = 0.1	a =0.25	a = 0.5	a = 0.75	a = 1.0	a = 2.5	a = 5.0	a = 7.5	a = 10.
1.1	1.0310	1.0192	0.90571	0.76406	0.64018	0.295	0.191	0.168	0.149
1.25	1.0274	0.99990	0.85661	0.70015	0.57535	0.282	0.159	0.0937	0.0586
1.5	1.0206	0.96446	0.77576	0.60451	0.48320	0.19675	0.0683	0.0323	0.0185
2.0	1.0036	0.88537	0.62720	0.44502	0.32754	0.082813	0.022291	0.010018	0.0056546
3.0	0.95824	0.71899	0.39761	0.23318	0.14785	0.027119	0.0068979	0.0030746	0.0017312
4.0	0.90148	0.56854	0.25386	0.13232	0.079031	0.013477	0.0033973	0.0015122	0.00085101
5.0	0.83796	0.44578	0.16986	0.083373	0.048597	0.0080729	0.0020285	0.00090236	0.00050774
6.0	0.77168	0.35077	0.11976	0.056922	0.032785	0.0053786	0.0013493	0.00060005	0.00033160
8.0	0.64234	0.22494	0.067600	0.031160	0.017752	0.0028792	0.00072118	0.00032064	0.00018038
10.0	0.52797	0.15272	0.043026	0.019566	0.011094	0.0017904	0.00044814	0.00019922	0.00011207

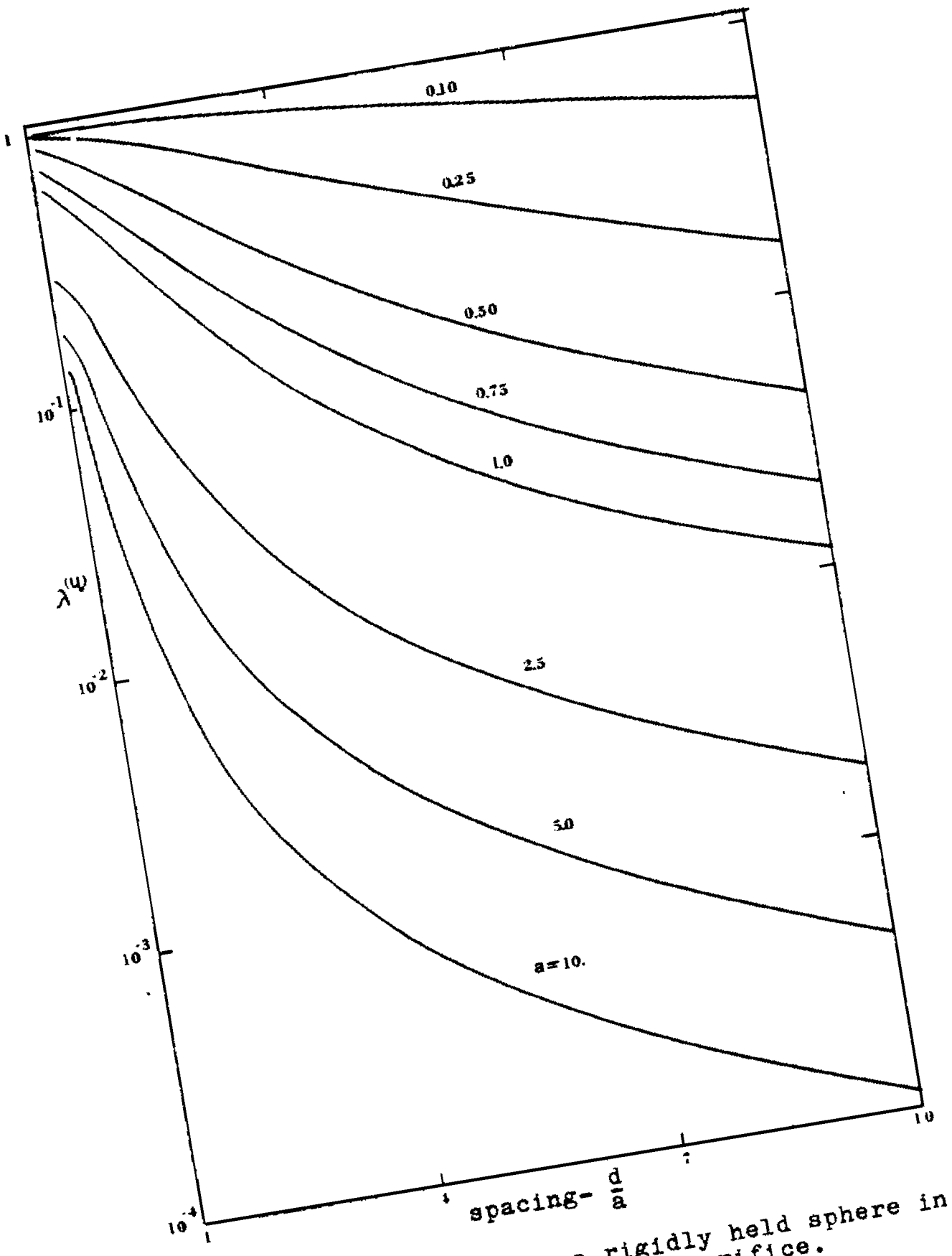

Figure III-3. Drag on a rigidly held sphere in flow through an orifice.

III-2.4 Pressure drop across the orifice.

The relations between the volumetric flow rate and the pressure drop across the orifice, in the presence of the sphere, can be obtained by integrating the axial velocity u_z^* over the area of the orifice opening. The integration can be performed analytically yielding the expression

$$Q = \frac{\Delta P}{3} + 4\sum_{n=2}^{\infty} \frac{B_n}{n}\left[\frac{1}{n-1} S_{n-1}(1,d) - C_n(d)\right] + D_2 \frac{2}{d^2+1}$$
$$+4\sum_{n=3}^{\infty}\left\{ D_n \frac{(2n-3)d}{n(n-1)}\left[\frac{S_{n-2}(1,d)}{n-2} - C_{n-1}(d)\right]\right.$$
$$\left. + D_{n+1}\frac{1}{n^2-1}\left[S_{n-2}(1,d) - (n-2)C_{n-1}(d)\right]\right\} \qquad \text{(III-2.57)}$$

where Q is the dimensionless volumetric flow rate defined in a similar manner to the stream function in (III-2.3a), S_n is defined by (III-2.47a) and

$$C_n(d) = \frac{\cos(n\cot^{-1}d)}{(1+d^2)^{n/2}} \qquad \text{(III-2.58)}$$

An important application of equation (III-2.57) is the operation of a ball valve in the low Reynolds number regime. In this application a ball whose dimensions are larger than the orifice is constrained from moving by a wire at a fixed distance above the orifice.

Clearly, when the sphere is far from the orifice ($d \to \infty$) equation (III-2.57) reduces to

$$Q = \frac{\Delta P}{3} \qquad \text{(III-2.59)}$$

which is in agreement with the exact solution for flow through an orifice in the absence of the sphere.

The relationship between Q and ΔP was computed for the case where the sphere is held rigidly at a prescribed distance from the orifice. These results are presented in figure III-4 for various sphere diameters. Examination of these results indicates that the volumetric flow rate decreases, for a prescribed pressure drop across the orifice, with decreasing spacing. For a sphere of diameter larger than the orifice diameter ($a > 1$) Q decreases rapidly when $\frac{d}{a} < 2$ and approaches zero when the sphere blocks the orifice opening entirely. The results for $\frac{d}{a} < 1.1$, when the sphere diameter is larger than that of the orifice, are extrapolated and shown by the dashed lines.

In the case of the sphere moving with velocity V towards the pore in quiescent fluid ($\Delta P=0$), the volumetric flow rate at the orifice opening Q_o is presented in figure III-5. Here, Q_o increases with increasing sphere size and decreasing distance between the sphere and the opening.

The total volumetric flow rate through the orifice for the general case when a sphere is moving with velocity V and the pressure drop across the orifice is prescribed by ΔP can be obtained by adding the two distinct contributions given in figures III-4 and III-5.

III-2.5 <u>The axisymmetric motion of a sphere in a flow through an orifice</u>.

In this subsection, solution for the velocity of a

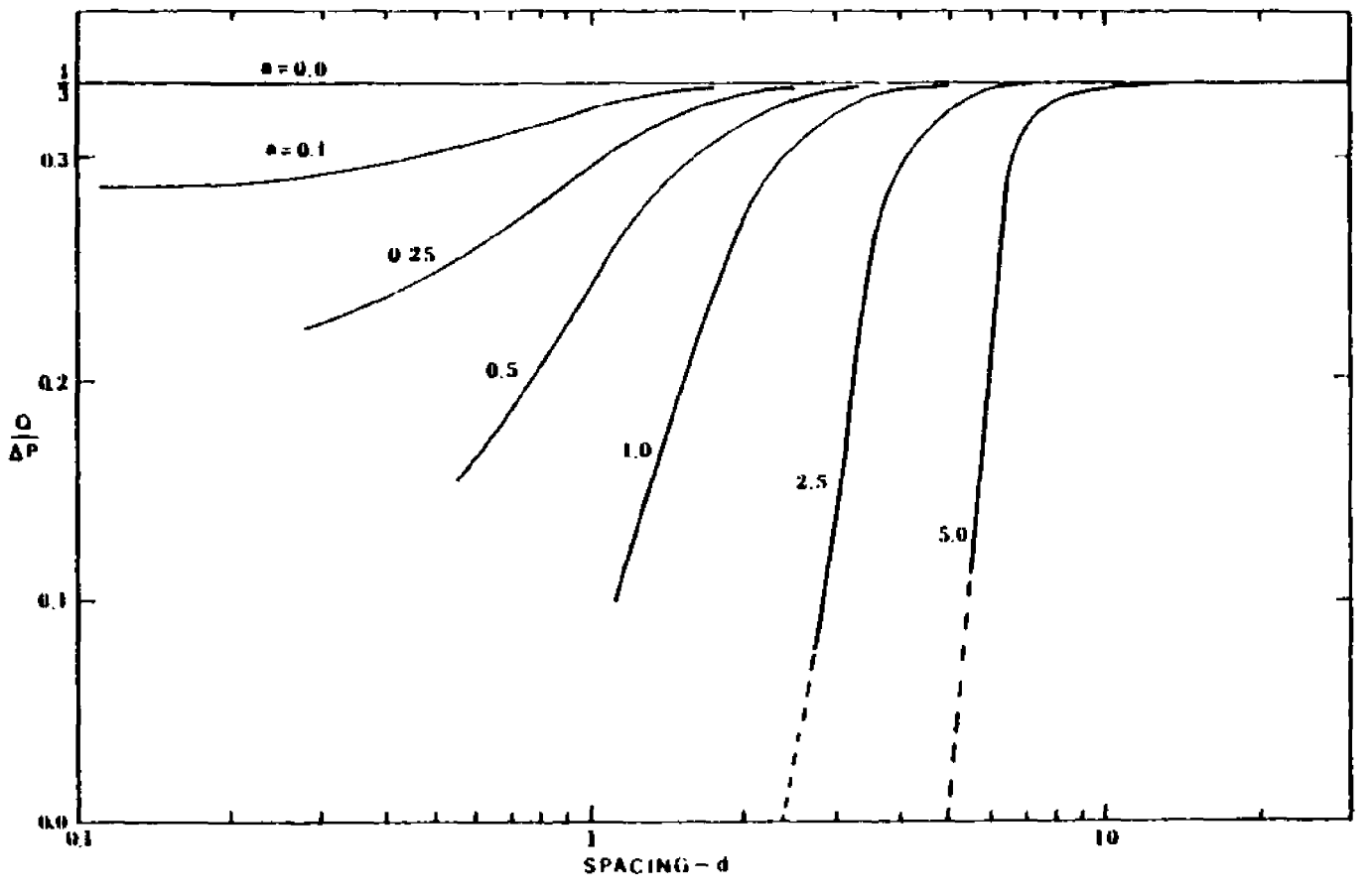

Figure III-4. Pressure drop across an orifice for flow past a rigidly held sphere. ---- extrapolated results.

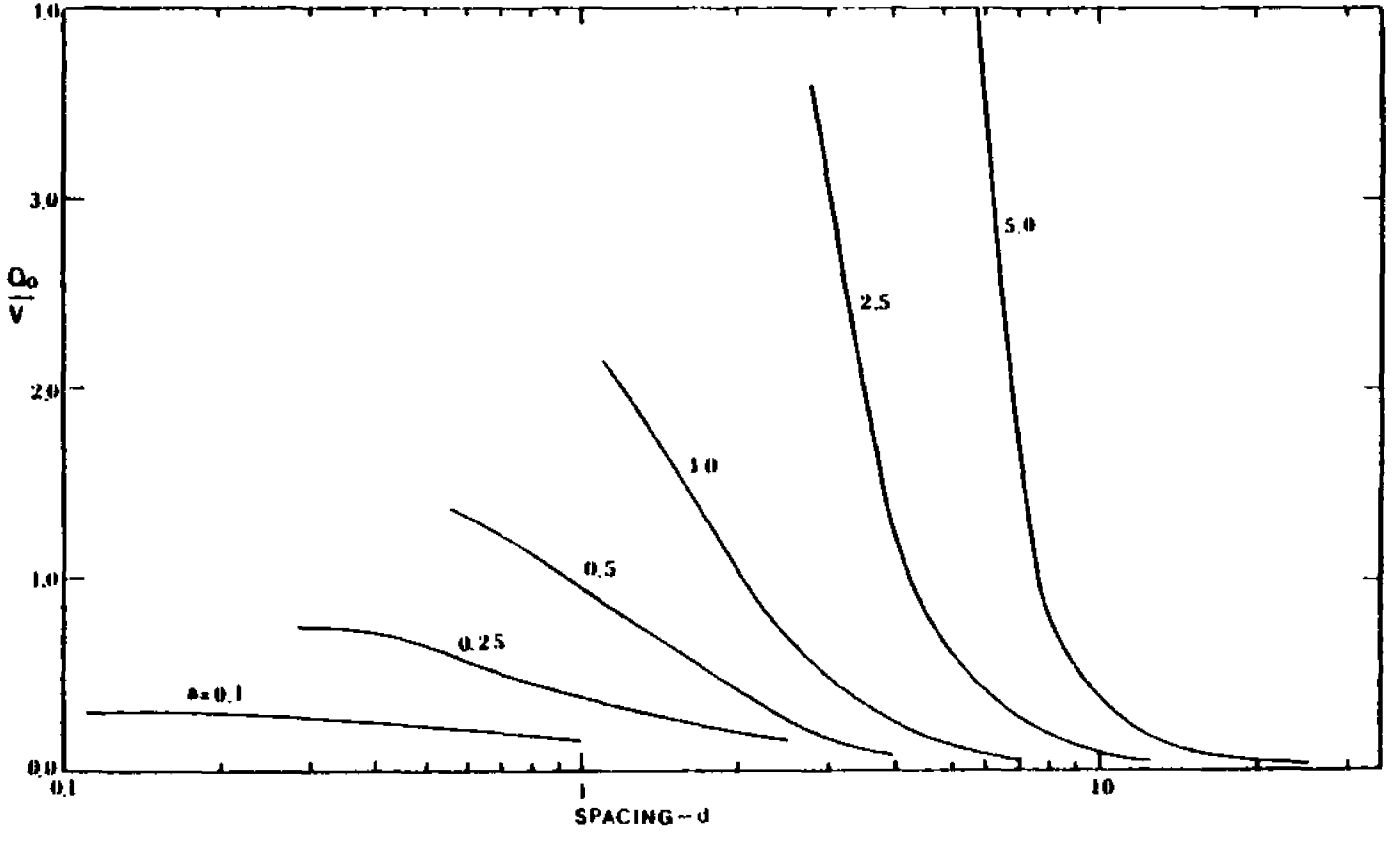

Figure III-5. Volumetric flow rate through an orifice due to the translatory motion of a sphere.

sphere carried by the fluid towards the orifice is presented by combining the axisymmetric solutions for the motion of a sphere in a quiescent fluid and the flow through an orifice past a stationary sphere.

One problem of interest considers a sphere suspended above the orifice in which fluid is being pumped against gravity. The flow rate required to keep the sphere stationary can be determined by setting V=0 in (III-2.56) and equating F to the force of gravity. The result is

$$U_0 = -\frac{V_t}{\lambda^{(\alpha_0)}} \qquad \text{(III-2.60)}$$

where V_t is the terminal settling velocity in an infinite medium.

Another application of interest, is the motion of a neutrally buoyant sphere carried by the flow towards the pore. In this case we require zero drag force on the sphere. Equation (III-2.56) reduces to

$$\frac{V}{U_0} = -\frac{\lambda^{(\alpha_0)}}{\lambda^{(\alpha)}} \qquad \text{(III-2.61)}$$

from which the local sphere velocity V is obtained.

Of particular interest is the slip velocity of a neutrally buoyant sphere defined by

$$V_{slip} = V - U \qquad \text{(III-2.62)}$$

where U is the local fluid velocity in the absence of the

sphere and can be related to U_o by

$$\frac{U}{U_o} = (1+d^2)^{-1} \qquad \text{(III-2.63)}$$

Hence

$$\frac{V_{slip}}{U} = -\left[\frac{\lambda^{(U_o)}}{\lambda^{(V)}}(d^2+1)+1\right] \qquad \text{(III-2.64a)}$$

or

$$\frac{V}{U} = -\frac{\lambda^{(U_o)}}{\lambda^{(V)}}(d^2+1). \qquad \text{(III-2.64b)}$$

Equation (III-5.64b) is plotted in figures III-6(a) and III-6(b). Figure III-6(a) shows the ratio of the sphere velocity to the undisturbed local fluid velocity for spheres with radius $a \leq 1$. The results indicate the the sphere velocity is smaller than the local fluid velocity. In contrast, for spheres larger than tne orifice diameter (Fig. III-6(b)) the sphere velocity increases rapidly as the sphere approaches the orifice and then drops sharply when $\frac{d}{a} < 1.25$. This behaviour can be explained by the fact that when the gap between the sphere and the orifice decreases, the fluid velocity rises quickly enhancing the motion of the sphere. With further decrease of the gap width the blocking of the orifice by the sphere reduces the volumetric flow rate (see figure III-4) which in turn retards the sphere motion. The dashed extensions in figure III-6(b) are extrapolated results for the sphere velocity for small spacings $\frac{d}{a} < 1.1$.

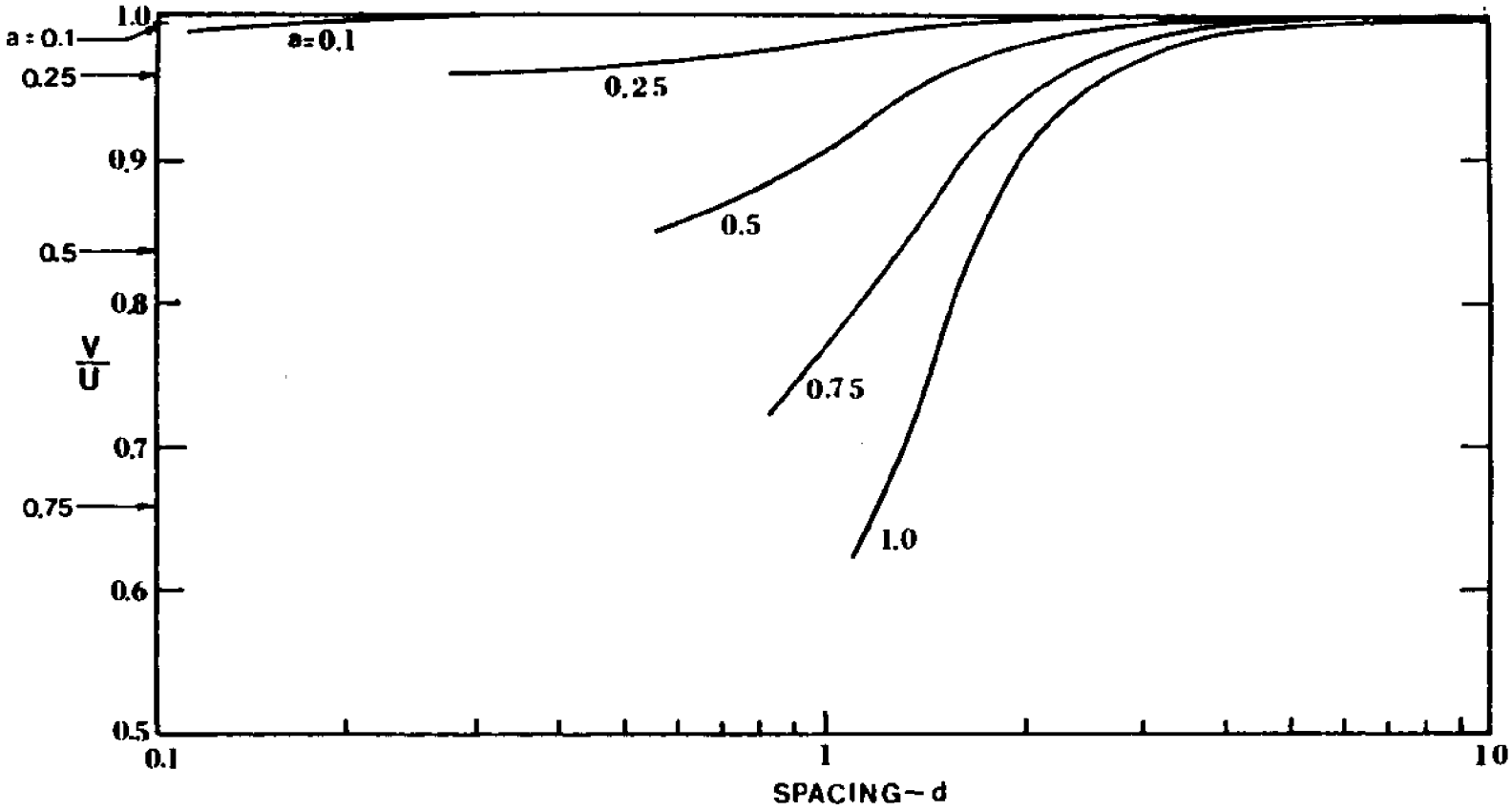

Figure III-6(a). Velocity of a neutrally buoyant sphere carried by the flow through an orifice. $a \leq 1.0$; ⟶ limiting value of the zero-drag velocity of a sphere in an infinite tube (Haberman & Sayre, 1958)

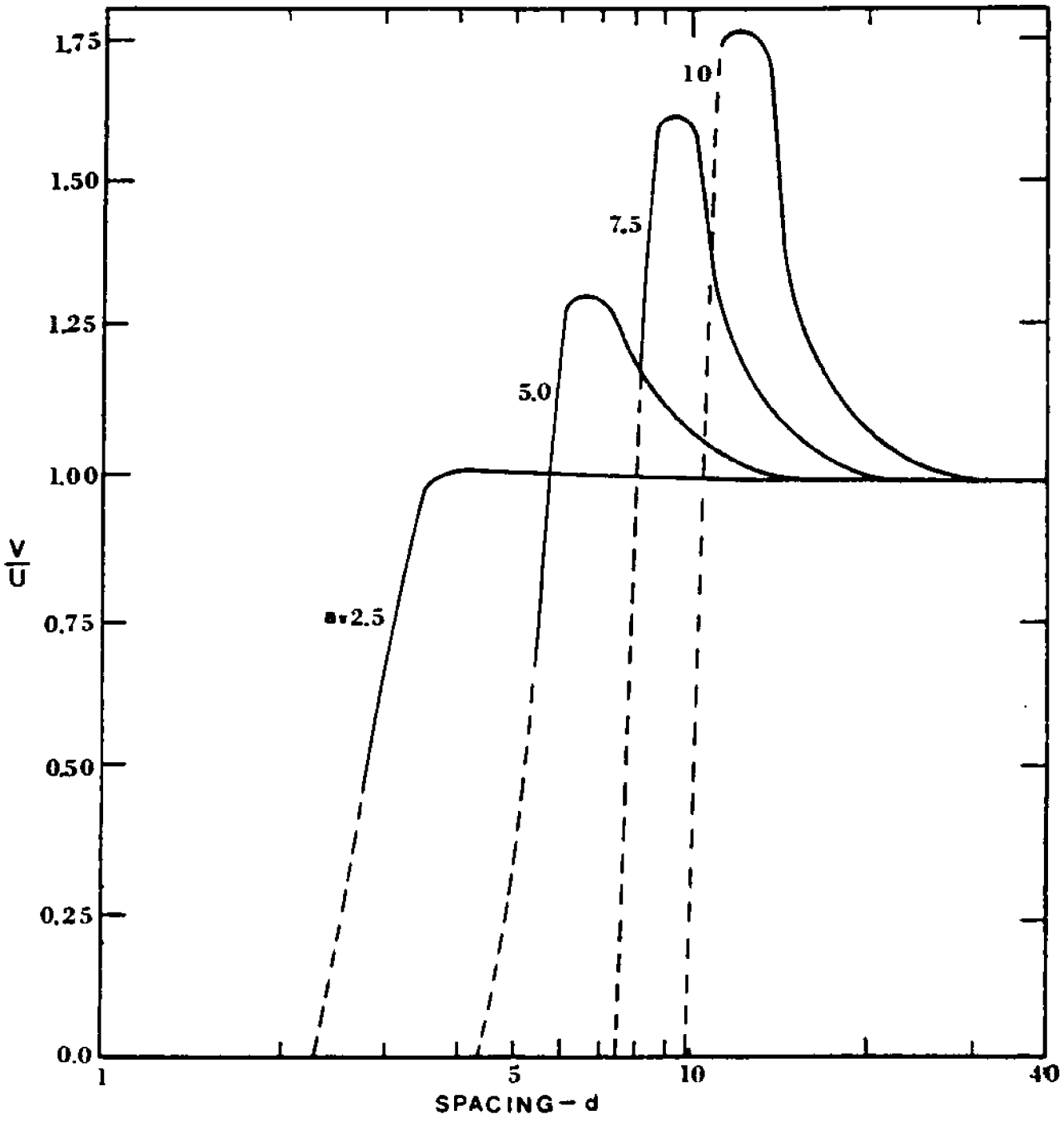

Figure III-6(b). Velocity of a neutrally buoyant sphere carried by the flow through an orifice. a > 1.0. ---- extrapolated results.

III-3. Motion of a sphere towards a disk.

In this section the application of the combined analytical-numerical solution procedure, employed in section III-2, for the problem of the axisymmetric motion of a sphere towards a disk of arbitrary size or the uniform flow past such configuration is presented. The strong interaction solutions presented herein are the first to explore the effect of a finite planar boundary on the motion of a sphere. One application is the motion of a sphere settling under gravity near the bottom of a falling ball viscometer.

The solution technique used in this section follows closely the procedure described in section III-2. Two different stream function representations are chosen, one for the region to the left of the plane of the disk containing the sphere and one for the remaining infinite half space to the right of the disk. The no-slip boundary conditions in each region are satisfied on the disk surface in terms of the unknown velocity at the plane of the disk. The two fields are matched dynamically at the interface providing a solution for the interfacial velocity expressed in terms of the remaining constant coefficients in the spherical series solution. Finally, the no-slip boundary conditions on the surface of the sphere are satisfied at discrete points yielding numerical results for the spherical coefficients.

This section is organized in 4 subsections. Subsection III-3.1 contains the formulation of the problem. Subsection III-3.2 presents solutions for both a sphere

translating in quiescent fluid and for the uniform flow past a fixed sphere-disk configuration. In subsection III-3.3 solutions for the drag force acting on the disk are presented . Finally, subsection III-3.4 considers the zero drag motion of a neutrally buoyant sphere carried by the flow towards the disk.

III-3.1 Mathematical formulation.

The formulation of the problem is similar to that presented in subsection III-2.1 and, therefore, will not be presented in great detail. Using similar notation, the problem consists of a sphere of radius a' translating axisymmetrically with a constant velocity V' towards a disk of radius b' held rigidly at a distance d' from the sphere. The fluid at infinity is assumed to have uniform velocity U_∞'. Figure III-7 shows the geometry using dimensionless variables (unprimed) and co-ordinates scaled to the disk radius. The dimensionless variables are defined by (III-2.3) with the disk radius playing the same role as the orifice radius.

The flow field is divided into two regions. The half space containing the sphere $Z \leq d$, and the infinite half space $Z \geq d$. Making use of the general solution of the creeping motion equations (III-2.4) for axisymmetric flow, one can write the stream function for the region $Z \leq d$ as the linear superposition

$$\Psi^I = \Psi_w + \Psi_s \qquad \text{(III-3.1)}$$

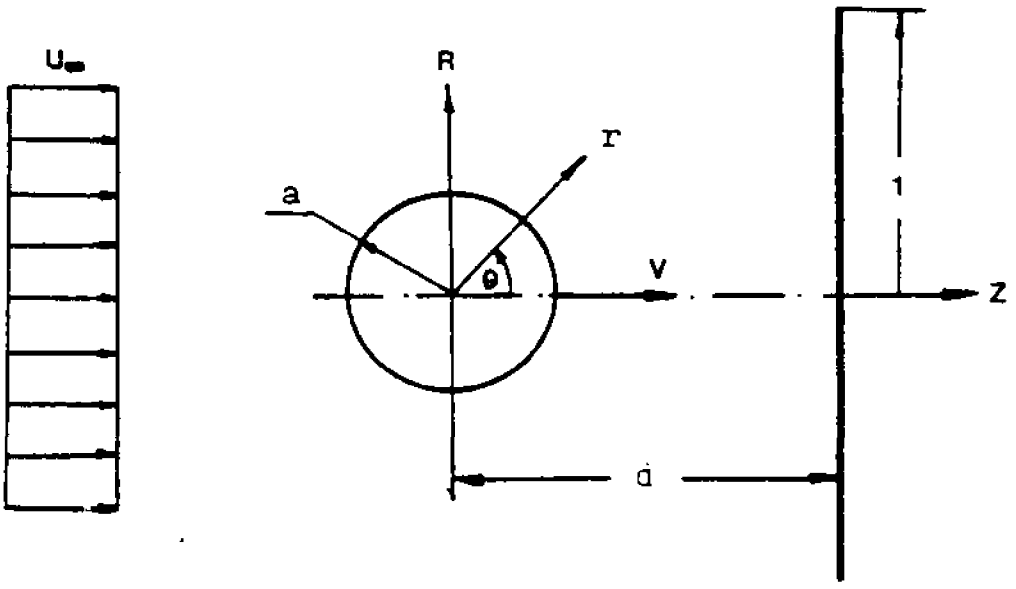

Figure III-7. Geometry for the problem of a sphere translating axisymmetrically towards a disk.

where Ψ_w represents the disturbance produced by the plane of the disk plus the uniform flow at infinity and is given by

$$\Psi_w = \tfrac{1}{2} U_\infty R^2 + \int_0^\infty R J_1(\omega R)\left[A_1(\omega) + Z B_1(\omega)\right] e^{\omega Z} d\omega \quad (Z \leq d) \quad \text{(III-3.2)}$$

where $A_1(\omega)$ and $B_1(\omega)$ are unknown functions of ω. The second part in (III-3.2), Ψ_s, represents the disturbance generated by the sphere and is given by (III-2.10).

For the region $Z \geq d$, a Fourier-Bessel representation is chosen for the stream function in the form of (III-3.2) which yields a uniform velocity as Z approaches infinity.

$$\Psi^{II} = \tfrac{1}{2} U_\infty R^2 + \int_0^\infty R J_1(\omega R)\left[A_2(\omega) + Z B_2(\omega)\right] e^{-\omega Z} d\omega \quad (Z \geq d) \quad \text{(III-3.3)}$$

where $A_2(\omega)$ and $B_2(\omega)$ are unknown functions of ω.

The velocity components at the plane of the disk can be defined in a general form by

$$\vec{u}(R,d) = \frac{1}{R}\left\{\left[f(R) + R U_\infty\right]\hat{z} - g(R)\hat{r}\right\} \qquad 1 < R < \infty \quad \text{(III-3.4)}$$

The kinematic boundary conditions in the matching plane Z=d require that the velocity vanish for $R \leq 1$ and that the velocity be continuous for $R > 1$.

$$u_z^i(R,d) = \begin{cases} \dfrac{f(R)}{R} + U_\infty & 1 < R \\ 0 & 0 < R < 1 \end{cases} \qquad i = I, II \quad \text{(III-3.5a)}$$

$$u_R^i(R,d) = \begin{cases} -\dfrac{g(R)}{R} & 1<R \\ \\ 0 & 0<R<1 \end{cases} \qquad i = I, \underline{II} \qquad \text{(III-3.5b)}$$

In addition, the dynamic matching of the two fields requiring a continuous stress tensor at the interface between the two regions is replaced, as described in chapter II, by matching the pressure and its gradient (Equations III-2.31a,b).

Application of the kinematic boundary conditions (III-3.5a,b) follows closely the mathematical development outlined in subsection III-2.1. This development leads to solutions for $A_1(\omega)$ and $B_1(\omega)$ in terms of the unknown constant coefficients in the spherical solution Ψ_s and the unknown velocity functions f(R) and g (R). The resulting velocity field in region I is given by

$$u_R^I = \int_0^\infty \Big\{ (\omega x - 1) \int_1^\infty g(t) J_1(\omega t)\, dt + v_\infty x J_1(\omega) - \omega x \int_1^\infty f(t) J_0(\omega t)\, dt \Big\} \omega J_1(\omega R) e^{-\omega x} d\omega + \sum_{n=2}^{\infty} \left[B_n \beta_n'(R,z) + D_n \delta_n'(R,z) \right] \qquad \text{(III-3.6a)}$$

$$u_z^I = v_\infty + \int_0^\infty \Big\{ (1+\omega x) \int_1^\infty f(t) J_0(\omega t) dt - \left(\frac{1}{\omega} + x\right) v_\infty J_1(\omega) - \omega x \int_1^\infty g(t) J_1(\omega t)\, dt \Big\} \omega J_0(\omega R) e^{-\omega x} d\omega +$$

$$+\sum_{n=2}^{\infty}\left[B_n\beta_n''(R,\bar{z})+D_n\delta_n''(R,\bar{z})\right] \qquad \text{(III-3.6b)}$$

where $x=d-Z$ and β_n', δ_n', β_n'', δ_n'' are given by equations (III-2.29). Similarly, an expression for the velocity field $\vec{u}^{II}$ can be obtained

$$u_R^{II} = -\int_0^{\infty}\left\{\left[1-\omega(\bar{z}-d)\right]\int_1^{\infty} g(t)J_1(\omega t)dt + (\bar{z}-d)U_\infty J_1(\omega) - \omega(\bar{z}-d)\int_1^{\infty} f(t)J_0(\omega t)dt\right\}\omega J_1(\omega R)e^{-\omega(\bar{z}-d)} \qquad \text{(III-3.7a)}$$

$$u_{\bar{z}}^{II} = U_\infty + \int_0^{\infty}\left\{\left[1+\omega(\bar{z}-d)\right]\int_1^{\infty} f(t)J_0(\omega t)dt - \left[1+\omega(\bar{z}-d)\right]U_\infty\frac{J_1(\omega)}{\omega} + \omega(\bar{z}-d)\int_1^{\infty} g(t)J_1(\omega t)dt\right\}\omega J_0(\omega R)e^{-\omega(\bar{z}-d)} \qquad \text{(III-3.7b)}$$

In order to apply the pressure matching conditions (III-2.31), the expression for the pressure field in each region is obtained. These expressions are given by equations (III-2.32) and (III-2.33) with $P_{-\infty}=P_\infty=0$. Application of the pressure matching conditions (expressions for $B_i(\omega)$ $i=1,2$ are given in the appendix) results in

$$\int_0^{\infty}\omega f^*(\omega)J_0(\omega R)d\omega = F^*(R) \qquad 1<R<\infty \qquad \text{(III-3.8a)}$$

$$\int_0^{\infty}\omega g^*(\omega)J_0(\omega R)d\omega = G^*(R) \qquad 1<R<\infty \qquad \text{(III-3.8b)}$$

where

$$f^*(\omega) = \omega\int_1^{\infty} f(t)J_0(\omega t)dt - U_\infty J_1(\omega) \qquad \text{(III-3.9a)}$$

$$g^*(\omega) = \omega^2 \int_1^\infty g(t)\, J_1(\omega t)\, dt \qquad \text{(III-3.9b)}$$

and F* and G* are given by equations (III-2.35a,b) with $\Delta P = 0$.

The integral equations (III-3.9) together with

$$\int_0^\infty f^*(\omega)\, J_0(\omega R)\, d\omega = -U_\infty \qquad 0 \le R < 1 \qquad \text{(III-3.10a)}$$

$$\int_0^\infty g^*(\omega)\, J_0(\omega R)\, d\omega = 0 \qquad 0 \le R < 1 \qquad \text{(III-3.10b)}$$

comprise two sets of dual integral equations for f* and g*. The solution of equations (III-3.9) and (III-3.10) follows from the results of Tranter (1951) yielding

$$\begin{Bmatrix} f^*(\omega) \\ g^*(\omega) \end{Bmatrix} = \begin{Bmatrix} M_f(\omega) \\ M_g(\omega) \end{Bmatrix} - \frac{2}{\pi} \int_0^1 dt \cos t\omega \int_0^\infty ds \cos ts \begin{Bmatrix} M_f(s) \\ M_g(s) \end{Bmatrix}$$

$$- \begin{Bmatrix} \frac{2}{\pi} U_\infty \frac{\sin \omega}{\omega} \\ 0 \end{Bmatrix} \qquad \text{(III-3.11)}$$

where

$$\begin{Bmatrix} M_f(\omega) \\ M_g(\omega) \end{Bmatrix} = \int_0^\infty \xi \begin{Bmatrix} F^*(\xi) \\ G^*(\xi) \end{Bmatrix} J_0(\omega\xi)\, d\xi \qquad \text{(III-3.12)}$$

The functions F* and G* are now substituted into

(III-3.12) and integrated. Then M_f and M_g are substituted into (III-3.11) where the inner integral can be performed analytically. The solutions for f* and g* are substituted back into the velocity field expressions. After considerable algebraic manipulation one obtains

$$u_R^I = \sum_{n=2}^{\infty} \left\{ B_n \left[B_n'(R,\xi) - \frac{2}{\pi} \int_0^1 B_n^*(R,\xi,\lambda)\, d\lambda \right] + D_n \left[D_n'(R,\xi) - \frac{2}{\pi} \int_0^1 D_n^*(R,\xi,\lambda)\, d\lambda \right] \right\} + \frac{2}{\pi} U_\infty \times S_1^\circ(R,x) \qquad \text{(III-3.13a)}$$

$$u_\xi^I = \sum_{n=2}^{\infty} \left\{ B_n \left[B_n''(R,\xi) - \frac{2}{\pi} \int_0^1 B_n^{**}(R,\xi,t)\, d\lambda \right] + D_n \left[D_n''(R,\xi) - \frac{2}{\pi} \int_0^1 D_n^{**}(R,\xi,t)\, d\lambda \right] \right\} + U_\infty \left\{ 1 - \frac{2}{\pi} \left[S_0^{-1}(R,x) + x S_0^\circ(R,x) \right] \right\} \qquad \text{(III-3.13b)}$$

where

$$B_n^*(R,\xi,\lambda) = (n+1)\, C_{n+2}(\lambda,d) \left[Q_1^{-1}(R,x,t) - x Q_1^\circ(R,x,t) \right] - x\, C_{n+1}(\lambda,d)\, Q_1^{-1}(R,x,t) \qquad \text{(III-3.14a)}$$

$$D_n^*(R,\xi,\lambda) = \left[(2n-3) d\, C_{n+1}(\lambda,d) - (n-2) C_n(\lambda,d) \right] \left[Q_1^{-1}(R,x,t) - x Q_1^\circ(R,x,t) \right] + \frac{x}{n} Q_1'(R,x,t) \left[(n-3) C_{n-1}(\lambda,d) - (2n-3) d\, C_n(\lambda,d) \right] \qquad \text{(III-3.14b)}$$

$$B_n^{**}(R,\xi,t) = Q_0^0(R,x,t)\,[C_{n+1}(t,d) + x(n+1)\,C_{n+2}(t,d)]$$

$$+ x\,Q_0^1(R,x,t)\,C_{n+1}(t,d) \qquad \text{(III-3.14c)}$$

$$D_n^{**}(R,\xi,t) = [\,Q_0^0(R,x,t) + xQ_0^1(R,x,t)]\,[\tfrac{2n-3}{n}\,d\,C_n(t,d) - \tfrac{n-3}{n}\,C_{n-1}(t,d)]$$

$$+ Q_0^0(R,x,t)\,x[(2n-3)\,d\,C_{n+1}(t,d) - (n-2)\,C_n(t,d)] \qquad \text{(III-3.14d)}$$

and

$$S_\nu^\mu(R,x) = \int_0^\infty \omega^\mu J_\nu(\omega R)\,e^{-\omega x}\sin\omega t\,d\omega \qquad \text{(III-3.15a)}$$

$$Q_\nu^\mu(R,x,t) = \int_0^\infty \omega^\mu J_\nu(\omega R)\,e^{-\omega x}\cos\omega t\,d\omega \qquad \text{(III-3.15b)}$$

$$C_n(t,d) = \frac{\cos[n\,\tan^{-1}\frac{t}{d}]}{(t^2+d^2)^{n/2}} \qquad \text{(III-3.16)}$$

The integrals defined by (III-3.14) can be evaluated using the results in Erdelyi (1954, vol. 1 p. 101; vol. 2 p. 11,19). Then

$$S_1^0(R,x) = \frac{x(1-h_1^2)}{R\,h_1 C_1^2} \qquad \text{(III-3.17a)}$$

$$S_0^0(R,x) = \frac{h_1}{C_1} \qquad \text{(III-3.17b)}$$

$$Q_1^{-1}(R,x,t) = \frac{h-x}{R} \qquad \text{(III-3.17c)}$$

$$Q_1^0(R,x,t) = \frac{1}{R}\left[1 - x\,\frac{t^2+h^2}{h\,C^2}\right] \qquad \text{(III-3.17d)}$$

$$Q_0^0(R,x,t) = \frac{h}{C} \qquad \text{(III-3.17e)}$$

$$Q_0^1(R,x,t) = \frac{x}{C^2}\left[\frac{4h(t^2+h^2)}{C} - \frac{t^2+3h^2}{h}\right] \qquad \text{(III-3.17f)}$$

$$Q_1^1(R,x,t) = \frac{t^2+h^2}{RhC}\left[1 + \frac{4x^2}{C} - \frac{x^2(t^2+h^2)}{C}\left(\frac{1}{h^2} + \frac{4}{C}\right)\right] \qquad \text{(III-3.17g)}$$

where h and h_1 are the roots of the algebraic equations

$$h^4 - h^2(R^2 + x^2 - t^2) - x^2t^2 = 0 \qquad \text{(III-3.18a)}$$

$$h_1^4 + h_1^2(R^2 + x^2 - 1) - x^2 = 0 \qquad \text{(III-3.18b)}$$

and C and C_1 are defined by

$$C = \left[(R^2 + x^2 - t^2)^2 + 4x^2t^2\right]^{1/2} \qquad \text{(III-3.19a)}$$

$$C_1 = \left[(R^2 + x^2 - 1)^2 + 4x^2\right]^{1/2} \qquad \text{(III-3.19b)}$$

The solution (III-3.13) satisfies the no-slip boundary conditions on the surface of the disk and the stress tensor matching condition with region II for any value of the constant coefficients B_n and D_n. The single integrals in the infinite series in (III-3.13) must be performed numerically. In this regard, it should be noted that the expressions for Q_1^{-1} and Q_1^0 given by (III-3.17c,d) are prone to large roundoff errors when R is small and $h \sim x$. Therefore Q_1^{-1} should be computed using the substitution

$$h - x = \frac{R^2h^2}{(h^2+t^2)(h+x)} \qquad \text{(III-3.20)}$$

which results directly from (III-3.18a). Q_1^0 can be obtained in an alternate form by differentiating Q_1^{-1} with respect to x. Hence

$$Q_1^0(R,x,t) = \frac{R}{h+x}\left[\frac{h^2}{h^2+t^2}\left(\frac{2x}{c^2}+\frac{1}{h+x}\right)+\frac{x}{c}\left(\frac{h}{h+x}-\frac{2}{c^2}\right)\right] \qquad \text{(III-3.21)}$$

The only boundary conditions that remain to be satisfied are those on the sphere surface

$$U_R = 0, \quad U_z = V \qquad (r=a) \qquad \text{(III-3.22a,b)}$$

where V is the velocity with which the sphere is translating towards the disk. The collocation technique presented in section III-2 may now be used for this purpose.

Using the notation in section III-2.1, the drag force acting on a sphere translating coaxially with velocity V towards a disk in quiescent fluid can be written as

$$F = 6\pi a V \lambda^{(v)} \qquad \text{(III-3.23a)}$$

where the drag correction factor $\lambda^{(v)}$ is defined by

$$\lambda^{(v)} = \frac{D_2^{(v)}}{1.5\,a\,V} \qquad \text{(III-3.23b)}$$

Similarly, for the case of uniform flow past a rigidly held sphere situated axisymmetrically at a distance d from a disk, the drag force is given by

$$F = 6\pi a U_\infty \lambda^{(U_\infty)} \qquad \text{(III-3.24a)}$$

and $\lambda^{(U_\infty)}$ is defined by

$$\lambda^{(U_\infty)} = \frac{D_2^{(U_\infty)}}{1.5\, a\, U_\infty} \qquad \text{(III-3.24b)}$$

In the general case, when both the fluid and the sphere are in motion the drag force is given by

$$F = 6\pi a \left(V \lambda^{(V)} + U_\infty \lambda^{(U_\infty)}\right) \qquad \text{(III-3.25)}$$

III-3.2 Solutions for the motion of a sphere towards a disk.

In this subsection, collocation solutions for the general axisymmetric motion of the sphere will be presented for both (i) translation of the sphere in quiescent fluid and (ii) uniform flow past the fixed sphere-disk configuration.

Before proceeding with the presentation of these results it should be noted that equations (III-3.13) can be simplified for the limiting case, a disk of infinite radius, by substituting the dimensional variables and allowing b' to approach infinity. The resulting equations for the velocity field are

$$u_R^I = \sum_{n=2}^{\infty} \left[B_n \beta_n'(R,Z) + D_n \delta_n'(R,Z)\right] \qquad \text{(III-3.26a)}$$

$$U_z^I = \sum_{n=2}^{\infty} \left[B_n \beta_n''(R,z) + D_n \delta_n''(R,z) \right] \qquad \text{(III-3.26b)}$$

Equations (III-3.26) represent the solution for the problem of a sphere translating perpendicular to an infinite plane wall. Application of the collocation technique for this case was demonstrated in the previous section and compared with the exact solution of Brenner (1961).

As in the case of the motion of a sphere towards an orifice, the most advantageous collocation boundary point to choose is $\Theta = \frac{\pi}{2}$, since this point has the greatest control of the projected area of the sphere normal to its direction of motion. In addition, the points $\Theta = 0, \pi$ were shown to have increasing effect on the speed of convergence of the results as the gap between the sphere and the disk is made very small. Therefore, the second scheme, described in subsectin III-2.2, will be employed. Unfortunately, the coefficient matrix becomes singular if these points are used. Therefore, convergence trials for the force correction factors using four adjacent points $\Theta = 0+\delta, \frac{\pi}{2} \pm \delta, \pi - \delta$ as $\delta \to 0$ were conducted. Tables III-13 and III-14 present the results of these tests for the two flows considered when a=1. Bearing in mind that the tests conducted for the case when the disk radius is infinite (table III-3(c)) apply as well for the present problem, convergence for $\lambda^{(v)}$ and $\lambda^{(\omega_z)}$ is obtained to five significant digits for $\delta \leq 0.01$ at all spacings tested. The rate of convergence of the

Table III-13. Drag correction factor for a sphere translating axisymmetrically towards a disk. M=4. Convergence tests for δ . a=1.

δ	$\alpha = 0.5$ $\frac{d}{a} = 1.13$	$\alpha = 1.0$ $\frac{d}{a} = 1.54$	$\alpha = 2.0$ $\frac{d}{a} = 3.76$	$\alpha = 3.0$ $\frac{d}{a} = 10.1$
10°	-22.003	-3.0344	-1.2110	-1.0284
1°	-36.008	-3.0716	-1.2112	-1.0284
0.1°	-36.241	-3.0720	-1.2112	-1.0284
0.01°	-36.244	-3.0720	-1.2112	-1.0284
0.001°	-36.244	-3.0720	-1.2112	-1.0284

Table III-14. Drag correction factor for a fixed sphere situated coaxially near a disk in uniform flow. M=4. Convergence tests for δ . a=1.

δ	$\alpha = 0.5$ $\frac{d}{a} = 1.13$	$\alpha = 1.0$ $\frac{d}{a} = 1.54$	$\alpha = 2.0$ $\frac{d}{a} = 3.76$	$\alpha = 3.0$ $\frac{d}{a} = 10.1$
10°	0.84878	0.77577	0.81699	0.89948
1°	0.87453	0.78129	0.81670	0.89948
0.1°	0.87484	0.78135	0.81670	0.89948
0.01°	0.87484	0.78135	0.81670	0.89948

solutions as the number of boundary points is increased is examined for various spacings and sphere radii in tables III-15 and III-16. The starting value of M for a given case in these tables is based on the results of similar tests conducted for the motion of a sphere towards an orifice presented in section III-2. The slowest rate of convergence is found at $\frac{d}{a}$=1.1 and a=10 for the two flows considered. Convergence to only three significant figures is obtained with M=34 for the sphere translating towards the disk and M=22 for the flow past a stationary sphere and disk configuration. Therefore for large values of a and small spacings, where convergence is slow, the solutions presented are accurate to only three significant digits. The slow rate of convergence for the case of the sphere translating towards the disk can be explained by the fact that large fluid velocities can be generated in the intervening fluid gap when its dimensions become small compared with the sphere radius. In the case of flow past a stationary sphere-disk configuration the slow convergence is due to the complexity of the flow in the gap between the two surfaces.

The final results for the hydrodynamic interaction coefficients $\lambda^{(v)}$ and $\lambda^{(\omega)}$ are shown in figures III-8 and III-9. In addition, for reference, converged values are presented in tables III-17 and III-18. Examination of the results reveals two interesting features. First, in the case of a sphere translating towards a disk (table III-17)

Table III-15. Convergence of $\lambda^{(\nu)}$ for various sphere radii and sphere-to-disk spacings.

$\frac{d}{a}$	M	a = 0.1	a = 0.5	a = 1.0	a = 10.
5.0	6	-1.2877	-1.2154	-1.1166	-1.0112
	8	-1.2877	-1.2154	-1.1166	-1.0112
2.0	6	-2.1258	-2.1798	-1.8930	-1.0619
	8	-2.1258	-2.1798	-1.8936	-1.0619
	10	-2.1258	-2.1798	-1.8936	-1.0620
	12			-1.8936	-1.0620
	14			-1.8936	-1.0620
1.5	8	-3.2054	-3.2951	-3.0812	-1.1059
	10	-3.2055	-3.2952	-3.0813	-1.1048
	12	-3.2055	-3.2952	-3.0812	-1.1046
	14	-3.2055	-3.2952	-3.0812	-1.1046
1.1	16	-11.458	-11.559	-11.786	-1.6444
	18	-11.459	-11.559	-11.784	-1.5708
	20	-11.459	-11.559	-11.784	-1.5338
	22	-11.459	-11.559	-11.784	-1.5238
	24				-1.5299
	26				-1.5417
	28				-1.5519
	30				-1.5579
	32				-1.5600
	34				-1.5601
	36				-1.5595

Table III-16. Convergence of $\lambda^{(2)}$ for various sphere radii and sphere-to-disk spacings.

$\frac{d}{a}$	M	a = 0.1	a = 0.5	a = 1.0	a = 10.
5.0	6	0.052987	0.65463	0.84075	0.98575
	8	0.052987	0.65463	0.84075	0.98575
2.0	6	0.0065800	0.37085	0.77523	0.99701
	8	0.0065800	0.37097	0.77459	0.99700
	10	0.0065800	0.37097	0.77463	0.99699
	12		0.37097	0.77463	0.99699
	14			0.77463	0.99699
1.5	8	0.0035577	0.27703	0.75386	1.0075
	10	0.0035578	0.27702	0.75383	1.0076
	12	0.0035578	0.27702	0.75391	1.0076
	14	0.0035578	0.27702	0.75390	1.0076
	16			0.75390	
1.1	16	0.0019244	0.19204	0.73206	1.0083
	18	0.0019244	0.19204	0.73200	1.0085
	20	0.0019244	0.19204	0.73200	1.0086
	22			0.73200	1.0086
	24				1.0086
	26				1.0085
	28				1.0084

Table III-17. Drag correction factor $\lambda^{(v)}$ for a sphere translating axisymmetrically towards a disk for various sphere radii a and sphere-to-disk spacings d/a.

$\frac{d}{a}$	a = 0.*	a = 0.1	a =0.25	a = 0.5	a =0.75	a = 1.0	a = 2.5	a = 5.0	a = 7.5	a = 10
1.1	-11.459	-11.459	-11.464	-11.559	-11.768	-11.784	-7.09	-3.04	-1.96	-1.56
1.25	-5.3053	-5.3054	-5.3123	-5.4051	-5.5172	-5.3773	-2.8182	-1.5704	-1.2854	-1.1790
1.5	-3.2054	-3.2055	-3.2147	-3.2952	-3.2954	-3.0812	-1.7408	-1.2643	-1.1513	-1.1046
2.0	-2.1255	-2.1258	-2.1394	-2.1798	-2.0776	-1.8936	-1.3152	-1.1354	-1.0851	-1.0620
3.0	-1.5692	-1.5700	-1.5878	-1.5543	-1.4392	-1.3417	-1.1292	-1.0613	-1.0401	-1.0297
4.0	-1.3802	-1.3818	-1.3953	-1.3272	-1.2417	-1.1848	-1.0719	-1.0350	-1.0231	-1.0172
5.0	-1.2851	-1.2877	-1.2916	-1.2154	-1.1536	-1.1166	-1.0459	-1.0226	-1.0150	-1.0112
6.0	-1.2279	-1.2314	-1.2247	-1.1521	-1.1064	-1.0805	-1.0318	-1.0158	-1.0105	-1.0078
8.0	-1.1625	-1.1672	-1.1440	-1.0872	-1.0579	-1.0450	-1.0179	-1.0089	-1.0059	-1.0044
10.0	-1.1262	-1.1305	-1.0989	-1.0563	-1.0382	-1.0287	-1.0115	-1.0057	-1.0038	-1.0028

* Solution for a sphere translating perpendicular to an infinite plane wall. $b' \to \infty$. (Brenner, 1961)

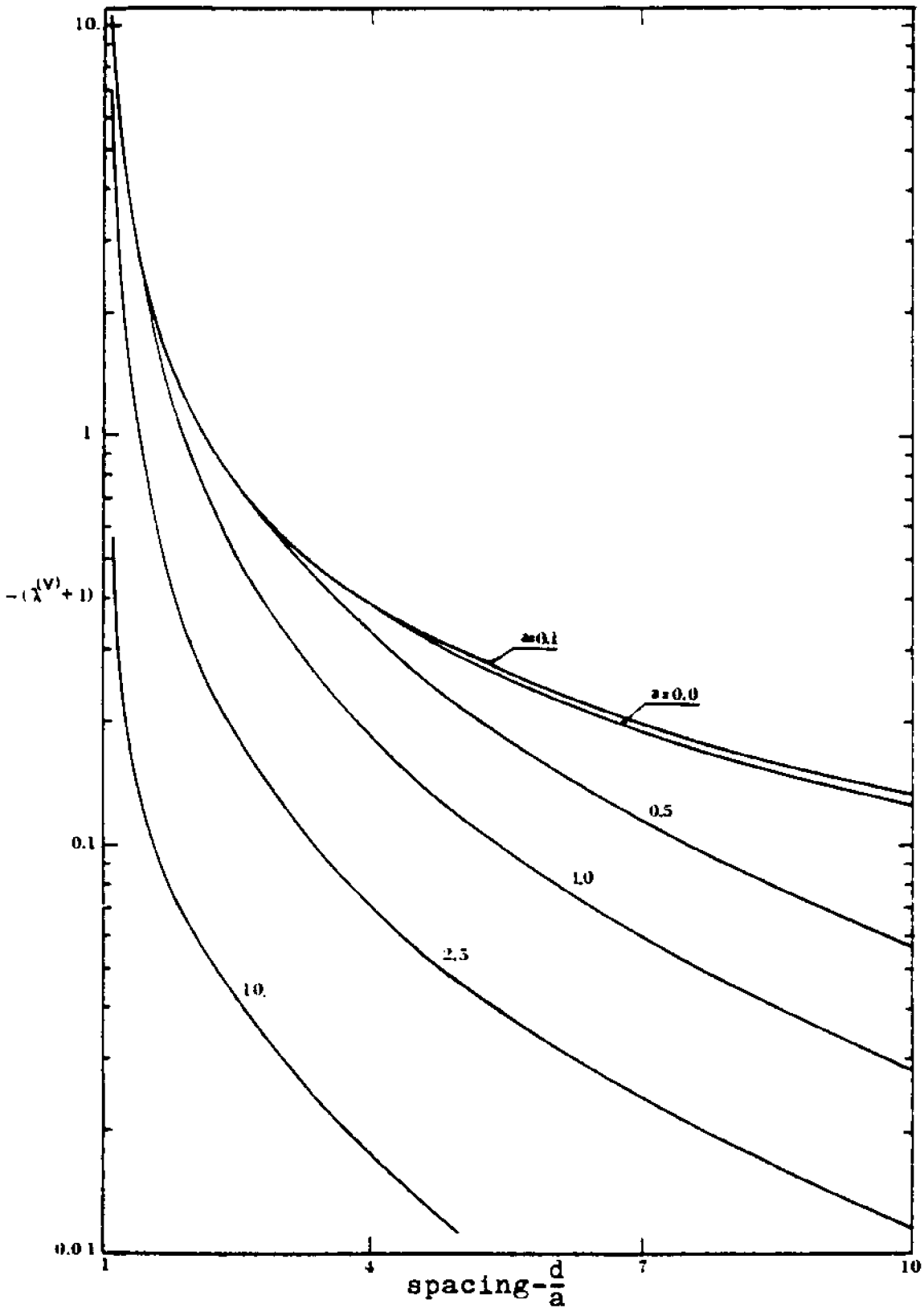

Figure III-8. Drag on a sphere translating axisymmetrically towards a disk.

Table III-18. Drag correction factor $\lambda^{(\infty)}$ for a flow past a stationary sphere situated coaxially near a disk for various sphere radii a and sphere-to-disk spacings d/a.

$\frac{d}{a}$	a = 0.1	a = 0.25	a = 0.5	a =0.75	a = 1.0	a = 2.5	a = 5.0	a = 7.5	a = 10.0
1.1	0.0019244	0.028422	0.19204	0.47616	0.73200	1.03	1.02	1.01	1.0
1.25	0.0024625	0.035592	0.22449	0.51115	0.74093	1.01	1.02	1.01	1.01
1.5	0.0035578	0.049394	0.27702	0.55879	0.75390	0.99551	1.0104	1.0092	1.0076
2.0	0.0065800	0.083163	0.37097	0.62668	0.77463	0.96585	0.99090	0.99536	0.99699
3.0	0.016469	0.16675	0.50853	0.70483	0.80212	0.94086	0.97337	0.98282	0.98732
4.0	0.031980	0.25566	0.59599	0.74920	0.82271	0.93780	0.97027	0.98047	0.98545
5.0	0.052987	0.33751	0.65463	0.78023	0.84075	0.94080	0.97114	0.98093	0.98575
6.0	0.078730	0.40790	0.69705	0.80424	0.85637	0.94516	0.97303	0.98212	0.98663
8.0	0.13985	0.51603	0.75559	0.83961	0.88101	0.95351	0.97696	0.98468	0.98853
10.0	0.20622	0.59223	0.79480	0.86444	0.89898	0.95016	0.98019	0.98682	0.99012

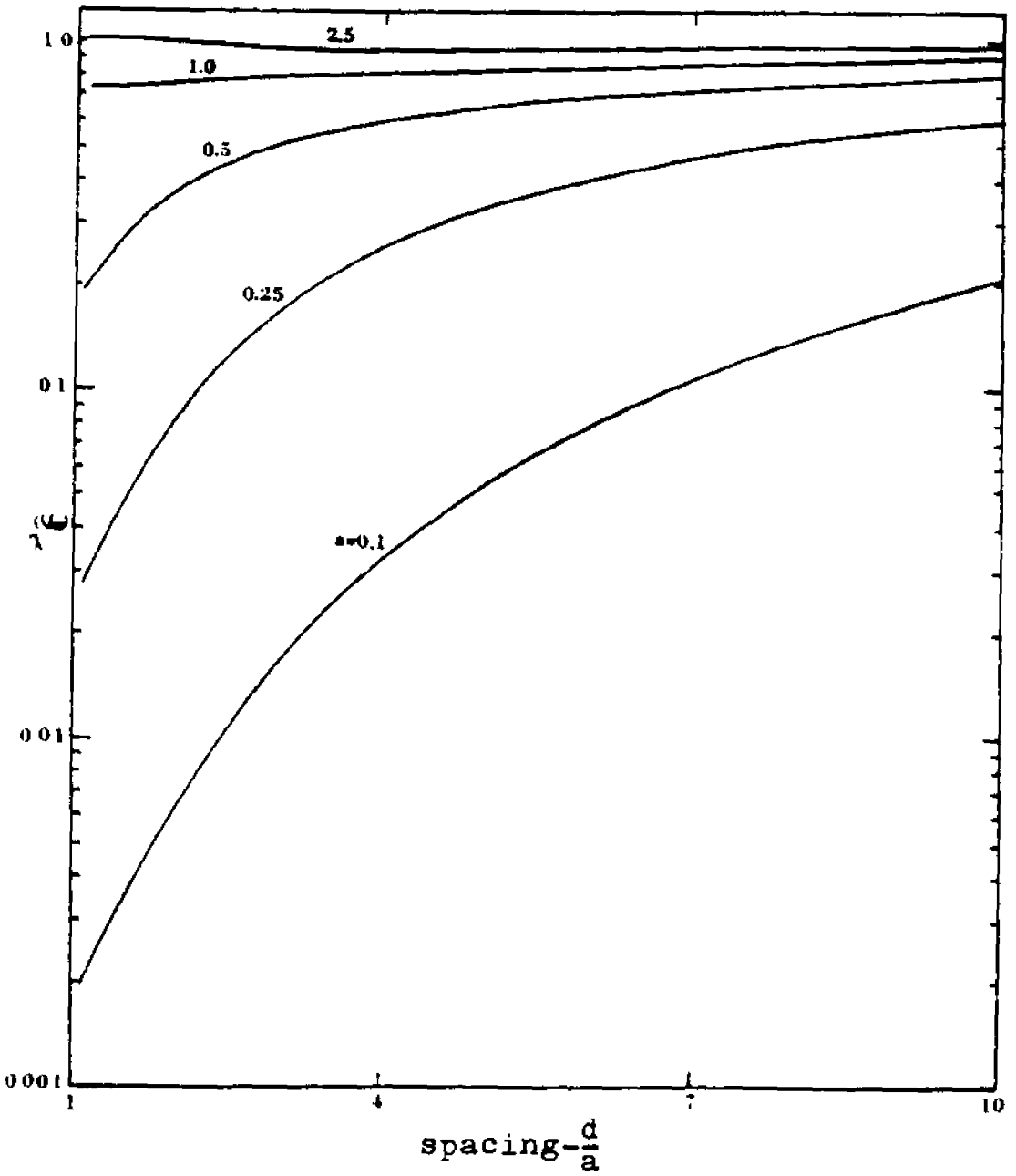

Figure III-9. Drag on a rigidly held sphere in uniform flow past a sphere-disk configuration.

the force acting on a sphere smaller than the disk increases above the value of the force acting on a sphere translating perpendicular towards an infinite plane wall (a=0), and approaches that value as the sphere approaches the disk. These results can be explained by the fact that the edge of a finite disk introduces a strong resistance to the fluid motion demonstrated by the singularity in the pressure field at R=1. This resistance can be greater than the total integrated resistance along an infinite wall where the fluid motion is almost parallel to the boundary. Hence, a larger force is required to push the fluid around the hinge point R=1 than along an infinite boundary. When the spacing between the sphere and the disk decreases further, the edge effect is diminished and the flow field in the vicinity of the sphere resembles the flow for the case of a sphere approaching an infinite wall.

The second interesting result is observed for the case of uniform flow past a rigidly held sphere and disk configuration. Here, for spheres larger than the disk, the drag force acting on the sphere for value of $\frac{d}{a}$ near 1.0 becomes slightly larger than the force acting on an isolated sphere in a uniform stream. These results motivated additional tests to assure that convergence was actually achieved. In the cases in question the number of boundary points was increased much beyond the upper limit shown in table III-18. Due to the limitation of excessive computation time when the spacing is small the tests were conducted

for intermidiate spacings up to $\frac{d}{a}$=1.5.(e.g. for a=10 and d/a=1.5 28 points were selected). The results obtained from these tests matched exactly the values in table III-18.

To help understand this intriguing behaviour the velocity field was examined for a=2.5 and various spacings. Figures III-10 and III-11 show the velocity field for the flow past a sphere-disk configuration in the gap between the two objects. The velocity vectors shown with arrowheads have been drawn to scale and show the magnitude and direction of the fluid motion. For cases where the magnitude of the velocity is too small to be visible on the scale shown the direction of the fluid motion is shown by a straight line without an arrow at the indicated point. Figure III-10 shows the flow field at $\frac{d}{a}$=2. Two wakes of trapped fluid are visible on the sides of the sphere and the disk facing each other.(additional computations have shown that there are no wakes in front of the sphere and behind the disk). Figures III-10(b),(c) show a more detailed description of the trapped fluid near each surface. The flow field shown is similar to the one presented in Davis et al (1976) for the flow past two equal spheres. At closer spacing $\frac{d}{a}$=1.5 (figure III-11) the wakes coalesce, and the two ring vortices have merged. At very small spacings ($\frac{d}{a} < 1.5$) the flow field cannot be computed accurately due to the insufficient convergence of the spherical constant coefficients B_n and D_n. In this case, as demonstrated by

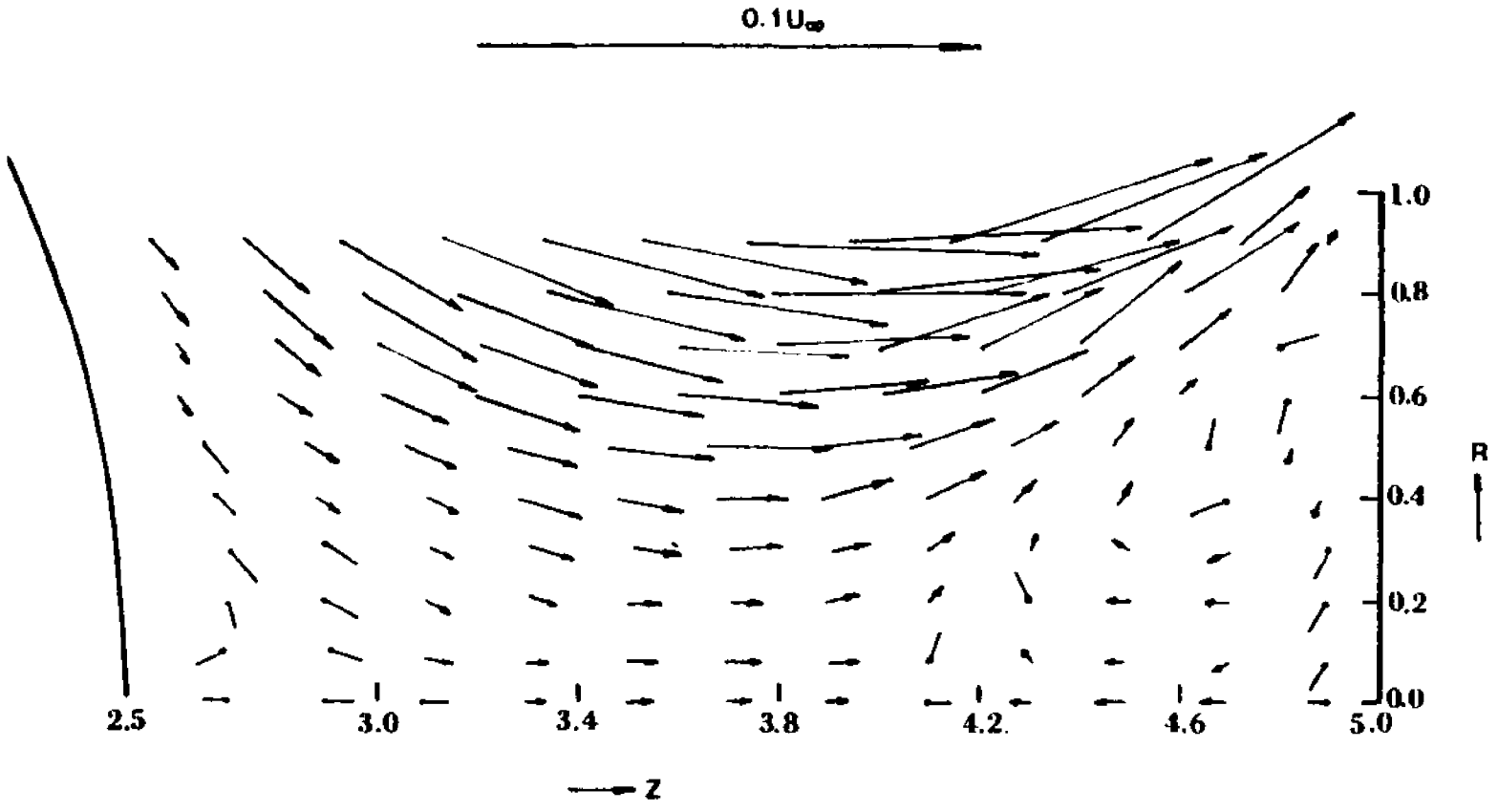

Figure III-10(a). Velocity field in the gap between a stationary sphere and disk configuration in a uniform stream, a=2.5, d/a=2.

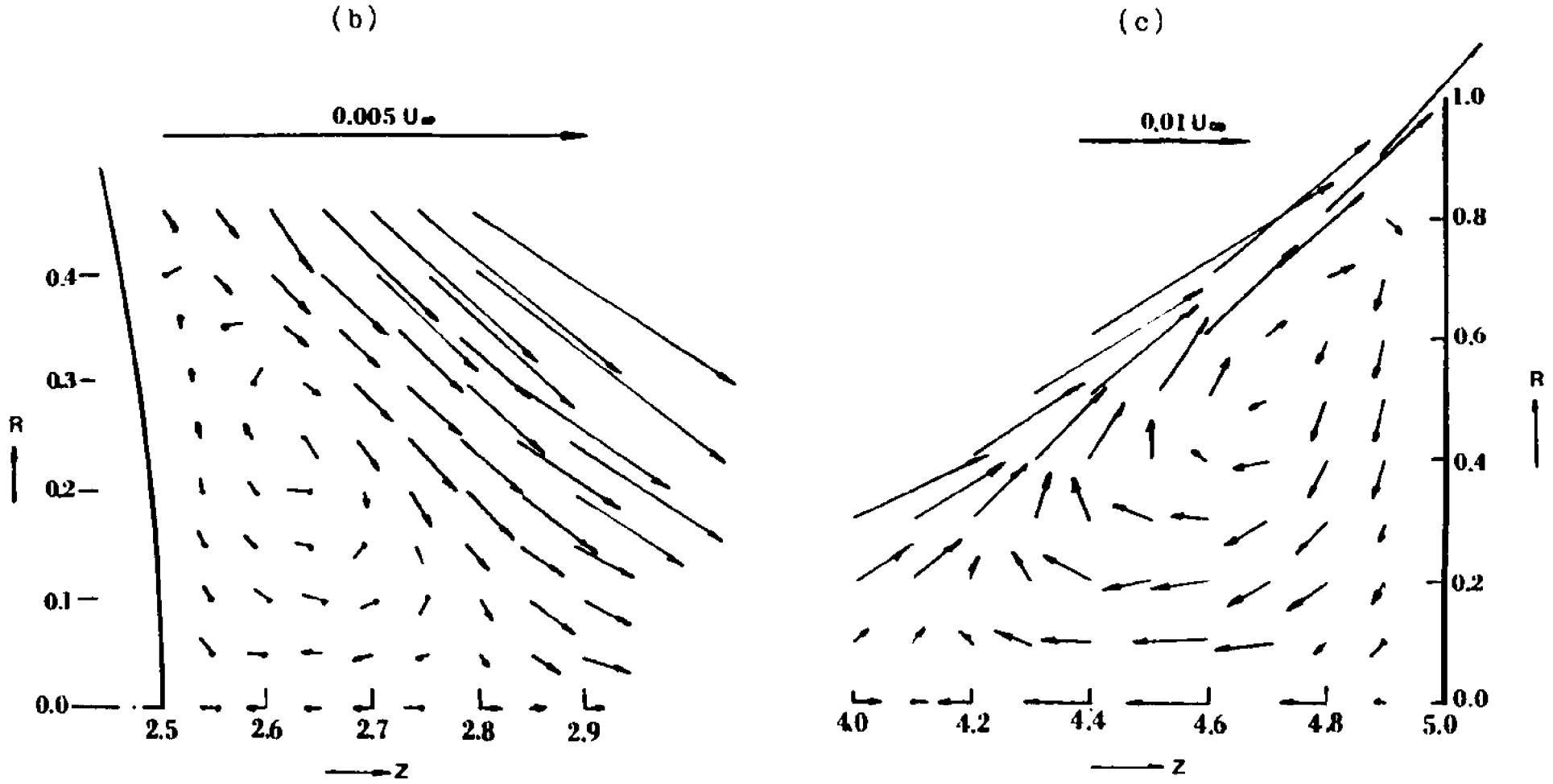

Figure III-10. Separated ring vortices near (b)the sphere surface and (c)the disk. a=2.5, d/a=2.

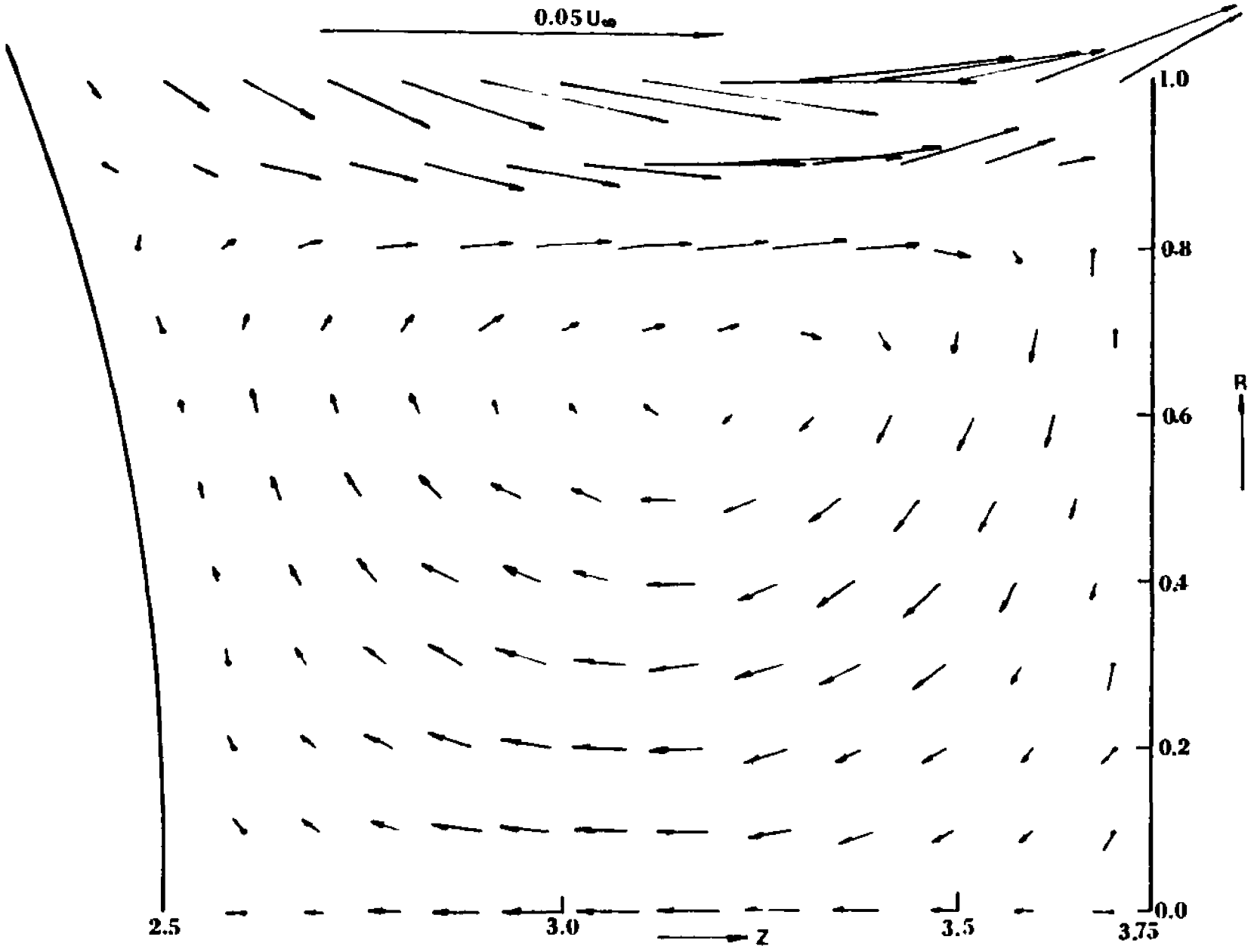

Figure III-11. The flow structure after coalescence of the two primary ring vortices. a=2.5, d/a = 1.5.

Davis et al (1976), the number of ring vortices increases and a very complex wake structure is formed. The formation of the primary ring vortices and their coalescence into one vortex shown in figure III-11 was examined by calculating the fluid velocity on the axis of symmetry R=0 in the gap between the sphere and the disk. The size of the wakes near the sphere l_s and near the disk l_d are shown in figure III-12 as a function of sphere to disk spacing d.

Although the flow field shown in figures III-10 and III-11 demonstrates clearly the separation of the flow from the boundaries, it does not offer an explanation for the increased drag on the sphere. Intuitively, this behaviour might result from the weak singularity in the pressure and the shear stress fields at R=1, which introduce high shear rates and pressure gradients in the vicinity of the disk edge that effect the force on the sphere when it is larger than the disk and in close proximity. In this context it should be noted that although the drag on the sphere exceeds the value of the drag on an isolated sphere in a uniform stream, the total drag force on the sphere and the disk (see subsection III-3.3) combined is smaller than the sum of the drag forces on an isolated sphere and an isolated disk in uniform flow.

III-3.3 Solutions for the drag force acting on the disk.

The expression for the drag force acting on the disk in the presence of the sphere can be obtained by

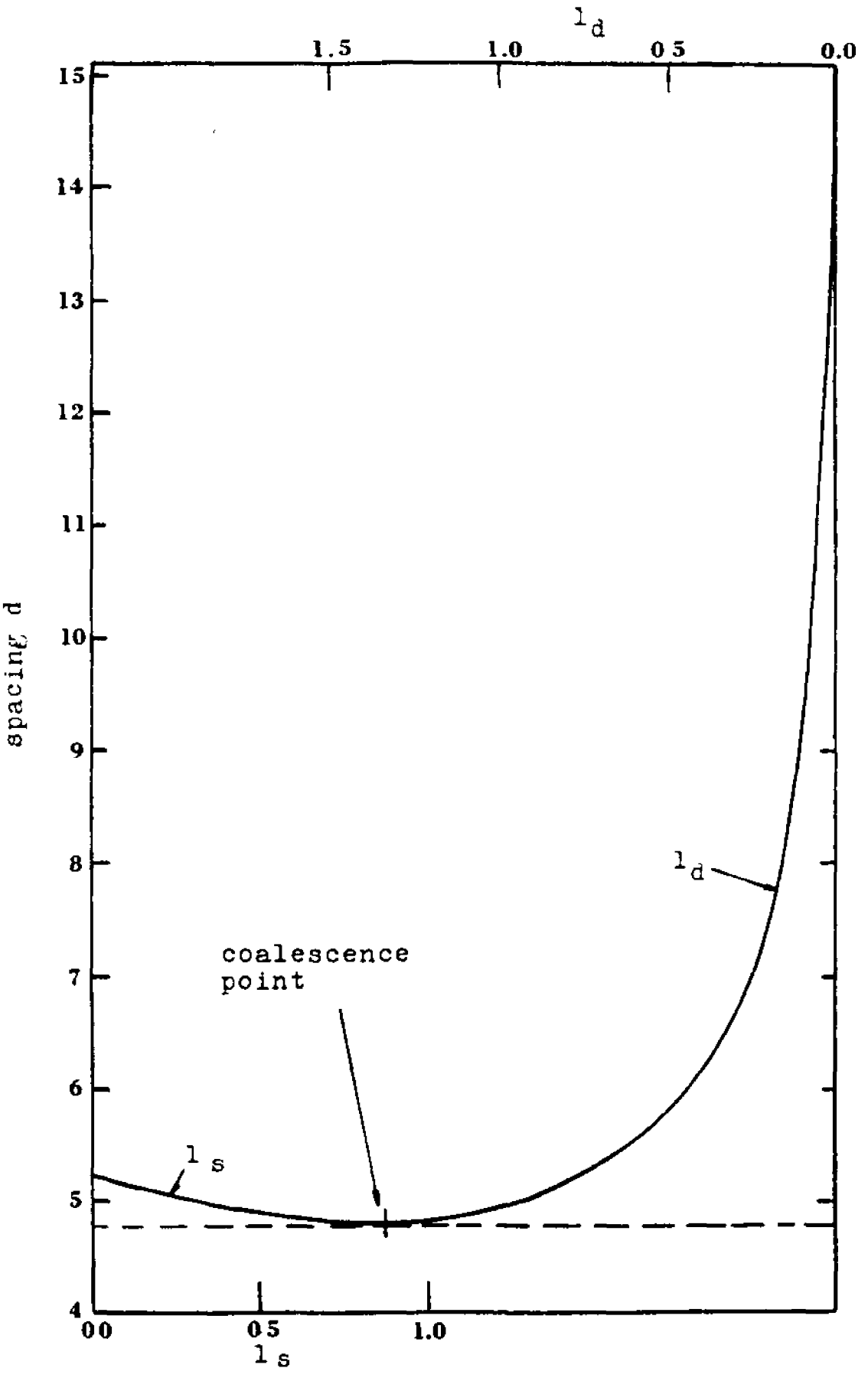

Figure III-12. Wake size : l_s for the sphere wake; l_d for the disk wake. a=2.5.

integrating the pressure over both the left and the right surfaces of the disk. The normal and tangential shear stress components on the surface of the disk have no contribution to the drag force. The normal component $\frac{\partial u_z}{\partial z}$, which can be expressed via the continuity equation in terms of the radial velocity component $\frac{1}{R}\frac{\partial R u_R}{\partial R}$, vanishes at Z=d and R< 1. The tangential component acts in the radial direction and, therefore, has no effect on the force in the Z direction. Hence,

$$F_d = 2\pi \int_0^1 \left[P^{I}(R,d) - P^{II}(R,d)\right] R\,dR =$$

$$16\,U_\infty + 16 \sum_{n=2}^{\infty} \left\{ B_n \frac{S_n(1,d)}{n} + D_n \frac{2n-3}{n(n-1)}\, d\, S_{n-1}(1,d) \right.$$

$$\left. - D_{n+1} \frac{n-2}{n^2-1} S_{n-1}(1,d) \right\} + \frac{1}{2} D_2 \cot^{-1} d \qquad \text{(III-3.27)}$$

were $S_n(1,d)$ is given by equation (III-2.47a)

Clearly, when the sphere is far from the disk ($d \to \infty$) equation (III-3.26) reduces to

$$F_d = 16\,U_\infty \qquad \text{(III-3.28)}$$

where F_d and U_∞ are dimensionless variables. Equation (III-3.28) is in agreement with the exact solution for uniform flow past a disk in the absence of the sphere.

The dimensionless drag force F_d was computed for both cases when the sphere is translating towards the disk and for the flow past the stationary sphere - disk

configuration. The drag correction factor for these two flows is defined respectively by

$$\lambda_d^{(v)} = \frac{F_d^{(v)}}{16\,V} \qquad \text{(III-3.29)}$$

$$\lambda_d^{(U_\infty)} = \frac{F_d^{(U_\infty)}}{16\,U_\infty} \qquad \text{(III-3.30)}$$

where U_∞ is the uniform stream velocity and V is the sphere velocity.

Results for $\lambda_d^{(v)}$ and $\lambda_d^{(U_\infty)}$ are shown in figures III-13 and III-14 respectively. Inspection of figure III-13 reveals that the drag on the disk increases monotonically with decreasing spacing when the sphere is moving towards the disk in quiescent fluid. When both the sphere and the disk are fixed in the uniform stream (figure III-14), the drag on a disk smaller than the sphere ($a \geq 1$) decreases monotonically with decreasing gap width to its minimum value at contact. However, when $a < 1$, the value of the drag is smallest before contact and increases slightly with decreasing gap width. A similar behaviour of the drag force has been shown for the motion of two unequal spheres along their line of centers (Cooley and O'Neill, 1968)

III-3.4 The axisymmetric motion of a neutrally buoyant sphere carried by a uniform flow towards a stationary disk.

In this subsection the motion of a neutrally

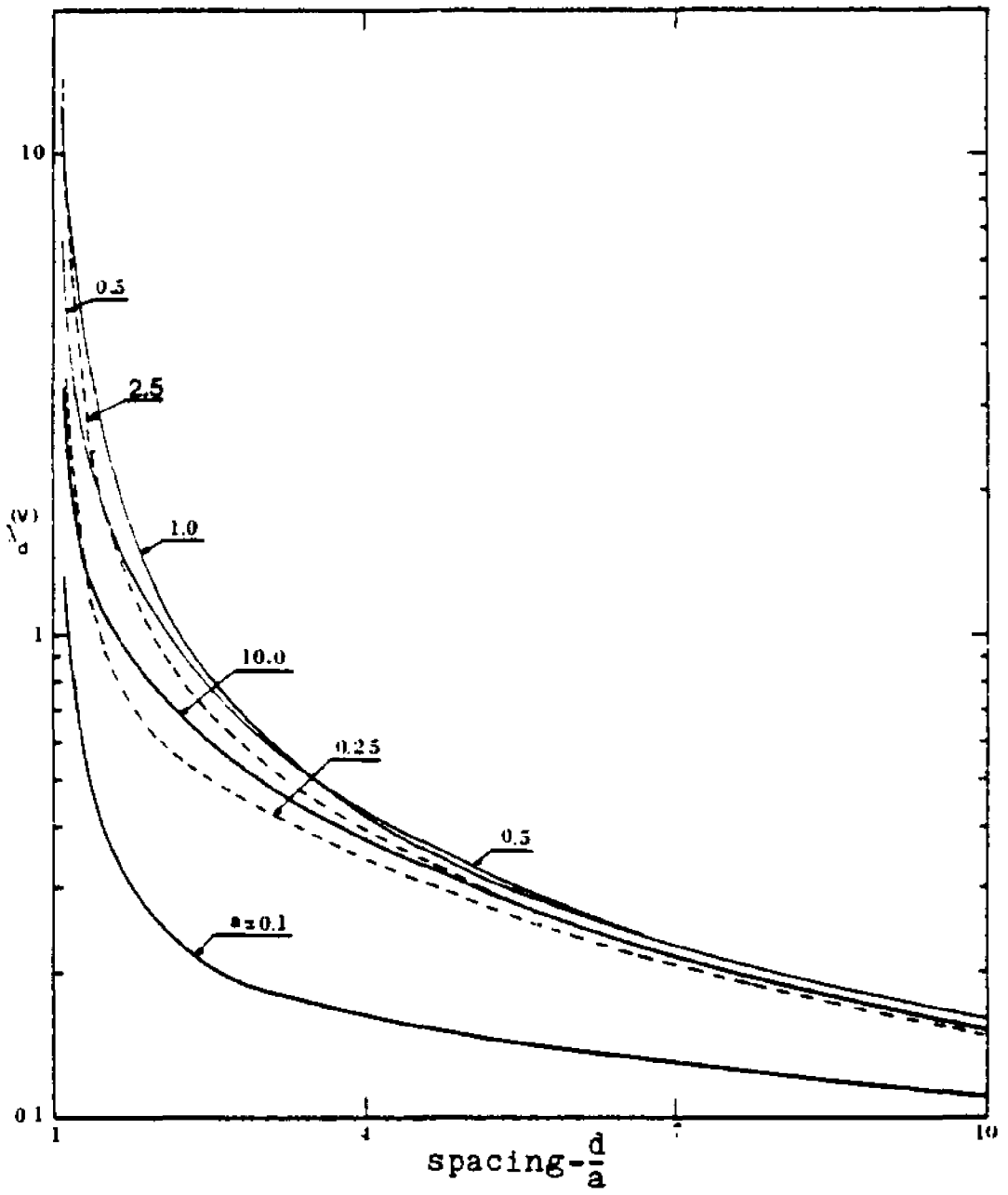

Figure III-13. Drag on a disk due to an axisymmetric motion of a sphere.

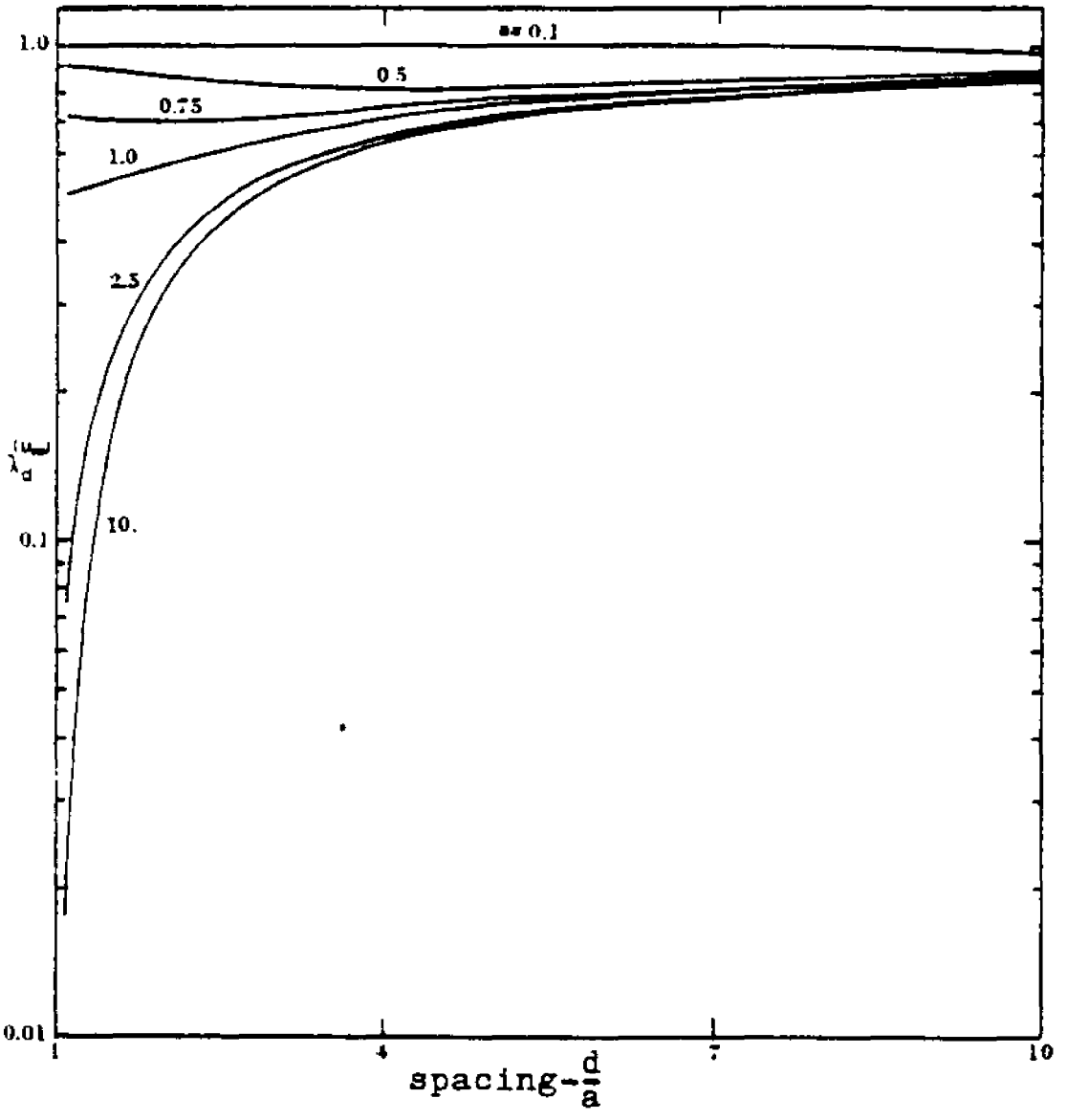

Figure III-14. Drag on a disk in a uniform flow past a sphere-disk configuration.

buoyant sphere carried by the flow towards a stationary disk is considered by superposing the two solutions presented in subsection III-3.2.

Using equation (III-3.25) and requiring zero net force on the sphere one obtains the expression for the sphere velocity V in the form

$$\frac{V}{U_\infty} = - \frac{\lambda^{(U_\infty)}}{\lambda^{(V)}} . \qquad \text{(III-3.31)}$$

Equation (III-3.31) can be written in an alternate form by introducing the local centerline velocity U in the absence of the sphere

$$\frac{U}{U_\infty} = \left[1 - \frac{2}{\pi}\left(\cot^{-1} d + \frac{d}{1+d^2}\right)\right]. \qquad \text{(III-3.32)}$$

Hence, (III-3.31) becomes

$$\frac{V}{U} = - \frac{\lambda^{(U_\infty)}}{\lambda^{(V)}} \left[1 - \frac{2}{\pi}\left(\cot^{-1} d + \frac{d}{1+d^2}\right)\right]^{-1} . \qquad \text{(III-3.33)}$$

Equation (III-3.33) is plotted in figure III-15 for various sphere sizes indicating that the sphere velocity increases above the local fluid velocity before it decays to zero as the sphere approaches the disk. The dashed extensions in this figure are extrapolated results for $\frac{d}{a} < 1.1$. Note that the actual distance d is plotted rather than $\frac{d}{a}$ so that the curves should not overlap.

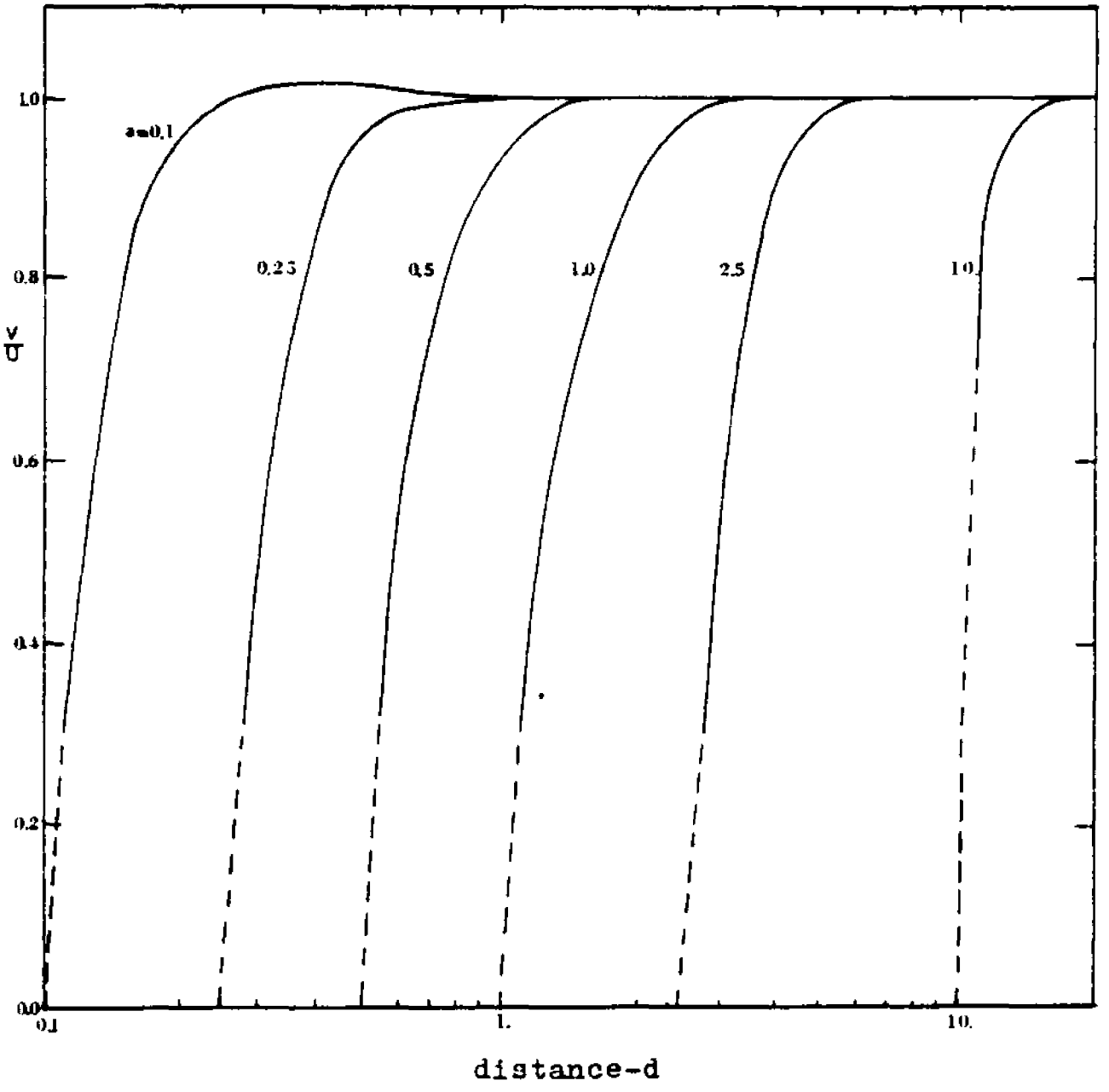

Figure III-15. Velocity of a neutrally buoyant sphere carried by a uniform flow towards a disk. ---- extrapolated results.

Appendix

This appendix contains a listing of the $A_i(\omega)$ and $B_i(\omega)$ functions (i=1,2) for the two problems considered in this chapter.

For the motion of a sphere towards an orifice, presented in section III-2 these functions are

$$A_1(\omega)\, e^{\omega d} = -\omega d \int_0^1 g(\xi) J_1(\omega\xi)\, d\xi + (1+\omega d)\int_0^1 f(\xi) J_0(\omega\xi)\, d\xi - \sum_{n=2}^{\infty} \left\{ B_n \left[B_n^{**}(\omega,d)(1+\omega d) + \omega d\, B_n^{*}(\omega,d) \right] + D_n \left[D_n^{**}(\omega,d)(1+\omega d) + \omega d\, D_n^{*}(\omega,d) \right] \right\} \qquad \text{(III-A-1)}$$

$$B_1(\omega)\, e^{\omega d} = \omega \left[\int_0^1 g(\xi) J_1(\omega\xi)\, d\xi - \int_0^1 f(\xi) J_0(\omega\xi)\, d\xi \right] + \omega \sum_{n=2}^{\infty} \left\{ B_n \left[B_n^{*}(\omega,d) + B_n^{**}(\omega,d) \right] + D_n \left[D_n^{*}(\omega,d) + D_n^{**}(\omega,d) \right] \right\} \qquad \text{(III-A-2)}$$

$$A_2(\omega)\, e^{-\omega d} = (1-\omega d)\int_0^1 f(\xi) J_0(\omega\xi)\, d\xi - \omega d \int_0^1 g(\xi) J_1(\omega\xi)\, d\xi \qquad \text{(III-A-3)}$$

$$B_2(\omega)\, e^{-\omega d} = \omega \left[\int_0^1 f(\xi) J_0(\omega\xi)\, d\xi + \int_0^1 g(\xi) J_1(\omega\xi)\, d\xi \right] \qquad \text{(III-A-4)}$$

For the motion of a sphere towards a disk, presented in section III-3.3, these functions are

$$A_1(\omega)\, e^{\omega d} = (1+\omega d)\int_1^{\infty} f(\xi) J_0(\omega\xi)\, d\xi - \omega \int_1^{\infty} g(\xi) J_1(\omega\xi)\, d\xi - \sum_{n=2}^{\infty} \left\{ B_n \left[B_n^{**}(\omega,d)(1+\omega d) + \omega d\, B_n^{*}(\omega,d) \right] + D_n \left[D_n^{**}(\omega,d)(1+\omega d) + \omega d\, D_n^{*}(\omega,d) \right] \right\} - V_\infty \left(\frac{1}{\omega} + d \right) J_1(\omega) \qquad \text{(III-A-5)}$$

$$B_1(\omega)\, e^{\omega d} = \omega \left[\int_1^\infty g(\xi) J_1(\omega\xi)\, d\xi - \int_1^\infty f(\xi) J_0(\omega\xi)\, d\xi \right]$$

$$+ U_\infty J_1(\omega) + \omega \sum_{n=2}^{\infty} \left\{ B_n \left[B_n^*(\omega, d) + B_n^{**}(\omega, d) \right] \right.$$

$$\left. + D_n \left[D_n^*(\omega, d) + D_n^{**}(\omega, d) \right] \right\} \qquad \text{(III-A-6)}$$

$$A_2(\omega)\, e^{-\omega d} = (1 - \omega d) \int_1^\infty f(\xi) J_0(\omega\xi)\, d\xi - \omega d \int_1^\infty g(\xi) J_1(\omega\xi)\, d\xi$$

$$- (1 - \omega d)\, U_\infty \frac{J_1(\omega)}{\omega} \qquad \text{(III-A-7)}$$

$$B_2(\omega)\, e^{-\omega d} = \omega \left[\int_1^\infty f(\xi) J_0(\omega\xi)\, d\xi + \int_1^\infty g(\xi) J_1(\omega\xi)\, d\xi \right]$$

$$- U_\infty J_1(\omega) \qquad \text{(III-A-8)}$$

CHAPTER IV

THREE DIMENSIONAL MOTION OF A SPHERE APPROACHING A PORE

IV-1. Introduction.

This chapter presents an approximate theory and validating experiments for the three-dimensional motion of a sphere approaching a circular cylindrical pore. Some recent biological applications where this flow geometry is important include the molecular sieving effects at the entrance to a pore in biological membranes, the filling of an attached plasmalemma vesicle with plasma proteins, and the non-uniform concentration profile that results when micron size particles such as red cells, enter a narrow tube from a feed reservoir (Fahraeus and Lindqvist, 1931). An important engineering application is the filtration of small aerosols through nuclepore filters.

The problem of three-dimensional creeping motion of a sphere approaching an orifice or a finite length pore in a plane wall cannot be treated by an exact theoretical approach because there is no natural co-ordinate system that can be used to satisfy the no-slip boundary conditions on the surface of the sphere and on the boundaries of the pore simultaneously. General three-dimensional problems involving the creeping motion of particles in viscous flow have been treated by four major approaches: the method of reflection, numerical finite difference schemes, the spherical bipolar co-ordinate transformation and the boundary collocation technique.

The method of reflection is a weak interaction theory that converges rapidly only when the sphere is five or more

diameters away from a boundary. Faxen (1923) used this method to obtain expressions for the force and torque acting on a sphere translating between two parallel planes using the five leading terms in the iterative series solution. This iterative method, which alternatly satisfies boundary conditions on the sphere and on the confining boundaries gives accurate results only if both walls are far removed from the surface of the sphere. At close sphere to wall spacings, the higher orderinteraction effects become significant and the leading terms of the iterative series give a poor description of the particle-wall interaction. Hence, the reflection technique cannot provide a good description of the motion of the sphere towards a pore when the sphere is close to the orifice wall.

The finite difference method has been used by Smith and Phillips (1975) and Parker and Buzzard (1977), who examined the problem of impaction of aerosol particles on a nuclepore filter. These authors first obtain numerical finite difference solutions to the Navier-Stokes equation for the fluid motion through the pore in the absence of the particle and then use this solution to calculate the trajectory of the sphere by applying a force balance in which the sphere's inertia is equated to the viscous drag force approximated by the local Stokes resistance for a particle in an unbounded fluid. This is a reasonable first approximation provided the particle is small and far from the boundaries of the pore where the sphere-orifice interaction

can be neglected. At best, the finite difference method can be used to describe a single three-dimensional flow configuration containing a finite size sphere in a vicinity of the pore, but the method is not presently feasible for treating time dependent motions involving continuously changing sphere-orifice configurations.

Useful information about the strong sphere-wall interaction when the sphere is near the orifice wall can be obtained from the results given by Brenner (1961) and Goldman, Cox and Brenner (1967a,b). The spherical bipolar co-ordinate transformation made it possible for Brenner (1961) to obtain an exact series solution for the drag on a sphere translating perpendicular to a single plane wall. Goldman, Cox and Brenner (1967a,b) used the same principle to obtain solutions for the rotation and translation of a sphere parallel to a plane wall in the presence of a linear shear field. This exact solution technique cannot be applied when the confining boundary is not an infinite plane wall since the solution is based on the limiting case of a spherical bipolar series expansion first introduced by O'Neill (1964) in which the radius of one of the spheres is taken as infinitely large. However, the results for the force and torque acting on a sphere near an infinite plane wall in those flow conditions can be used to estimate the force and torque acting on a particle approaching a pore when it is in close proximity of the confining wall provided the effect of the transverse curvature of the pore

is small.

In addition to the results obtained by Brenner (1961) and Goldman, Cox and Brenner (1967a,b) it is necessary to investigate the force acting on the sphere in the direction perpendicular to the orifice wall due to the pore induced velocity. The general flow problem of a sphere held rigidly in a velocity field perpendicular to the wall has not been studied before. This problem, which is treated by the boundary collocation technique, is an extension to the problem of flow past a sphere perpendicular to a disk presented in chapter III when the disk radius is much larger than the radius of the sphere. Although the boundary collocation technique is a strong interaction three-dimensional theory, it cannot be used to treat the general three-dimensional motion of a sphere towards a pore because of the long computation time required for the evaluation of the inversion integrals representing the disturbances generated by the sphere and detected on the pore boundaries.

Existing theoretical analyses by Pich(1964), Smith and Phillips (1975), Parker and Buzzard (1977) and Manton (1978), of the impaction of aerosols in the neighborhood of a circular hole in connection with the study of filtration through nuclepore filters, have neglected the hydrodynamic interaction between the particle and all boundaries, as mentioned previously, and considered only the effect of the particle inertia on its trajectory. In general, these studies predict that a particle will enter the pore when

its trajectory is within the critical trajectory along which a particle will impact the edge of the orifice. In the limit of zero Reynolds number the particle trajectory will become identical with the fluid streamline in the unperturbed flow since the sphere's interaction with the walls of the orifice is neglected. The critical streamline for this case is the one whose closest approach to the edge of the pore is equal to the particle radius and all particles outside this critical stream tube will be excluded from entering the pore.

The present study examines, for the first time, the effects of hydrodynamic interaction on the trajectory of the particle and demonstrates that for zero Stokes number the concept of the critical trajectory is invalid. The particle-wall interaction causes the particle trajectory to deviate significantly from the unperturbed fluid streamline when the particle is close to the wall. The particle will enter the pore regardless of its initial location. The initial position of the particle is important in determining the total time required for the particle to enter the pore from a specified distance. In this context it is necessary to redefine the critical trajectory based on the concept of "time dependent exclusion" of a particle from entering the pore.

In the present study an approximate solution procedure is developed for determining the trajectory of a neutrally buoyant sphere approaching a pore, valid in the far field and near the orifice wall provided the effect of

the transverse curvature of the pore is much smaller than the resistance to motion introduced by the planar boundary. In the immediate vicinity of the pore the hydrodynamic interaction coefficient is greatly affected by the complex three-dimensional entrance geometry and hence cannot be easily simplified. Therefore, for the near field, an experimental study is employed to determine the trajectory of a neutrally buoyant sphere and its departure from the approximate theory as well as the fluid streamline of the undisturbed flow field.

The general motion of a sphere towards the pore can be determined by superposition of three distinct flow situations: translation of a sphere in quiescent fluid near the wall in which the orifice is located, rotation of the sphere in fixed position near the orifice wall in quiescent fluid and flow past a rigidly held sphere into the pore. The total force and torque acting on the sphere is the vector sum of the contributions from these three flows. The formulation of this theory is presented in section IV-2. Section IV-3 contains the solutions for the far field particle trajectory. In section IV-4 the experimantal apparatus and method for determining the near field particle trajectory are described. In section IV-5 the experimental results are discussed and compared with the prediction of the three-dimensional far field theory. Finally, section IV-6 contains some comments about the particle exclusion effect for flow into a pore.

IV-2. Formulation of an approximate theory for the arbitrary motion of a sphere towards a pore.

In this section, the formulation for the trajectory of a sphere of arbitrary size in asymmetric flow towards a pore of finite diameter will be presented for the flow situation where the spacing between the sphere and the orifice wall is of the order of the sphere diameter. For these small spacings the boundary interaction produces significant deviations of the sphere trajectory from the undisturbed fluid streamline, and the critical trajectory does not coincide any longer with the critical streamline of the fluid in the absence of the sphere.

The geometry of the flow configuration is shown in figure IV-1. A neutrally buoyant sphere of radius a moves towards a pore of radius c with an instantaneous velocity (U_x, U_z) at an instantaneous position (X_o, Z_o) in the plane bisecting the sphere and containing the pore axis. The solution for the flow through a pore of finite length presented in chapter II, has established that the unperturbed flow field is properly described by Sampson's solution (1891) for the flow through a zero thickness orifice except for distances of less than half the pore radius from the edge of the pore opening. Hence, the length of the pore is immaterial in the formulation of the far field particle trajectory. Furthermore, even when the sphere is present in the flow field, the far field remains unchanged except in the vicinity of the sphere. Hence, the

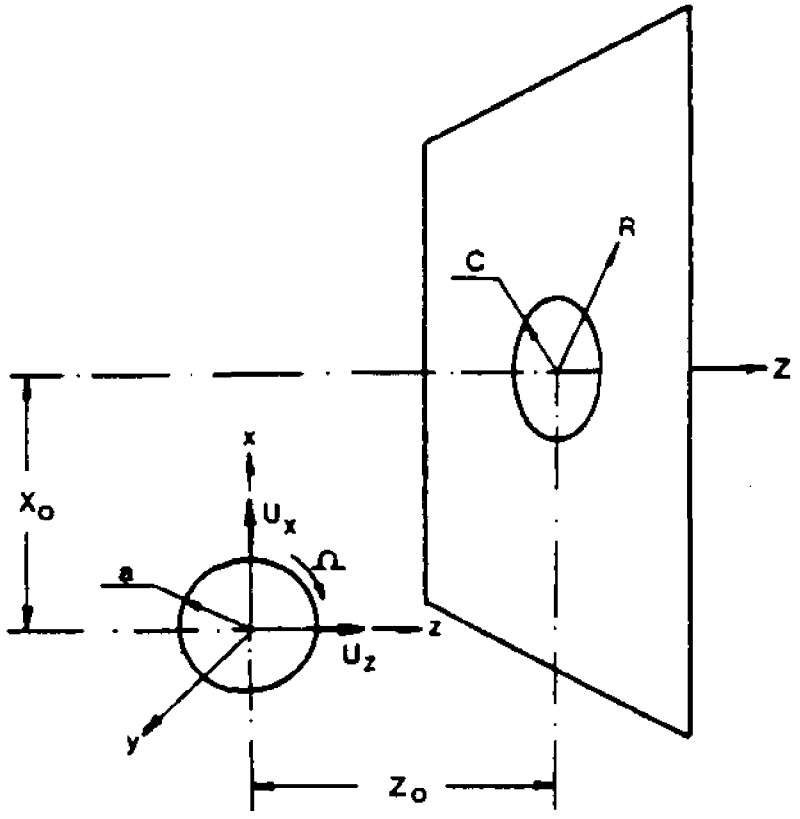

Figure IV-1. Geometry for the arbitrary motion of a sphere towards a pore.

fluid motion far from the pore entrance is well defined by Sampson's solution given by

$$\Psi = -\frac{Q}{2\pi}(1 - q^3) \qquad \text{(IV-2.1)}$$

where Ψ is the stream function, Q the volumetric flow rate and q is an oblate spheroidal co-ordinate that can be expressed in terms of cylindrical co-ordinates (R,Z) as follows

$$q^2 = 1 - \frac{1}{4C^2}(R_1 - R_2)^2 \qquad \text{(IV-2.2a)}$$

where

$$R_{1,2} = [Z^2 + (R \mp C)^2]^{1/2} \qquad \text{(IV-2.2b)}$$

Due to the linearity of the governing equations for Stokes flow, the general motion of a sphere towards a pore can be constructed from the superposition of the following asymmetric flows:

(a) translation without rotation of the sphere towards the pore parallel to the orifice wall, and translation without rotation perpendicular to the wall in quiescent fluid;

(b) rotation without translation of the sphere near the orifice wall in quiescent fluid;

(c) flow into the pore past a rigidly held sphere which obeys Sampson's solution at infinity.

These three flow situations exactly define the three-dimensional motion of the sphere. The flow in the

plane of the pore entrance is unknown but is not required in the solution procedure.

We will make use of the convenient notation of Goldman, Cox and Brenner (1967a,b) to define the force and the torque acting on the sphere in the problems outlined above, bearing in mind that these definitions are used here for a different flow configuration. For each of the problems mentioned, the force and torque are considered separately for motions perpendicular and parallel to the orifice wall.

The force and torque acting on a sphere translating without rotation parallel to the orifice wall with velocity U_x are defined as follows:

$$\vec{F} = 6\pi\mu a U_x F_x^t \hat{\imath}, \quad \vec{T} = 8\pi\mu a^2 U_x T_y^{t,x} \hat{\jmath} \qquad \text{(IV-2.3a,b)}$$

while for translation perpendicular to the orifice wall with velocity U_z they are given by

$$\vec{F} = 6\pi\mu a U_z F_z^t \hat{k}, \quad \vec{T} = 8\pi\mu a^2 U_z T_y^{t,z} \hat{\jmath} \qquad \text{(IV-2.4a,b)}$$

For a sphere rotating with angular velocity Ω about the y-axis in quiescent fluid the force is written in terms of its components as follows:

$$\vec{F} = 6\pi\mu a^2 \Omega F_x^r \hat{\imath} + 6\pi\mu a^2 \Omega F_z^r \hat{k} \qquad \text{(IV-2.5a)}$$

and the torque is

$$\vec{T} = 8\pi\mu a^3 \Omega T_y^r \hat{\jmath} \qquad \text{(IV-2.5b)}$$

The force and torque acting on a stationary sphere for flow into the pore is considered first in the x-direction:

$$\vec{F} = 6\pi\mu a\, V_R\, F_x^s\, \hat{\imath}, \qquad \vec{T} = 4\pi\mu \frac{a^3}{Z_o}\, V_R\, T_y^{s,x}\, \hat{\jmath} \qquad \text{(IV-2.6a,b)}$$

where V_R is the undisturbed local radial fluid velocity and the superscript s represents Sampson's solution for the flow through an orifice. The definition of the torque in (IV-2.6b) is based on a similar definition for shear flow past a sphere near an infinite wall.

Similar definitions for the force and the torque acting on the sphere in the z-direction are:

$$\vec{F} = 6\pi\mu a\, V_Z\, F_z^s\, \hat{k}, \qquad \vec{T} = 6\pi\mu \frac{a^3}{X_o}\, T_y^{s,z}\, \hat{\jmath} \qquad \text{(IV-2.7a,b)}$$

where V_Z is the local undisturbed axial fluid velocity.

The undisturbed fluid velocity components can be obtained directly from equations (IV-2.1) and (IV-2.2) and are given by

$$V_R = -\frac{1}{R}\frac{\partial \Psi}{\partial Z} = \frac{3Q}{8\pi C^2}\, \frac{|Z|}{R}\, \eta\, (R_1 - R_2)\left(\frac{1}{R_1} - \frac{1}{R_2}\right) \qquad \text{(IV-2.8a)}$$

$$V_Z = \frac{1}{R}\frac{\partial \Psi}{\partial R} = -\frac{3Q}{8\pi C^2}\, \frac{\eta}{R}\, (R_1 - R_2)\left(\frac{R-C}{R_1} - \frac{R+C}{R_2}\right) \qquad \text{(IV-2.8b)}$$

The total force and torque acting on the sphere is simply the vector sum of the individual contributions, i.e.

$$\vec{F} = 6\pi\mu a \left[\left(U_x F_x^t + V_R F_x^s + a\Omega F_x^r \right) \hat{i} + \left(U_z F_z^t + V_z F_z^s + a\Omega F_z^r \right) \hat{k} \right] \qquad \text{(IV-2.9)}$$

$$\vec{T} = 8\pi\mu a^2 \left(U_x T_y^{t,x} + U_z T_y^{t,z} + \frac{a}{2Z_o} V_R T_y^{s,x} + \frac{a}{2X_o} V_z T_y^{s,z} + a\Omega T_y^r \right) \hat{j} \qquad \text{(IV-2.10)}$$

For the special case of interest of a neutrally buoyant sphere being carried by the flow into the pore the conditions of zero force and torque on the sphere require:

$$U_x F_x^t + V_R F_x^s + a\Omega F_x^r = 0 \qquad \text{(IV-2.11a)}$$

$$U_z F_z^t + V_z F_z^s + a\Omega F_z^r = 0 \qquad \text{(IV-2.11b)}$$

$$U_x T_y^{t,x} + U_z T_y^{t,z} + \frac{1}{2Z_o} V_R T_y^{s,x} + \frac{1}{2X_o} V_z T_y^{s,z} + a\Omega T_y^r = 0 \qquad \text{(IV-2.11c)}$$

Simultaneous solution of these equations for the sphere velocity components and angular velocity yields

$$a\Omega = \left[T_y^r - \frac{F_x^r}{F_x^t} T_y^{t,x} - \frac{F_z^r}{F_z^t} T_y^{t,z} \right]^{-1} X$$

$$\left\{ V_R \left[\frac{F_x^s}{F_x^t} T_y^{t,x} - \frac{a}{2Z_o} T_y^{s,x} \right] + V_z \left[\frac{F_z^s}{F_z^t} T_y^{t,z} - \frac{a}{2X_o} T_y^{s,z} \right] \right\} \qquad \text{(IV-2.12a)}$$

$$U_x = -\frac{1}{F_x^t} \left(V_R F_x^s + a\Omega F_x^r \right) \qquad \text{(IV-2.12b)}$$

$$U_z = -\frac{1}{F_z^t} \left(V_z F_z^s + a\Omega F_z^r \right) \qquad \text{(IV-2.12c)}$$

Using this results and the relations

$$\frac{d}{dt}\left(X_o\,\hat{\imath} + Z_o\,\hat{k}\right) = U_x\,\hat{\imath} + U_z\,\hat{k} \qquad \text{(IV-2.13)}$$

the governing equation for the trajectory of the sphere is

$$\frac{dZ_o}{dX_o} = \frac{F_x^t}{F_z^t}\cdot\frac{V_z F_z^s + a\Omega F_z^r}{V_R F_x^s + a\Omega F_x^r} \qquad \text{(IV-2.14)}$$

where V_R and V_Z are given by equations (IV-2.8a,b), Ω by equation (IV-2.12a) and the right hand side of (IV-2.14) is evaluated at the center of the sphere (X_o, Z_o).

Clearly, the exact sphere trajectory can be obtained by integrating (IV-2.14) provided the hydrodynamic interaction coefficients are known. These coefficients, defined by equations (IV-2.3)-(IV-2.7), cannot be obtained exactly for the problem at hand. Therefore, by order of magnitude analysis, the hydrodynamic interaction coefficients will be estimated and an approximate equation for the sphere trajectory will be derived.

IV-2.1 Simplification of equation (IV-2.14).

For small sphere to wall spacings the transverse curvature effect of the circular pore on the hydrodynamic correction coefficients is much smaller than the resistance to motion introduced by the planar boundary. Hence, the force and torque are essentially similar to those acting on a sphere near an infinite plane wall under the same flow conditions. The problem of a sphere near an infinite plane

wall under various flow conditions has been studied extensively. Results for the force and torque acting on a sphere translating parallel to a wall or held rigidly in Couette flow parallel to the wall are presented in Goldman, Cox and Brenner (1967a,b), while the problem of a sphere translating perpendicular to a wall is given in Brenner (1961).

First, we examine the results for the resistance coefficients for the forces acting in the x-direction due to sphere or fluid motion and the torque due to sphere rotation or fluid motion parallel to the orifice wall. The magnitude of these coefficients is shown in figure IV-2 for $1.1 \leq \frac{Z_o}{a} \leq 10$. Examination of these results indicate that the ratio of the force coefficient for a sphere in shear flow to the force coefficient for translation is of order one, while the force coefficient in the x-direction due to rotation is one order of magnitude smaller when the gap width is 0.1a, and decreses in magnitude to $O(10^{-6})$ at $\frac{Z_o}{a} \sim O(10)$. In addition, the torque coefficient for a sphere due to rotation or shear flow is found to be of order one, while the torque coefficient for translation in the x-direction is $O(10^{-1})$ for small gap width and decreases with increasing distance between the sphere and the wall. Hence

$$\left|\frac{F_x^s}{F_x^t}\right| T_y^{t,x} \ll \frac{a}{2Z_o} T_y^{s,x} \qquad \text{(IV-2.15a)}$$

$$\left|\frac{F_x^r}{F_x^t}\right| T_y^{t,x} \ll T_y^r \qquad \text{(IV-2.15b)}$$

$$F_x^r \ll F_x^s \qquad \text{(IV-2.15c)}$$

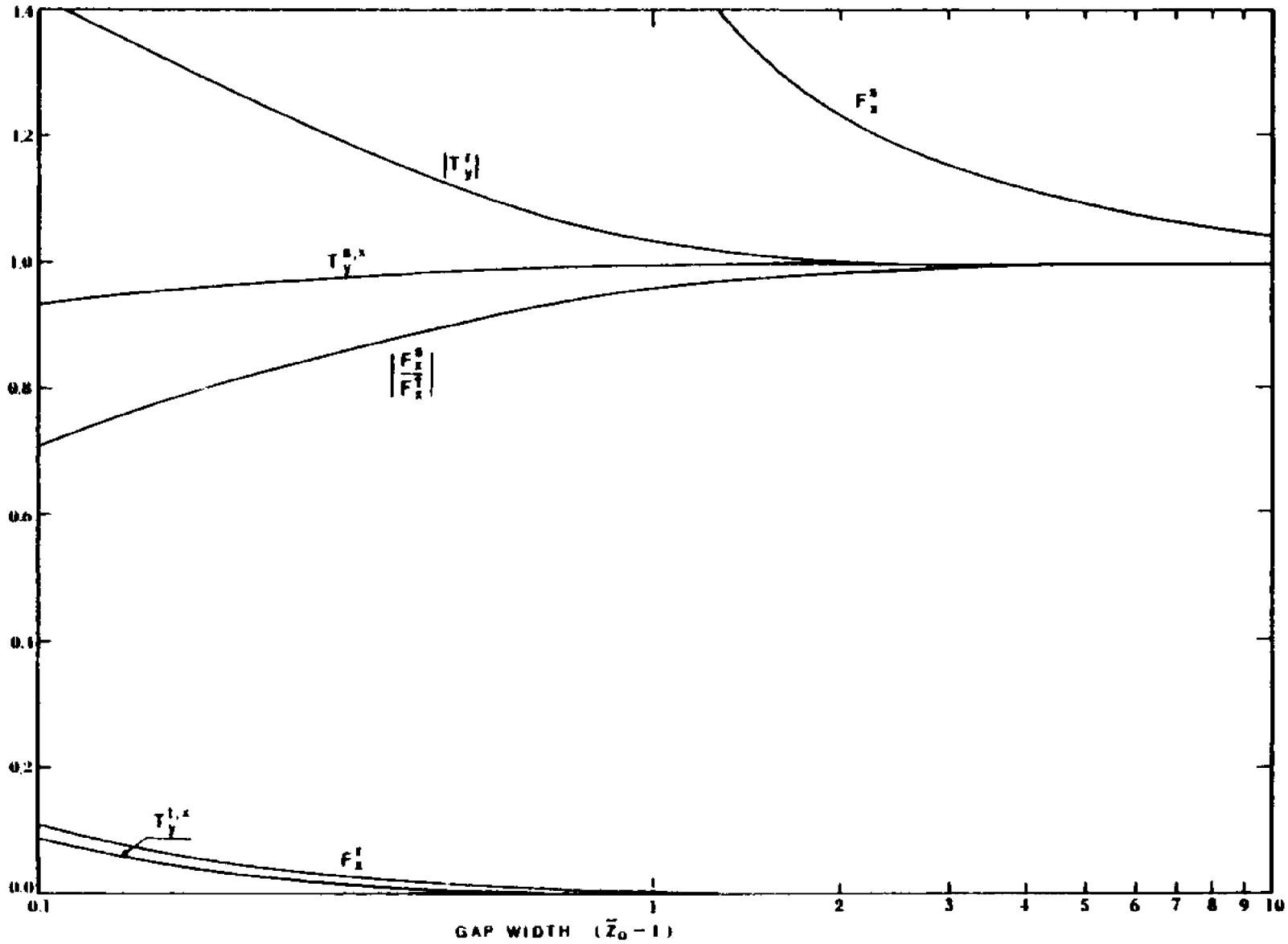

Figure IV-2. Hydrodynamic interaction coefficients for the force and torque acting on a sphere parallel to a plane wall. (plotted from the results given in Goldman, Cox & Brenner, 1967a,b)

The resistance coefficients for the motion of the sphere in the z-direction and for the flow past a sphere with velocity V_Z are expected to have similar relative importance as those for the parallel motion. The perpendicular three-dimensional motion of a sphere towards a planar boundary with an orifice can be approximated by an axisymmetric motion of a sphere towards an infinite plane. This approximation neglects the induced velocity at the orifice opening which is very small when the sphere is moving in quiescent fluid near the orifice wall. Hence, the contributions to the force in the z-direction due to rotation and the torque due to translation perpendicular to the wall are neglected. Namely

$$F_z^r \ll 1. \qquad \text{(IV-2.16a)}$$

$$T_y^{t,z} \ll 1. \qquad \text{(IV-2.16b)}$$

Making use of the observations (IV-2.15) and (IV-2.16) when $\frac{z_o}{a} \geq 1.1$, equations (IV-2.12) reduce to

$$\Omega = -\frac{1}{T_y^r}\left(\frac{V_R}{2z_o} T_y^{s,x} + \frac{V_z}{2x_o} T_y^{s,z}\right) \qquad \text{(IV-2.17a)}$$

$$U_x = -V_R \frac{F_x^s}{F_x^t} \qquad \text{(IV-2.17b)}$$

$$U_z = -V_z \frac{F_z^s}{F_z^t} \qquad \text{(IV-2.17c)}$$

and the resulting governing equation for the sphere trajectory becomes:

$$\frac{dZ_o}{dX_o} = \frac{V_z}{V_R}\left[\frac{F_z^s}{F_z^t}\cdot\frac{F_x^t}{F_x^s}\right] \qquad \text{(IV-2.18)}$$

The approximate trajectory equation (IV-2.18) excludes the effect of rotation on the motion of the sphere. This is consistent with the strong interaction solutions presented by Ganatos, Pfeffer and Weinbaum (1978, Fig.10) for the settling of three equally spaced spheres under gravity, and for the arbitrary motion of a sphere between two parallel plates in Poiseuille flow (private communications with Dr. P. Ganatos). The effect of rotation on the sphere trajectory in both cases was found to be very small. Furthermore, the angular velocity itself given by (IV-2.17a) cannot be evaluated because there is no existing solution for the hydrodynamic interaction coefficient $T_y^{s,z}$, representing the torque on a stationary sphere near a plane wall due to shear flow perpendicular to the wall.

In order to solve equation (IV-2.18) it is necessary to obtain numerical values for the translation force coefficients F_x^t and F_z^t and the force coefficients arising from the flow past a rigidly held sphere into the pore F_x^s and F_z^s. The evaluation of these coefficients will now be presented.

IV-2.2 Hydrodynamic force coefficients for pure translation.

Due to the small induced velocity at the pore opening in pure translatory motio. of the sphere, the motion

can be approximated by translation towards an infinite plane wall, provided the sphere is not in the vicinity of the pore opening.

Numerical results for the hydrodynamic resistance coefficients for a sphere translating perpendicular to an infinite plane wall have been obtained by Brenner (1961) and will be used to represent F_z^t. The force coefficient, representing F_x^t, for motion parallel to an infinite wall was first obtained by O'Neill (1964) and is presented in Goldman et al (1967a). Values of these translation coefficients are given in table IV-1 for various sphere to wall spacings Zo/a. The results are also presented for values of $\alpha = \cosh^{-1}\left(\frac{z_o}{a}\right)$ which is the bipolar co-ordinate parameter used in Brenner (1961).

IV-2.3 Hydrodynamic force coefficients due to flow past a rigidly held sphere into the pore.

The flow past a stationary sphere into a pore can be separated into two distinct cases: flow parallel to the orifice wall and flow perpendicular to the wall where the far field satisfies Sampson's solution (1891) for the flow through an orifice. When the sphere is rigidly held near the orifice wall the Sampson velocity component V_R parallel to the wall resembles simple Couette flow. Neglecting the small induced velocity at the pore opening and the transverse curvature effect of the pore, one can approximate the behaviour of F_x^s by the force coefficient due to Couette

Table IV-1. Hydrodynamic force coefficients for pure translation and for flow past a rigidly held sphere into a pore.

$\alpha=\cosh^{-1}\frac{Z_o}{a}$	$\frac{Z_o}{a}$	F_z^{t} *	F_x^{t} **	F_z^{s}	F_x^{s} ***
0.0	1.0	$-\infty$	$-\infty$	--	1.7005
0.5	1.1276	-9.2518	-2.1514	3.3584	1.6160
1.0	1.5431	-3.0361	-1.5675	2.4858	1.4391
1.5	2.3524	-1.8375	-1.3079	1.8248	1.2780
2.0	3.7622	-1.4129	-1.1738	1.4429	1.1671
3.0	10.068	-1.1252	-1.0591	1.1332	1.0587
∞	∞	-1.0	-1.0	1.0	1.0

* Brenner (1961)
** Goldman, Cox & Brenner (1967a)
*** Goldman, Cox & Brenner (1967b)

flow past a sphere held near an infinite plane wall. Numerical values of this coefficient were obtained by Goldman et al (1967b) and are presented in table IV-1.

The force coefficient F_z^s arising from the problem of the flow perpendicular to the orifice wall past a stationary sphere near the orifice wall can be approximated by considering the axisymmetric uniform flow past a sphere perpendicular to a disk (Fig.IV-3) in the limit when the sphere radius a' is much smaller than the radius of the disk c'. This approximation is valid near the orifice wall, since the velocity gradient in the radial direction is small and can be neglected. When the disk radius is large compared to the sphere radius, the velocity profile at the plane of the disk Z'=d' for $R' > c'$ is similar to the undisturbed profile in the absence of the sphere. Thus, the problem can be solved in the infinite half space containing the sphere with a prescribed velocity profile at the plane of the disk. which vanishes at the surface of the disk and satisfies Sampson's solution (1891) for $R' > c'$. The solution procedure (see appendix) is similar to that shown in chapter III, but with the shear stress matching condition at Z'=d' relaxed since Sampson's disk velocity profile is assumed at the plane of the disk. We first satisfy the no-slip boundary condition on the surface of the disk analytically using Hankel inversion formulae. Then, the boundary collocation technique is employed to satisfy the no-slip boundary conditions at discrete points on the surface of the sphere.

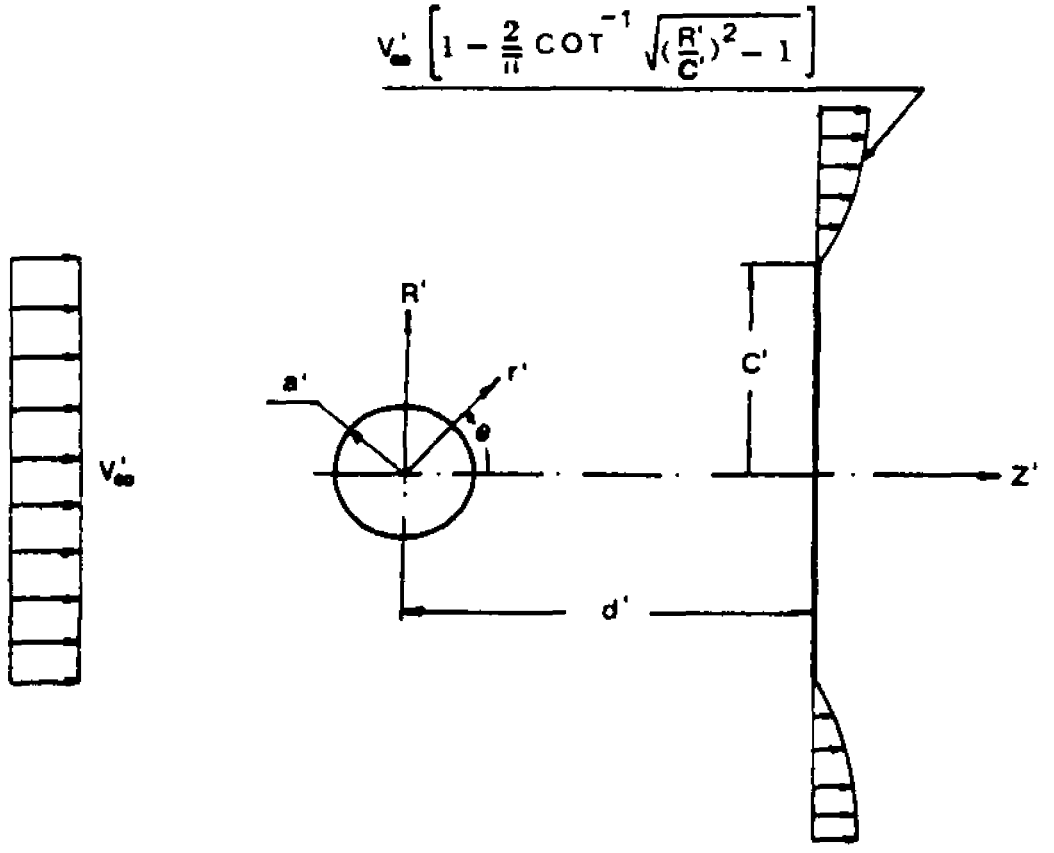

Figure IV-3. Geometry for the problem of flow past a sphere held rigidly near a disk with imposed velocity profile at the plane of the disk.

The drag correction factor λ is defined as follows:

$$F = 6\pi\mu a' V_\infty' \lambda \qquad \text{(IV-2.19)}$$

where F is the force acting on the sphere. Numerical values of λ are presented in table IV-A-1 for various sphere radii and sphere to wall spacings. The results are also plotted in figure IV-4 excluding the curve for $\frac{a'}{c'} = 0.01$ due to the small magnitude of λ for this configuration.

An alternate expression for the force acting on the sphere can be written using the undisturbed local fluid velocity as follows

$$F = 6\pi\mu a' V_L' \lambda_L \qquad \text{(IV-2.20)}$$

where V_L is given by Sampson (1891) for flow past a disk in the absence of the sphere

$$\frac{V_L'}{V_\infty'} = 1 - \frac{2}{\pi}\left[\cot^{-1}\frac{d'}{c'} + \frac{\frac{d'}{c'}}{1 + \left(\frac{d'}{c'}\right)^2}\right] \qquad \text{(IV-2.21)}$$

Hence, the hydrodynamic interaction coefficient λ_L can be obtained from the equation

$$\lambda_L = \lambda \frac{V_\infty'}{V_L'} \qquad \text{(IV-2.22)}$$

Results for λ_L are plotted in figure IV-5. Clearly, for small ratios of sphere to disk radius the results

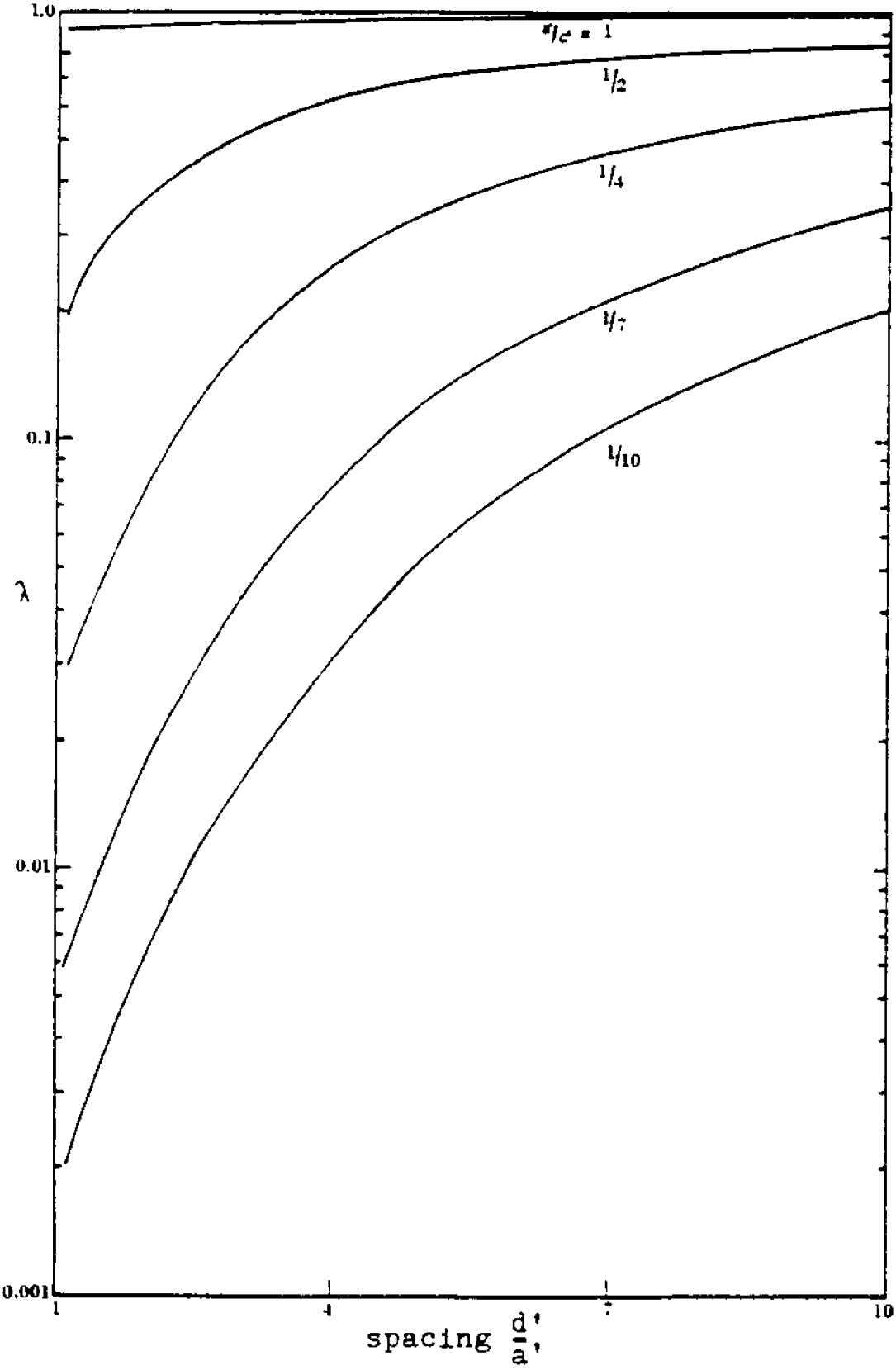

Figure IV-4. Drag on a sphere held rigidly in an imposed velocity field at the plane of the disk.

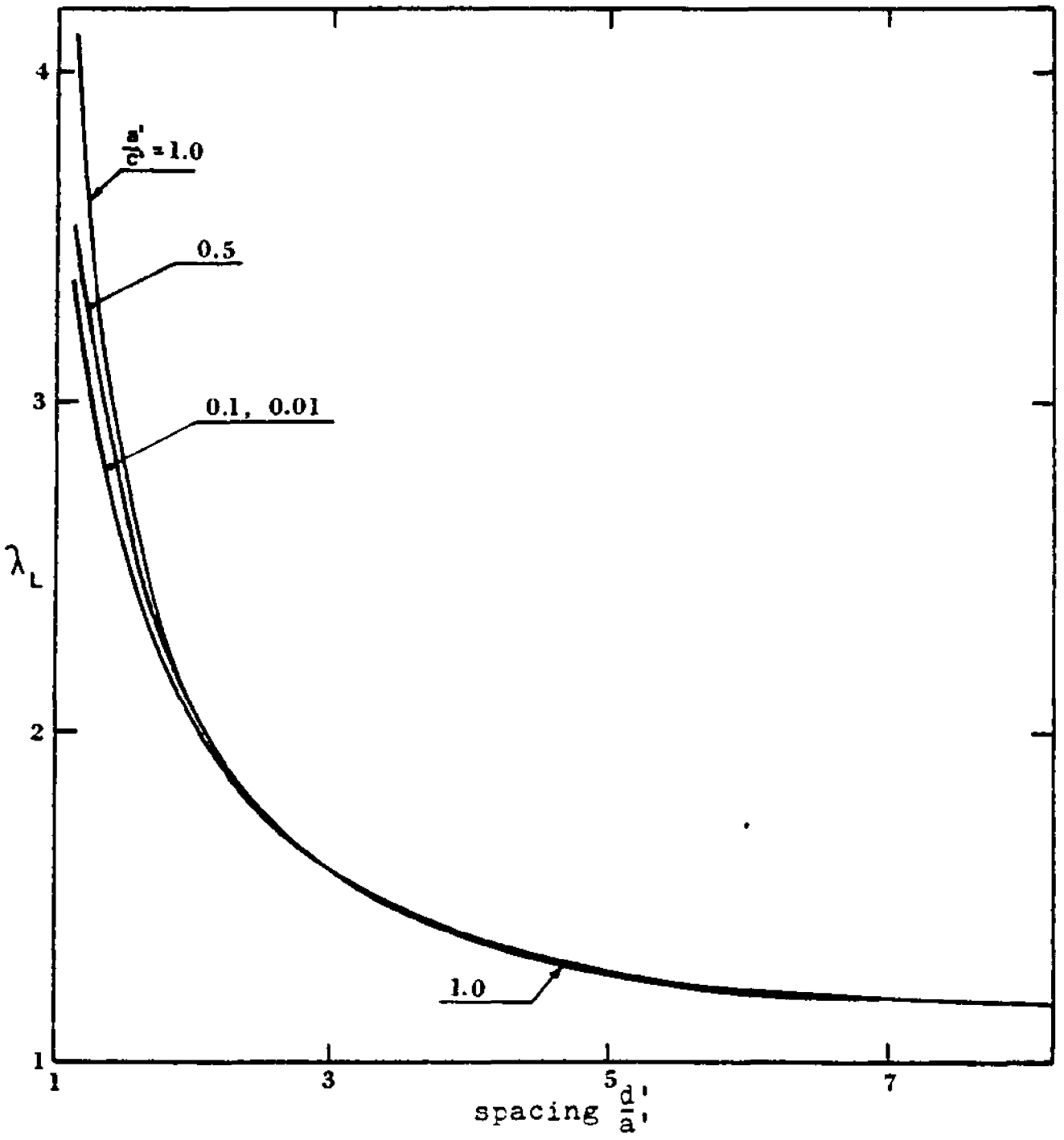

Figure IV-5. Rescaled drag on a sphere held rigidly in an imposed velocity profile at the plane of the disk.

converge into a single curve independent of that ratio. The values of λ_L which will be used to represent F_z^s are shown in table IV-1.

IV-3. Solution for the far field sphere trajectory.

For the purpose of numerical integration of (IV-2.18) it is advantageous to scale the co-ordinates with respect to the pore radius c. Substituting (IV-2.8) into (IV-2.18) and rescaling one obtains the equation

$$\frac{d\tilde{Z}_o}{d\tilde{X}_o} = \left[\frac{(\tilde{R}_1+\tilde{R}_2)^2}{4\tilde{X}_o} - \tilde{X}_o\right]\frac{\lambda(\tilde{Z}_o)}{\tilde{Z}_o} \qquad \text{(IV-3.1a)}$$

where the tilde denotes dimensionless variables, $\tilde{R}_1$ and $\tilde{R}_2$ are evaluated at $\tilde{R}=\tilde{X}_o$, $\tilde{Z}=\tilde{Z}_o$ and $\lambda(\tilde{Z}_o)$ is given by

$$\lambda(\tilde{Z}_o) = \frac{F_z^s}{F_z^t}\cdot\frac{F_x^t}{F_x^s} \qquad \text{(IV-3.1b)}$$

Numerical values for $\lambda(\tilde{Z}_o)$ are presented in table IV-2. $\tilde{Z}_o$ represents the distance of the sphere from the wall in sphere radii, and the bispherical parameter α is defined by $\alpha=\cosh^{-1}\tilde{Z}_o$. $\lambda(1)$, representing the value of the interaction function when the sphere is in contact with the wall, was calculated using the leading terms of the asymptotic expressions for small gap width obtained by Goldman et al (1967) and Brenner (1967) for F_x^t and F_z^t. The value of F_z^s for this limiting case , although undetermined, is finite and does not affect the value of $\lambda(\tilde{Z}_o)$ when $\tilde{Z}_o \to 1$.

The correction function $\lambda(\tilde{Z}_o)$ is a first order approximation for the hydrodynamic sphere-orifice interaction which neglects the curvature of the radial co-ordinate system and the effect of the sphere rotation. Examination

of the numerical values of $\lambda(\tilde{Z}_o)$ indicates that it is slightly larger than 1.0 for $\tilde{Z}_o \gtrsim 2.35$ and decreases to 1.0 as $\tilde{Z}_o \to \infty$ with a maximun value of about 1.03 at $\tilde{Z}_o \simeq 3.76$. This behaviour is intuitively unexpected because it predicts that the sphere trajectory will be closer to the orifice wall than the undisturbed streamline passing through the same initial position. This behaviour results from the axisymmetric approximation for the perpendicular motion discussed in section IV-2.3. As shown in chapter III (see also appendix, Fig. A-1), a neutrally buoyant sphere carried by a uniform flow at infinity translates towards a disk with a velocity larger than the local fluid velocity in the absence of the sphere for $\frac{d'}{a'} \gtrsim 2.5$. This effect should necessarily be diminished in asymmetric flow such as to maintain $0 \lesssim (\tilde{Z}_o) \lesssim 1$ for all $\tilde{Z}_o$. Furthermore, since $\lambda(\tilde{Z}_o)$ represents only first order effects it is sufficient to employ a convenient expression to estimate its numerical value. Two approximate expression have been chosen for this purpose and are compared with the theoretically predicted values of $\lambda(\tilde{Z}_o)$ in table IV-2.

Numerical integration of (IV-2.18) has been carried out for $\frac{a}{c}=\frac{1}{2}$ and the two proposed functions $\lambda_1(\tilde{Z}_o)$ and $\lambda_2(\tilde{Z}_o)$. The resulting trajectories are shown in figure IV-6 and are compared with Sampson's solution for the streamlines in the flow through an orifice in the absence of the sphere. The results indicate that the motion of the sphere departs significantly from the fluid streamline with a marginal

Table IV-2. Hydrodynamic interaction functions.

$\alpha = \cosh^{-1}\tilde{z}_o$	$\tilde{z}_o$	$\lambda(\tilde{z}_o)$	$\lambda_1(\tilde{z}_o) = \tanh(\alpha)$	$\lambda_2(\tilde{z}_o) = \tanh(\sinh\alpha)$
0.0	1.0	0.0	0.0	0.0
0.5	1.13	0.483	0.462	0.478
1.0	1.54	0.892	0.762	0.824
1.5	2.35	1.02	0.905	0.975
2.0	3.76	1.03	0.964	0.998
3.0	10.1	1.01	0.995	1.0
∞	∞	1.0	1.0	1.0

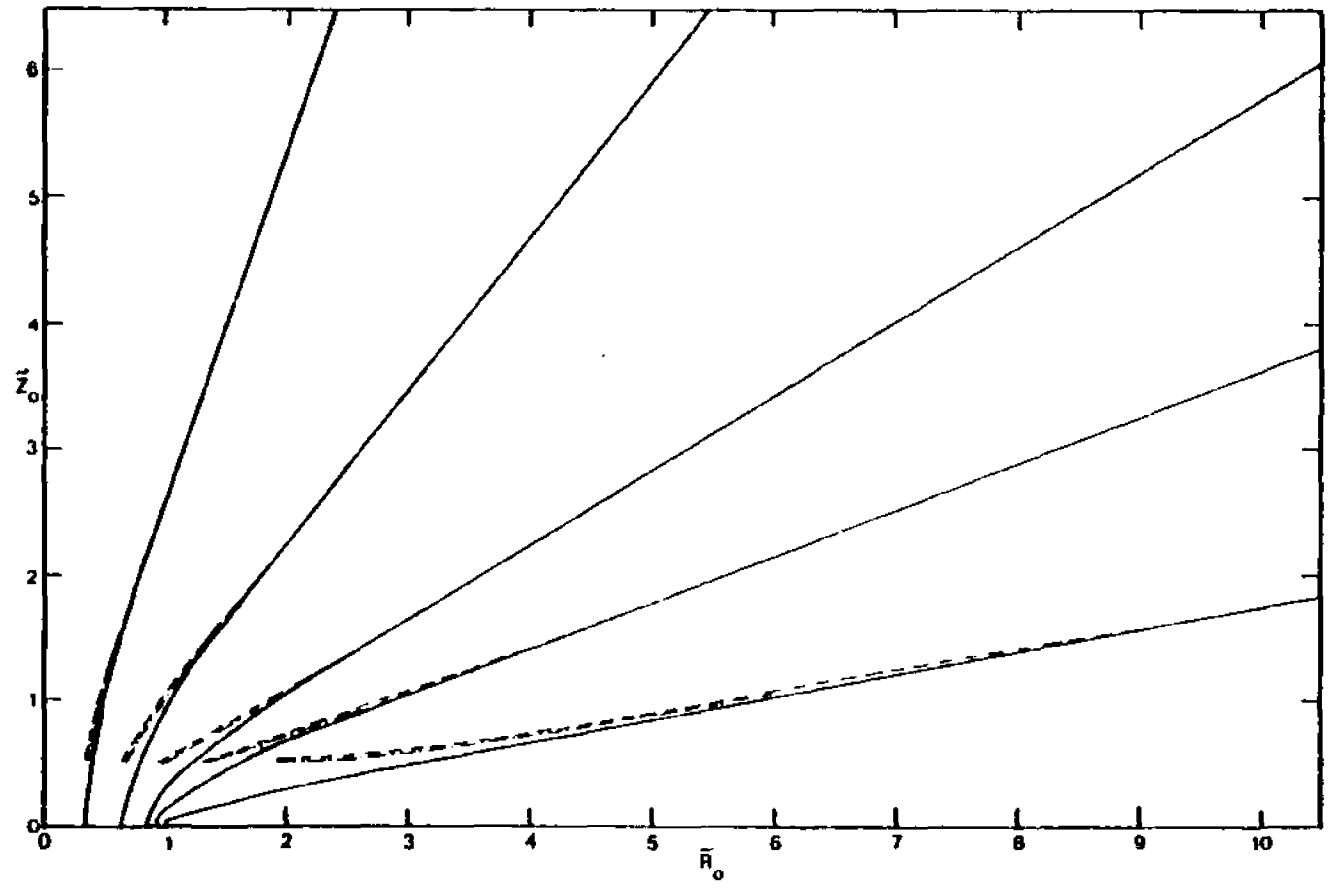

Figure IV-6. Theoretically predicted trajectories for a neutrally buoyant sphere carried by the fluid towards a pore. a/c=0.5; ———— undisturbed fluid streamlines, - - - - trajectories calculated with $\lambda_1(\tilde{Z}_o)$, -·-·-·- trajectories calculated with $\lambda_2(\tilde{Z}_o)$.

shift based on the choice of the correction function $\lambda(\tilde{Z}_o)$.

Bearing in mind the simplicity of the computation involved in the solution presented, the results seem to be qualitatively encouraging. However, a quantitative comparison between the theoretical results and experimantal measurements is necessary especially for the behaviour in the vicinity of the pore opening where the transverse curvature effect is considerable. Thus, an experimental study of the motion of a neutrally buoyant sphere towards a pore was undertaken.

IV-4. Experimental apparatus and method.

This section is devoted to a description of the experimental apparatus and the method of measuring the trajectory of a neutrally buoyant sphere towards a pore of finite length and diameter.

The apparatus constructed consists of a square glass tank 18in.x18in.x82in. in which a glass tube 2 in. long with I.D of $1\frac{1}{8}$ in. was installed between two parallel plates as shown in figure IV-7, and suspended with wires from the top of the tank. A dropping mechanism, consisting of a thin-walled brass tube with an O.D. of $\frac{1}{8}$ in., was attached to a sliding block and carefully mounted on the top of the tank so that the tube can be moved laterally and vertically to any desirable location. The tube was connected through a flexible hose to a vacuum pump which was used to hold the sphere at the lower end of the tube. The tank was equipped with a closed nipple set between two $1\frac{1}{4}$ in. brass gate valves to control the flow.

The experiments were performed in a relatively constant temperature room which was maintained at 70°F by a thermostatically controlled room air conditioner in order to insure that the viscosity of the fluid and its density remain constant. The fluid used, a polyalkylene glycol type UCON HB-3520 fluid, shows a comparatively small change in viscosity and density with temperature and is also extremely stable. The viscosity was measured using Brookfield Synchro-Lectric LVT viscometer and the density was measured

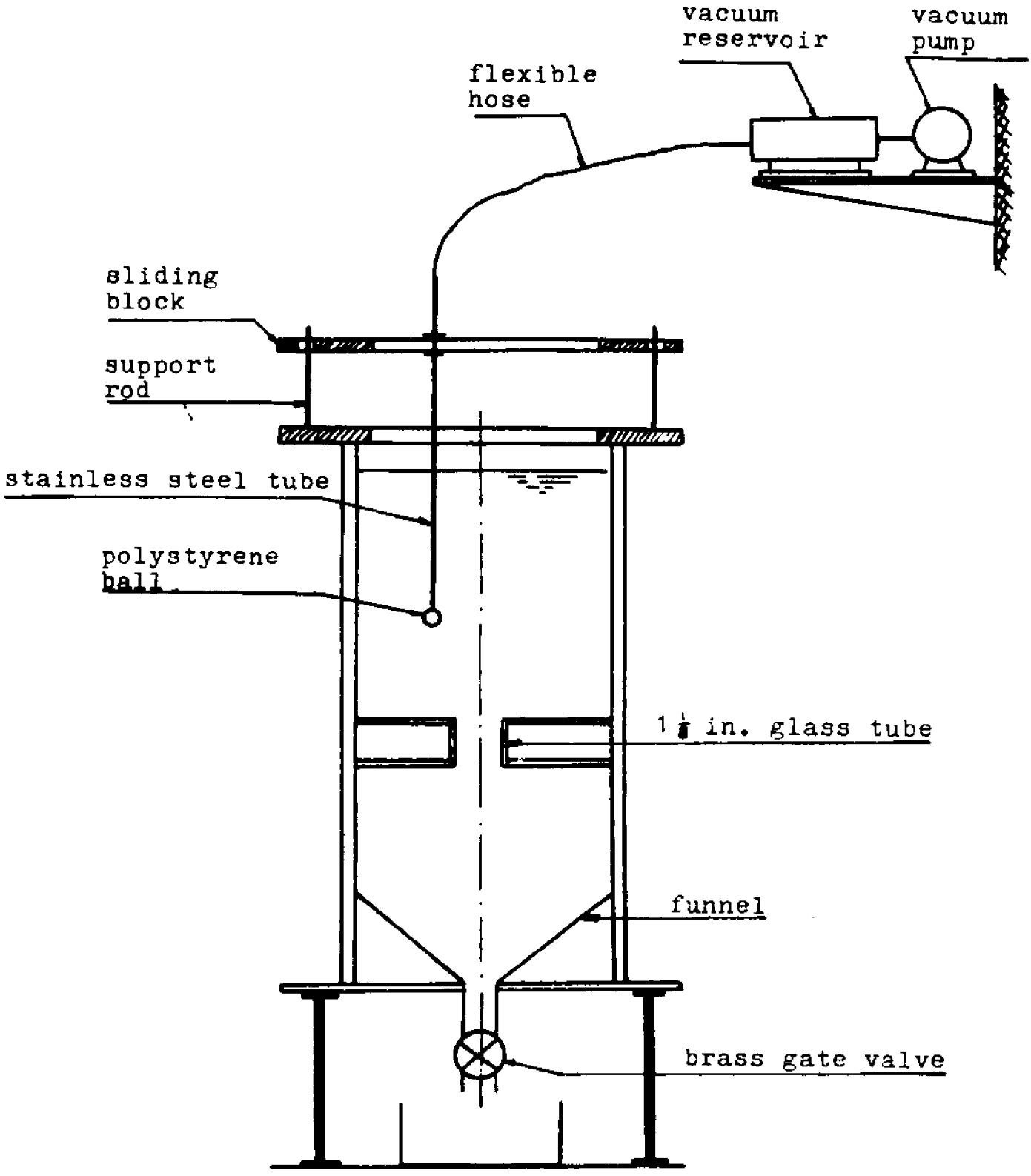

Figure IV-7. Schematic illustration of experimental apparatus.

with a constant volume pycnometer. Viscosity measurements were made at the begining and end of each series of runs to insure that there are no changes due to temperature variation.

The spheres used in the experiment were $\frac{1}{2}$ in. solid polystyrene balls. The balls were extremely smooth and insoluble in the fluid. To insure that the test spheres are neutrally buoyant preliminary measurements of the terminal settling velocity were made to select the spheres with a settling velocity of less than 1mm/min. Since each run lasts about 3 min. the error introduced by the discrepancy between the sphere density and the fluid density is within the permissible range.

The test sphere was placed in the fluid above the pore in a predetermined location. By opening the valves at the bottom of the tank the flow field was established. The sphere was photographed by a Bauer C-Royal 6-Zoom Super 8 movie camera at one frame per sec.. The length of each run was timed and the fluid volume extracted was measured to determine the Reynolds number. A Kodak Ektagraphic MFS-8 movie projector was used to project the film onto a grid from which measurements of the radial and axial position were taken, excluding the first ten frames in the begining of each run to account for possible transient effects before the flow becomes fully developed.

IV-5. Results and discussion.

The results obtained experimentally are presented in figure IV-8 and are compared with the theoretical prediction of the trajectory based on the interaction function $\lambda_2(Z_o)$. The Reynolds number for these runs was calculated based on the average fluid velocity in the tube and was kept at 0.2. Lower Reynolds number increases the time needed to complete a run, requiring increased accuracy of the sphere buoyancy. Unfortunately, these commercially made polystyrene spheres had small internal bubbles which were filled with polystyrene latex and then tested for their settling velocity. Settling velocity of 1mm/min. introduces a measurable error if the run lasts longer than 4 min.. Therefore, the volumetric flow rate was controlled to keep each run under 4 min. and, in turn, the Re at about 0.2. Although the Re is slightly higher than desired, the motion should be very close to zero Re behaviour. In fact, Bond (1921) and Johanson (1930) demonstrated that inertial effects in a flow through an orifice are negligible for $Re \ll 6$.

The results shown in figure IV-8 are in good agreement with the predicted theoretical trajectory in the far field and near the orifice wall. In the vicinity of the pore, the agreement is good when the initial position is close to the axis of the pore or its wall. A sphere approaching the pore at an angle of about 45° departs from the theoretical curve and is closer to the fluid streamline. This behaviour results from the transverse curvature effects which are

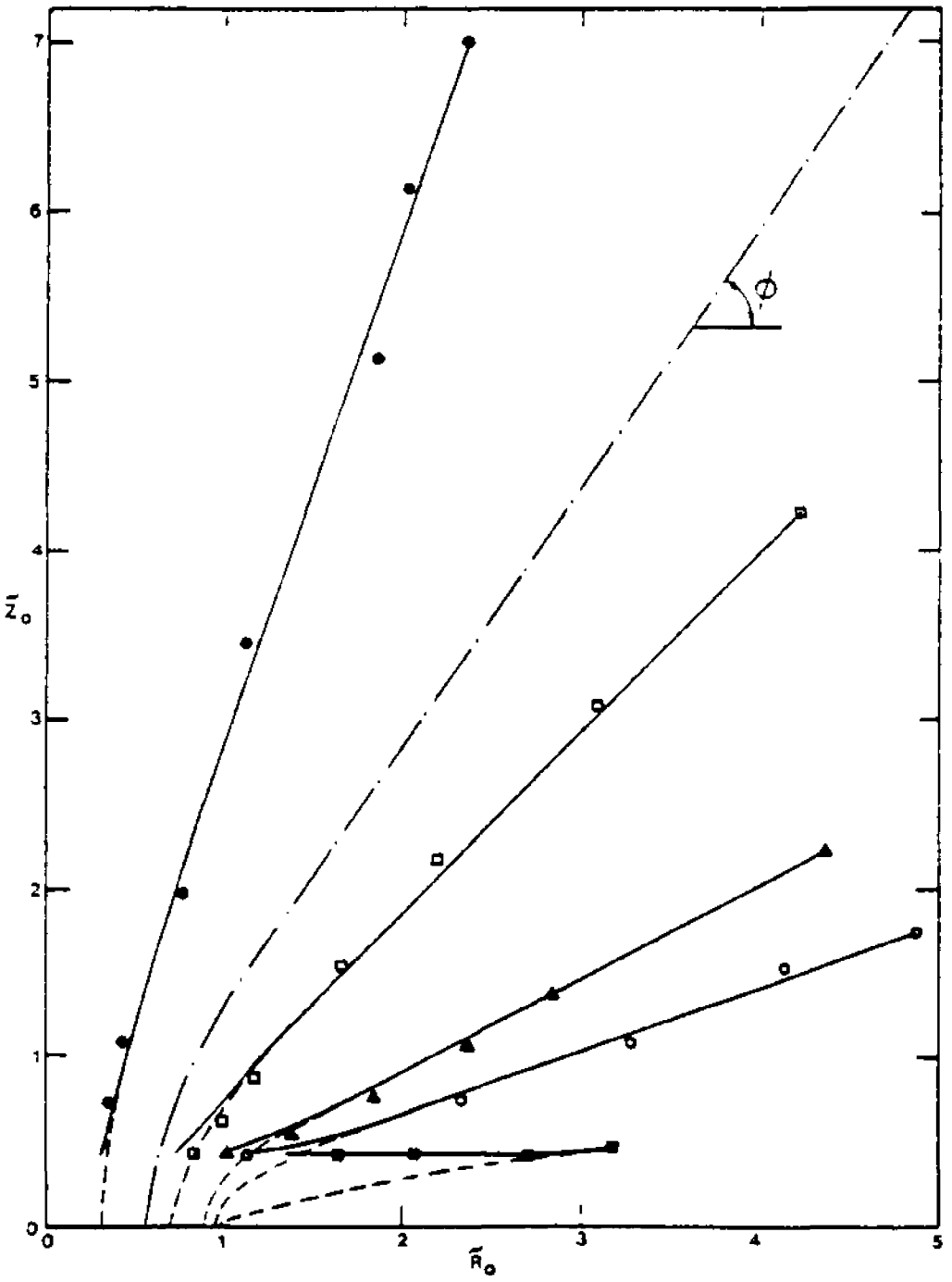

Figure IV-8. Comparison between theory and experiment for sphere trajectories. a=0.5 in., c=1.125 in. ——— theoretical solutions; - - - undisturbed fluid streamlines; —·—·— critical trajectory.

neglected in the theoretical formulation. Results for the sphere entering the pore are not presented for $Z < a$ because the parallax prevented accurate measurements in that region.

The most striking result observed is that the sphere always enters the pore even in the extreme case where it moves parallel to the boundary at minimum gap width. According to the critical trajectory concept, which has been used extensively in the nuclepore filter literature, all particles originating on streamlines whose angle ϕ in the far field was less than 56° would have been excluded from entering the pore for the case shown in figure IV-8. This behaviour is in agreement with the results presented by Hocking (1959) who have shown that the collision efficiency for small inertaless drops approaches zero when hydrodynamic interaction effects are taken into account. In general, collection of particles on the orifice wall will occur when adhesive forces at small gap width are significant and can offset the repelling hydrodynamic forces.

IV-6. Comments on the particle exclusion effect at the entrance to a pore.

It is evident that when inertial effects are negligible the undisturbed streamline which passes by the edge of the pore with a minimum clearance equal to the sphere radius does not properly describe the exclusion of particles entering the pore. Figure IV-8 shows that when the particle is not small compared to the diameter of the orifice the simple definition of a "geometric critical trajectory" can lead to very substantial errors in the collection efficiency of filters. The hydrodynamic interaction of the particle with the wall of the orifice, which heretofore has been neglected, will cause large particles to deviate strongly from fluid streamlines as the boundary is approached. Since the fluid gap between the sphere and the wall can never vanish (this would require an infinite force in creeping motion) the sphere must eventually translate nearly parallel to the wall and rotate with an angular velocity approaching $0.5676\frac{U_\infty}{a}$ as demonstrated by Goldman et al (1967b) for the free motion of a sphere almost touching a plane wall in a shear field.

It is, therefore, the time dependent behaviour which distinguishes between various trajectories. Namely, the time required for a sphere to enter the pore from a prescribed distance depends strongly on the initial position and is greatly increased when the sphere translates close to the wall due to velocity retardation. Furthermore, since

there is no real exclusion of particles, the critical trajectory in the zero inertia limit coincides with the path made by a particle center that just touches the orifice wall.

In the case of multiparticle flow into the pore, particles can be collected on the wall due to hydrodynamic interaction between the particles themselves, surface roughness and the adhesive forces which are significant at small gap width. In addition, when the particles are small compared with the pore diameter the force acting on the particles due to concentration gradients can affect the particle trajectories. These effects are neglected in the present analysis.

For a dilute suspension in which particles are not collected the entrance effects can be investigated by examining the steady state average volumetric concentration of particles across a hemispherical surface of radius r with its origin at the center of the opening. From physical considerations, when a suspension flows into the pore, there cannot be any particle centers near the orifice wall closer than the particle radius. Therefore, one can assume the existence of a particle depleted wall layer whose thickness is one particle radius in which the flux is zero.

Since there is no real exclusion, it is required that

$$H_\infty \bar{V} = H \bar{U}_p \qquad \text{(IV-6.1)}$$

where H_∞ is the concentration far from the pore, $\bar{V}$ is the average fluid velocity on the hemispherical surface and $\bar{U}_p$

is the average velocity calculated over the hemispherical surface excluding the particle free layer. The average concentration H is defined by the ratio of the particle flux to the volumetric flow rate across the same hemispherical surface. Hence

$$\bar{V} = \int_0^{\pi/2} (V_R^2 + V_Z^2)^{1/2} \sin\theta \sin(\theta + \alpha_f)\, d\theta \qquad \text{(IV-6.2a)}$$

where

$$\alpha_f = \tan^{-1} \frac{V_Z}{V_R} \qquad \text{(IV-6.2b)}$$

and

$$\bar{U}_p = \frac{\int_0^{\pi/2 - \sin^{-1}\frac{a}{r}} (U_x^2 + U_Z^2)^{1/2} \sin\theta \sin(\theta + \alpha_p)\, d\theta}{(1 - \frac{a}{r})} \qquad \text{(IV-6.3a)}$$

where

$$\alpha_p = \tan^{-1} \frac{U_Z}{U_x} \qquad \text{(IV-6.3b)}$$

In the equations above, θ is the cone angle measured from the Z axis, the fluid velocity components are given by equations (IV-2.8a,b) and the particle velocity components are approximated by equations (IV-2.17b,c) neglecting the hydrodynamic interaction between the particle themselves.

Equation (IV-6.1) has been solved for the local average concentration and the results are shown in figure IV-9 for various particle radii. The concentration decreases with decreasing distance r from the pore opening and this concentration defect increases with increasing particle size. This behaviour is in agreement with the observations made by Fahraeus (1929) showing that when blood flows from a feed reservoir into a tube of diameter less than 500μm the

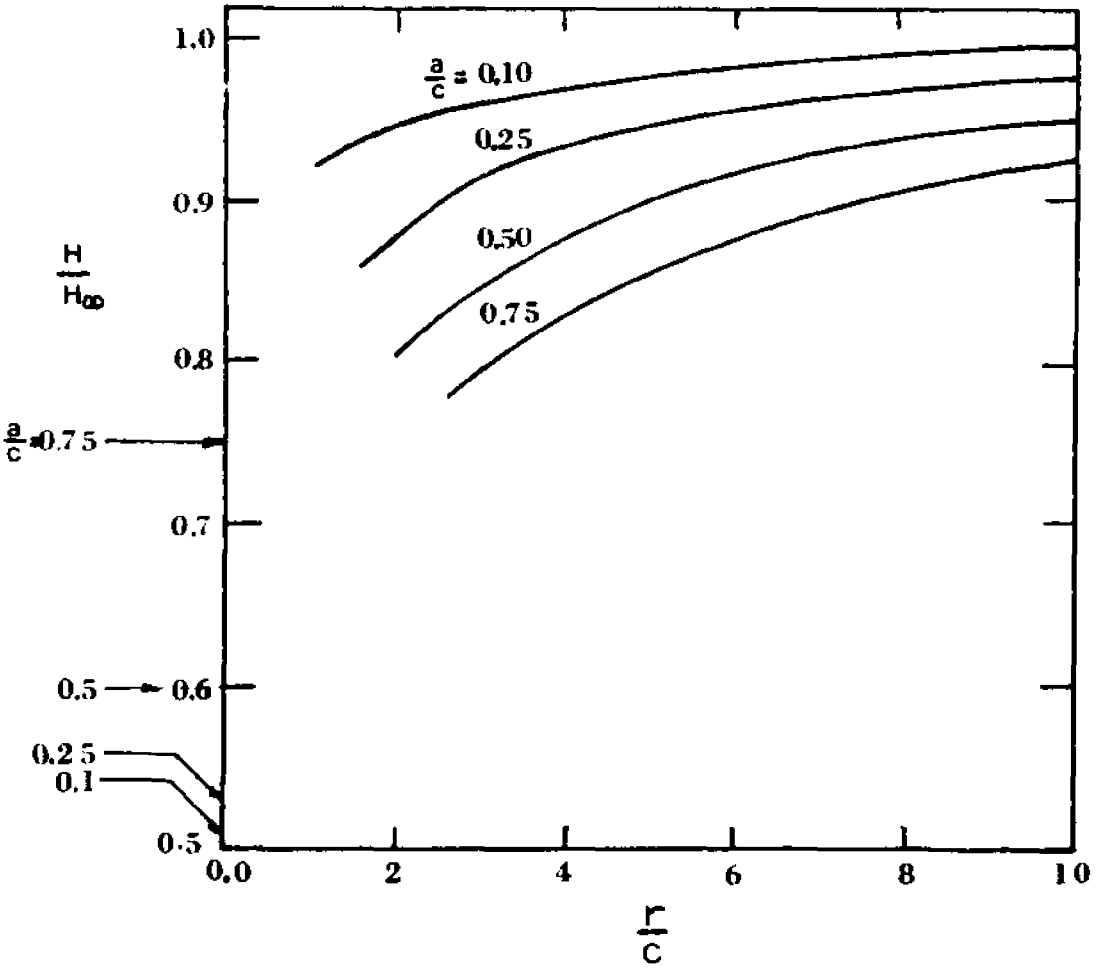

Figure IV-9. Concentration defect in a flow into a pore. ——→ values for a chain of spheres carried axisymmetrically in an infinite tube (Wang & Skalak, 1969)

instantaneous hematocrit within the tube is always less tnan that of the blood in the reservoir.

The results shown in figure IV-9 were computed for decreasing value of r until r=c+2a. For smaller values of r the approximate theory presented in this chapter is not valid because the effect of the pore opening on the particle trajectory becomes significant. Nevertheless, the results for small values of r are compared with the limiting value for a chain of spheres moving coaxially in an infinite tube (Wang and Skalak, 1969) shown in figure IV-9 by the arrow-heads. Examining these values one can observe that for large particles (a/c=0.75) the present results approach this value, while for small particles the concentration defect is much smaller than the one described by a flow of an axial chain of spheres in an infinite tube. This behaviour can be explained by the fact that when the particle radius is large compared with the pore radius only one particle can enter the pore through its opening area creating a chain of spheres inside the pore. For particles much smaller then the pore, many particles can enter the pore at the same time and a non-uniform concentration profile is established which cannot be described by a chain of coaxial spheres.

Some insight into the formation of a non-uniform concentration profile can be attained by examining concentration change along trajectory tubes. For this purpose the generating arc of the hemispherical surface $\frac{r}{c}=10$ was

divided into nine equal arc lengths ($\theta=10^{o},20^{o},30^{o},\cdots$) creating nine circular surfaces on the hemisphere. Since particles cannot cross trajectory lines, one can obtain trajectory tubes by calculating the particle trajectories starting from the nine points on the generating arc.

Thus, conservation of flux requires that at any r

$$H\int \vec{U}\cdot\hat{n}\ dS = H_{\infty}\left(\int \vec{U}\cdot\hat{n}\ dS\right)_{r=10} = \text{constant} \qquad (IV\text{-}6.4)$$

where the integral is evaluated over the surface area bounded by each trajectory tube at any distance r.

Equation (IV-6.4) was evaluated for various sphere radii a and dimensionless distances $\tilde{r}$ ($\tilde{r}=\frac{r}{c}$), and the average local concentration was plotted as a function of θ (figures IV-10a,b,c,d). Clearly, this procedure gives a rough quantitative description of the concentration profile, however it provides for the first time a graphic account of the concentration evolution in the flow towards a pore.

Figure IV-10 shows that the concentration decreases near the axis of the pore and increases near the orifice wall. This effect increases with decreasing values of the distance $\tilde{r}$ and the particle radius a. In this context it should be noted that near the orifice wall the trajectory tube is bounded by the trajectory of the particle which almost touches the wall. For computational purposes this trajectory was defined at a distance of 1.01a from the orifice wall.

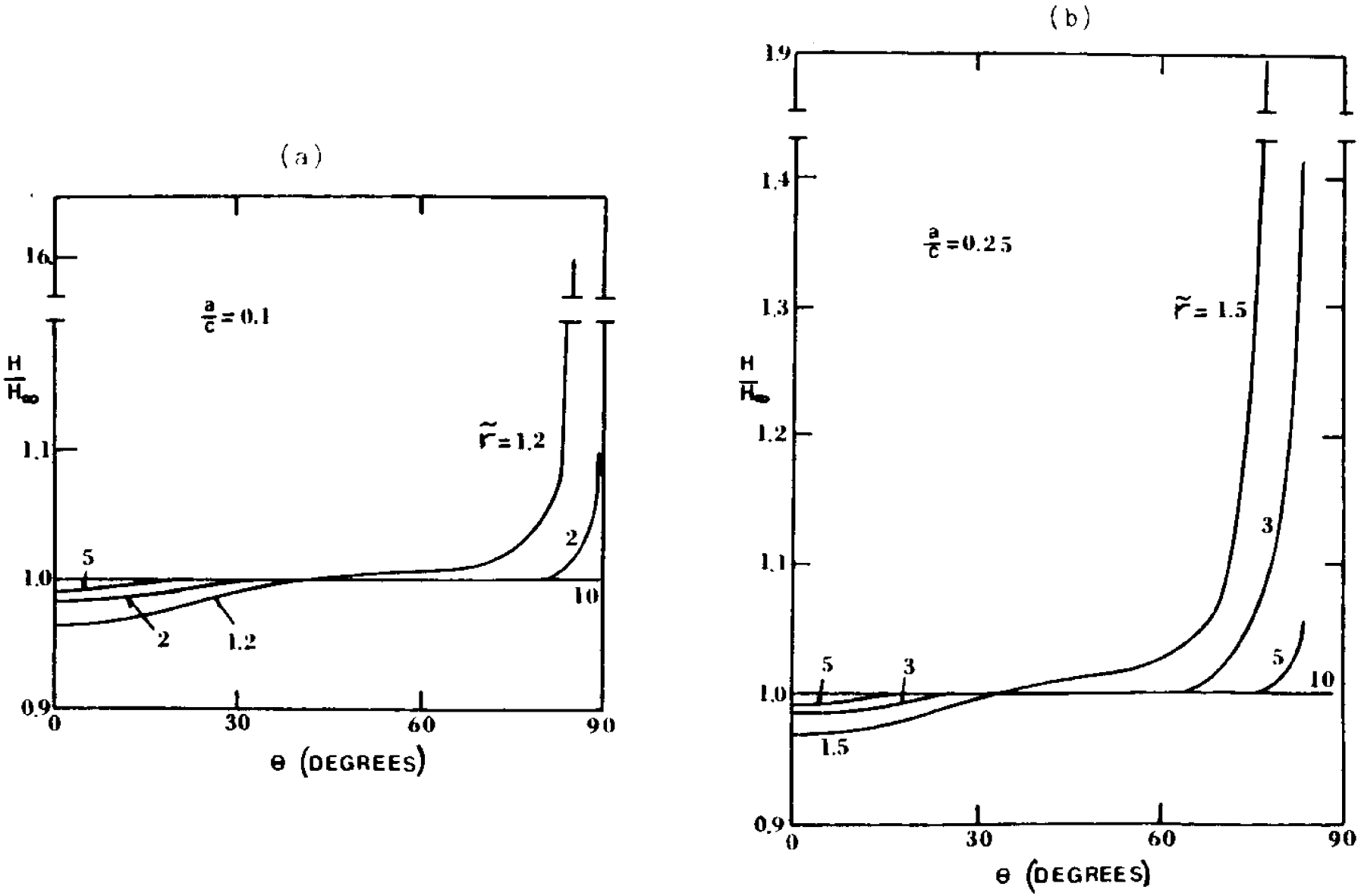

Figure IV-10. Concentration profiles in a flow towards a pore. (a) a/c=0.1; (b) a/c=0.25.

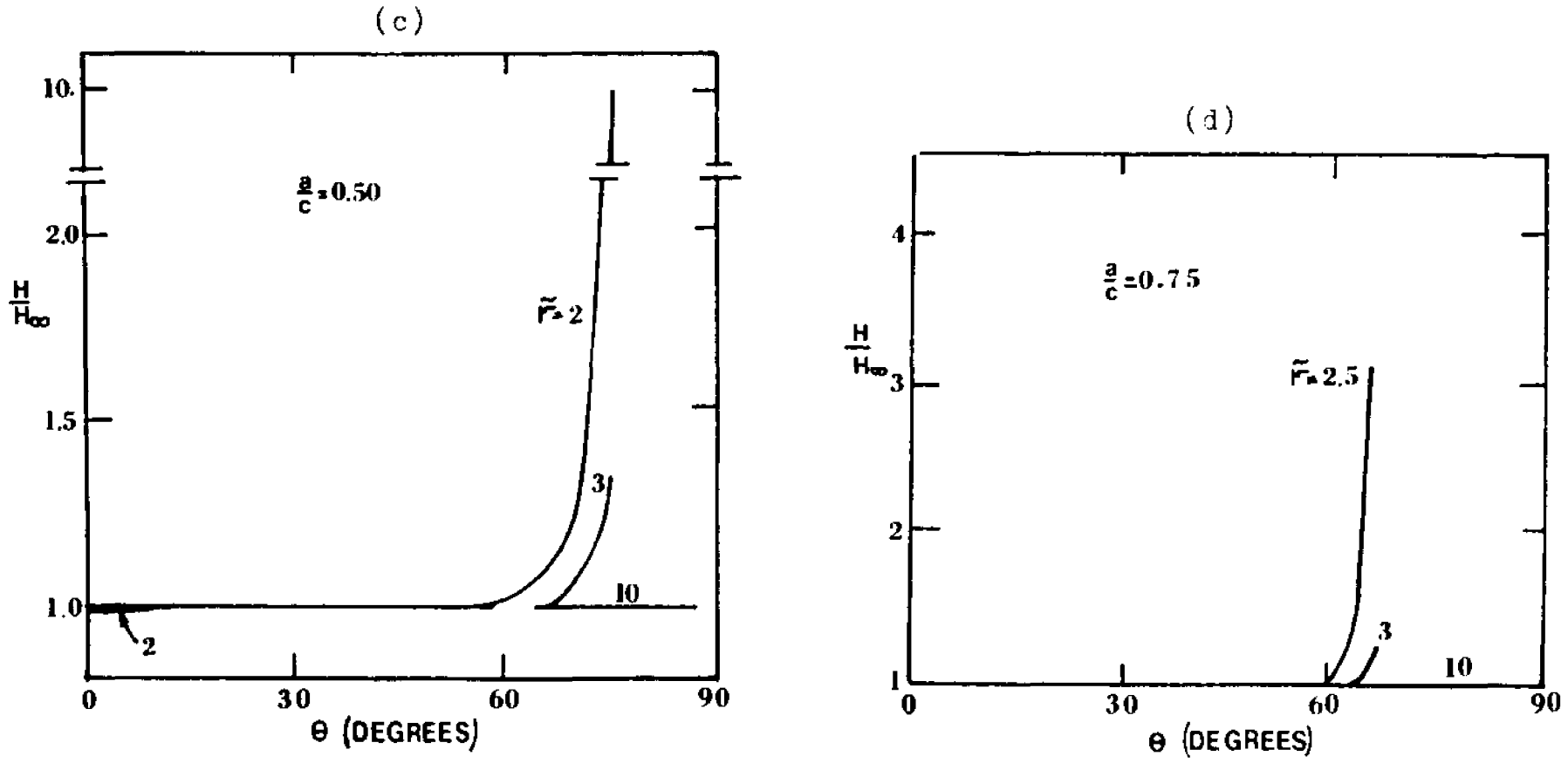

Figure IV-10. Concentration profiles in a flow towards a pore. (c) a/c=0.5; (d) a/c=0.75.

The variation of the concentration profile shown in figure IV-10 is a direct result from the hydrodynamic interaction between the particles and the orifice wall. Near the wall this interaction significantly reduces the particle velocity causing particle aggregation. On the other hand, near the pore axis (θ=0.) the hydrodynamic interaction with the confining boundaries is small allowing the particles to move with large velocities which in turn reduce the local concentration.

The theory in the present form is unable to predict the complete transition from the reservoir to tube concentration because the analysis breaks down in the vicinity of the pore opening. An important extension of the present theory is to study this transition region.

Appendix: <u>The axisymmetric uniform flow past a sphere perpendicular to a disk for a'<< c'.</u>

We consider a sphere of radius a' held rigidly at a distance d' from a disk of radius c' (Fig. IV-3). For c' >> a' the velocity profile at Z'=d' can be assumed to be similar to the profile given by Sampson (1891) for flow past a disk in the absence of the sphere.

The general solution of the creeping motion equations for the axisymmetric flow is constructed by superposing the disturbaces from the plane of the disk and the spherical series solution representing the disturbances generated by the sphere. In dimensionless form it can be written as follows

$$\Psi = \frac{1}{2} V_\infty R^2 + \int_0^\infty R J_1(\omega R)\left[A(\omega) + Z B(\omega)\right] e^{\omega Z} d\omega + \sum_{n=2}^{\infty} \left[B_n r^{-n+1} + D_n r^{-n+3}\right] I_n(\cos\theta) \qquad \text{(IV-A-1)}$$

Here, the notation is similar to that used in chapter III, $A(\omega)$ and $B(\omega)$ are unknown functions of ω and the dimensionless variables are given by

$$(R, Z, r, a, d) = \frac{1}{c'}(R', Z', r', a', d') \qquad \text{(IV-A-2a)}$$

$$\psi = \frac{\Psi'}{c'\nu} \quad , \quad u = \frac{\nu}{c'} u' \qquad \text{(IV-A-2b,c)}$$

The boundary conditions at the plane of the disk require

$$u_R(R, d) = 0 \qquad (R > 0) \qquad \text{(IV-A-3a)}$$

$$u_z(R,d) = \begin{cases} V_\infty \left(1 - \frac{2}{\pi}\cot^{-1}\sqrt{R^2-1}\right) & (R>1) \\ 0 & (0<R<1) \end{cases} \qquad \text{(IV-A-3b)}$$

Application of (IV-A-3) utilizing the Hankel inversion formula results in

$$\left[A(\omega)+B(\omega)\left(\frac{1}{\omega}+d\right)\right]e^{\omega d} = \sum_{n=2}^{\infty}\left[B_n B_n^*(\omega,d)+D_n D_n^*(\omega,d)\right] \qquad \text{(IV-A-4a)}$$

$$\left[A(\omega)+d\,B(\omega)\right]e^{\omega d} = -\sum_{n=2}^{\infty}\left[B_n B_n^{**}(\omega,d)+D_n D_n^{**}(\omega,d)\right]-\frac{2V_\infty \sin\omega}{\pi\omega^2} \qquad \text{(IV-A-4b)}$$

where B*, D*, B** and D** are given by (III-2.26).

Equations (IV-A-4a,b) are solved simultaneously for $A(\omega)$ and $B(\omega)$ in terms of the unknown spherical coefficients B_n and D_n. This solution is then substituted back into (IV-A-1) from which the radial and axial velocity components are obtained

$$u_R = \frac{2}{\pi}V_\infty \times \int_0^\infty J_1(\omega R)\sin\omega\, e^{-\omega x}\,d\omega + \sum_{n=2}^{\infty}\left[B_n\beta_n'(R,Z)+D_n\delta_n'(R,Z)\right] \qquad \text{(IV-A-5a)}$$

$$u_z = V_\infty - \frac{2}{\pi}V_\infty \int_0^\infty J_0(\omega R)\,e^{-\omega x}(1+\omega x)\frac{\sin\omega}{\omega}\,d\omega + \sum_{n=2}^{\infty}\left[B_n\beta_n''(R,Z)+D_n\delta_n''(R,Z)\right] \qquad \text{(IV-A-5b)}$$

where $x=d-Z$, β_n', δ_n', β_n'', and δ_n'', are defined by (III-2.29)

and the integrals in (IV-A-5) are given by (III-2.48).

The remaining boundary conditions to be satisfied on the surface of the sphere, r=a, are

$$U_R = 0, \qquad U_Z = 0 \qquad \text{(IV-A-6a,b)}$$

These conditions are applied by making use of the collocation technique presented in chapter III. The boundary conditions are satisfied at discrete points on the sphere's surface and the infinite series in (IV-A-5) is truncated into a finite one. If the no-slip boundary conditions are to be satisfied at N points on the generating arc of the sphere, the infinite series is truncated after the Nth term resulting in a set of 2N linear algebraic equations for the 2N B_n and D_n unknown coefficients.

The drag correction coefficients can be written in the form

$$\lambda = \frac{D_z}{1.5\, a\, V_\infty} \qquad \text{(IV-A-7)}$$

Solutions for λ were obtained with increasing number of boundary points until convergence of the first five significant digits was achieved. The results are presented for various sphere to disk spacings and sphere radii in table IV-A-1, and are plotted in figure IV-4.

The velocity of a neutrally buoyant sphere carried towards a disk can now be approximated by equating the force acting on a sphere translating with velocity V_s perpendicu-

Table IV-A-1. Hydrodynamic interaction coefficient λ for uniform flow past a rigidly held sphere perpendicular to a disk.

$\alpha = \cosh^{-1}\frac{d'}{a'}$	$\frac{d'}{a'}$	$\frac{a'}{c'}=1.$	$\frac{a'}{c'}=\frac{1}{2}$	$\frac{a'}{c'}=\frac{1}{4}$	$\frac{a'}{c'}=\frac{1}{7}$	$\frac{a'}{c'}=\frac{1}{10}$	$\frac{a'}{c'}=\frac{1}{100}$
0.5	1.13	0.91480	0.19323	0.29510×10^{-1}	0.58018×10^{-2}	0.20170×10^{-2}	0.20434×10^{-5}
1.0	1.54	0.92493	0.28227	0.51599×10^{-1}	0.10698×10^{-1}	0.37724×10^{-2}	0.38753×10^{-5}
1.5	2.35	0.94061	0.43206	0.10973	0.25815×10^{-1}	0.94444×10^{-2}	0.10075×10^{-4}
2.0	3.76	0.95859	0.60441	0.23286	0.69673×10^{-1}	0.27741×10^{-1}	0.32555×10^{-4}
2.5	6.13	0.97383	0.74942	0.41881	0.17571	0.82181×10^{-1}	0.12081×10^{-3}
3.0	10.1	0.98420	0.84849	0.60953	0.35533	0.20773	0.48488×10^{-3}

lar to an infinite wall given in Brenner (1961) and the force acting on a rigidly held sphere in the flow past a disk for the case $a' \ll c'$ presented in figure IV-5. The solution for Vs when $a'/c'=0.01$, shown in figure IV-A-1, indicates that the sphere velocity is slightly larger than the undisturbed local fluid velocity in the absence of the sphere for $d'/a' \gg 2.3$, and decreases rapidly to zero as it approaches the disk.

The solution procedure presented here, for $a' \ll c'$, provides numerical results without the need for numerical evaluation of the integral expressions in the exact series solution obtained in chapter III (equation III-3.13) Hence, the computation time is much shorter and convergence to five significant figures is achieved with less boundary points.

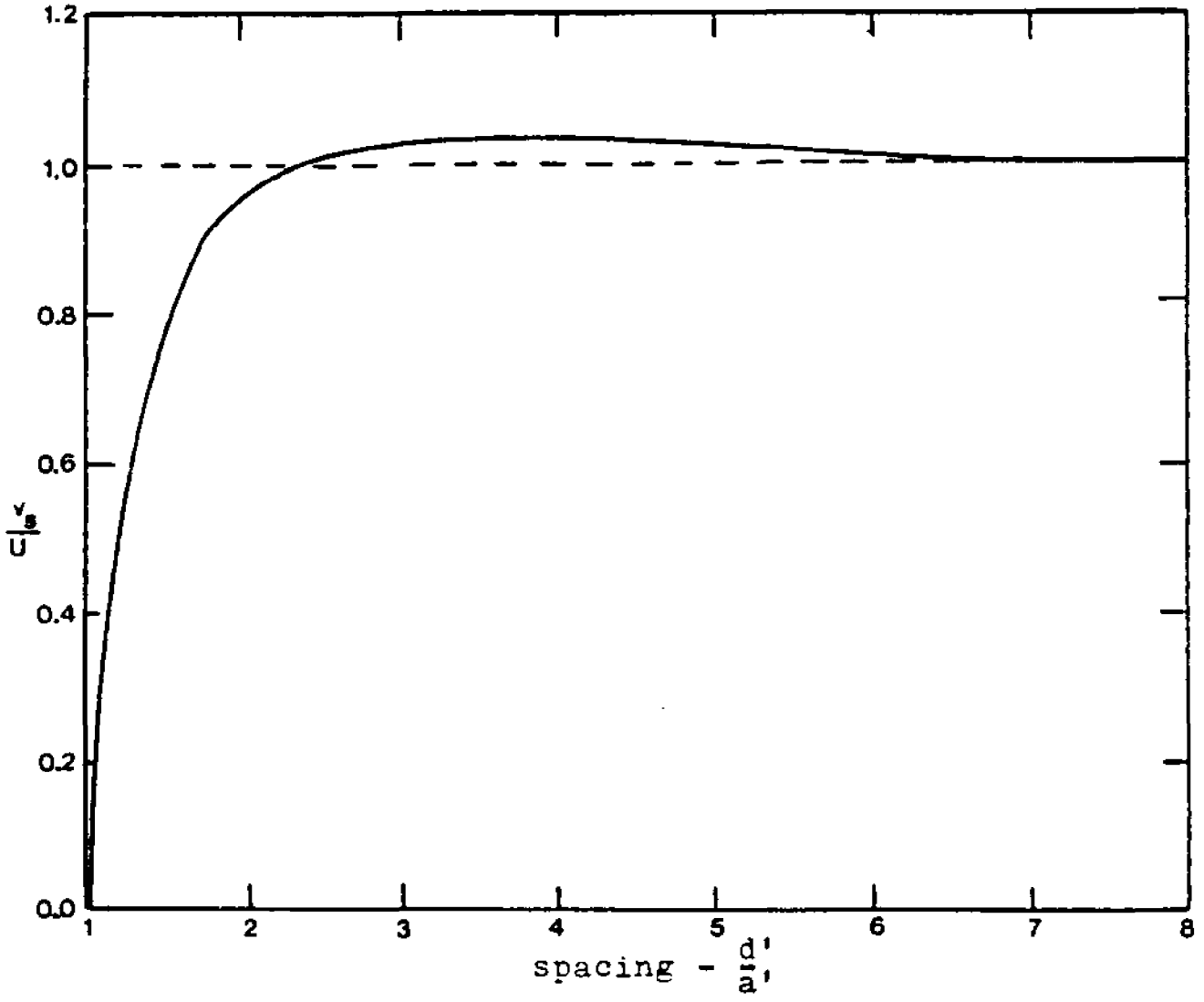

Figure IV-A-1. Velocity of a neutrally buoyant sphere carried by a uniform flow towards a disk for $a'/c' \ll 1$. $a'/c'=0.01$, Sampson (1891) profile in the plane of the disk.

CHAPTER V

CONCLUDING REMARKS

Entrance effects in creeping motion of viscous fluid into a pore have been presented by detailed solutions of three entrance flow problems: the creeping flow through a pore of finite length, the axisymmetric motion of a sphere towards an orifice, and the three-dimensional motion of a sphere towards a pore.

The problem of the flow through a finite length pore has been treated by a newly developed matching procedure. The flow field is divided into two simply bounded regions. Analytic solutions are first obtained in each region in terms of unknown functions representing the velocity components at the interface between the regions. These functions are then determined by matching the stress tensor at the interface between the two regions. The procedure reduces the boundary value problem into a set of integral equations that can be solved for the interfacial velocity components.

By combining the solution technique mentioned above and the boundary collocation method, the slow axisymmetric motion of a sphere towards an orifice has been examined. The procedure has been extended further to obtain the solution for the problem of uniform flow past a sphere moving axisymmetrically towards a rigidly held disk. In this context it is important to note that the stream function representing the disturbances generated by the sphere can be used in the form of equation (III-2.10) only when the sphere does not penetrate the orifice opening.

The reason for this restriction is that the orthogonality properties of the Gegenbauer functions in the present representation cannot be used to satisfy the no slip boundary conditions on the surface of a spherical cap. In the case when the sphere penetrates the plane of the opening, a different stream function representation has to be chosen to account for the disturbances genarated by the spherical caps on each side of the orifice. These functions, which are orthogonal on the surface of a spherical cap, are given by Dorrepaal, O'Neill and Ranger (1976) and by Majumdar, O'Neill and Brenner (1974).

The combined matching-collocation technique can be easily extended to treat bounded axisymmetrix multiparticle flows by superposing the flow field disturbances created by the particles and satisfying the no slip boundary conditions on the closed surfaces at discrete points.

Although in principle a similar analysis can be applied for three-dimensional flows, the numerical computation time required in applying the collocation method may be excessive. Therefore, an approximate strong interaction theory has been developed for determining the trajectory of a neutrally buoyant sphere carried by the fluid towards a pore which is valid when the spacing between the sphere and the confining wall is of the order of the sphere diameter. An overall hydrodynamic interaction function has been obtained by neglecting high order contributions and transverse curvature effects in the

vicinity of the pore opening. Results indicate that the sphere trajectory departs significantly from the undisturbed fluid streamlines and that the particle velocity is greatly reduced near the orifice wall. The theory has been used also to predict the onset of hematocrit defect that one observes when particles enter a tube from a feed reservoir. These results are consistant with the observations of Fahreaus and demonstrate, for the first time, the exclusion effect at the entrance to the pore. Furthermore, the concentration distribution indicates that particles aggregate near the orifice wall and a non-uniform profile is established with minimum concentration at the pore axis.

The theory is not valid near the pore opening and cannot predict the behaviour in the transition region between the reservoir the the tube. The study of the particle motion in the transition region and inside the pore is an important continuation of the present research.

REFERENCES

Bond, W.N. 1921 Proc. Phys. Soc. 33, 225.

Brenner, H. 1961 Chem. Eng. Sci. 16, 242.

Cooley, M.D.A. & O'Neill, M.E. 1969 Proc. Camb. Phil. Soc. 66,407.

Cox, G.R. & Brenner, H. 1967 Chem. Eng. Sci. 22,1753.

Davis, A.M.J., O'Neill, M.E., Dorrepaal, J.M. & Ranger, K.B. 1976 J. Fluid Mech. 77, 625.

Dean, W.R. & Montagnon, P.E. 1949 Proc. Camb. Phil. Soc. 45, 389.

Dorrepaal, J.M., O'Neill, M.E. & Ranger, K.B. 1976 J. Fluid Mech. 75,273.

Erdelyi, A. 1954 Tables of Integral Transforms, vols. 1,2, McGraw-Hill.

Fahraeus, R. 1929 Physiol. Rev. 9, 241.

Fahraeus, R. & Lindqvist, T. 1931 Amer. J. Physiol. 96, 562.

Faxen, H. 1923 Arkiv. Mat. Astron. Fys. 17, No. 27.

Ganatos, P., Pfeffer, R. & Weinbaum, S. 1978 J. Fluid Mech. 84, 79.

Ganatos, P., Pfeffer, R. & Weinbaum, S. 1980b J. Fluid Mech. 99, 775.

Ganatos, P., Weinbaum, S. & Pfeffer, R. 1980a J. Fluid Mech. 99, 739.

Gluckman, M.J., Pfeffer, R. & Weinbaum, S. 1971 J. Fluid Mech. 50, 705.

Goldman, A.J., Cox, R.G. & Brenner, H. 1967a Chem.Eng. Sci. 22, 637.

Goldman, A.J., Cox, R.G. & Brenner, H. 1967b Chem. Eng. Sci. 22, 653.

Haberman, W.L. & Sayre, R.M. 1958 David W. Taylor Model Basin Report No. 1143, Washington D.C.

Happel, J. & Brenner, H. 1973 Low Reynolds Number Hydrodynamics, 2nd ed. Noordhoff.

Hocking, L.M. 1959 Q.J. Roy. Met. Soc. 85,44.

Johanson, F.C. 1930 Proc. Roy. Soc. A126, 231.

Kanaoka, C., Emi, H. & Nskada, K. 1974 Kagaku Kogaku 38, 223.

Leichtberg, S., Pfeffer, R. & Weinbaum, S. 1976 Int. J. Multiphase Flow 3, 147.

Leichtberg, S., Weinbaum, S., Pfeffer, R. & Gluckman, M.J. 1976 Phil. Trans. Roy. Soc. A 282, 585.

Lugt, H.J. & Schwiderski, E.W. 1965 Proc. Roy Soc. A, 382.

Luke, Y.L. 1969 The Special Functions and Their Approximation, vol. 2, Academic Press.

Majumdar, S.R., O'Neill, M.E. & Brenner, H. 1974 Mathematika 21,147.

Manton, I.L. 1978 Atmos. Environ. 12, 1669.

Oberhettinger, F. 1972 Tables of Bessel Transforms, Springer Verlay.

O'Neill, M.E. 1964 Mathematika 11, 67.

Parker, R.D. & Buzzard, G.H. 1978 J. Aerosol Sci. 9, 7.

Parmet, I.L. & Saibel, E. 1965 Commun. on Pure and Applied Math. XVIII, 17.

Pich, J. 1964 Collec. Czech. Chem. Commun. 29, 2223.

Payne, L.E. & Pell, W.H. 1959 Fluid Mech. 7, 529.

Sampson, R.A. 1891 Phil. Trans. Roy. Soc. A 182, 449.

Skalak, R.A., Chen, P.H. &Chein, S. 1972 Biorheol. 9, 67.

Smith, T.N. & Phillips, C.R. 1975 Environ. Sci. Tech. 9, 564.

Tranter, C.J. 1951 Quart. J. Math. 2, 60.

Wang, H. & Skalak, R. 1969 J. Fluid Mech. 38, 75.

Weinbaum, S. 1968 J. Fluid Mech. 33, 38.

Weinbaum, S. & Caro, C.C. 1976 J. Fluid Mech. 74, 611.